MULTICOLOUR PHOTOMETRIC STUDY OF PULSATIONS IN A PRE-MAIN SEQUENCE STAR V351 ORI (HD 38238)

By

Getinet Feleke Ayane

A dissertation submitted in fulfilment of the requirements for the M.Sc. degree in the Faculty of Agriculture, Science and Technology

NORTH WEST UNIVERSITY

Supervisor: **Prof. Medupe R.**

November 2013

Abstract

V351 Ori is a member of the Herbig Ae stars that are characterized by large infrared excess, emission in hydrogen lines and non periodic photometric and spectroscopic variability. Some of them have been detected to pulsate in radial and non-radial modes. V351 Ori has been found to pulsate in different frequencies of radial mode and possible existence of non-radial mode is also suggested. Before 1986 the brightness of this star showed changes due to dust obscuration. However, after 1986 such variability disappeared. The lack of variability was explained as the disappearance of obscuring material around the star. These several peculiarities of the star easily justify the definition "remarkable". V351 Ori is projected on to the region of the Orion belt, where the Orion complex and the region of star formation lie nearby. In addition, the unstable pattern of light variations and the apparent indications of accretion of matter onto the star are consistent with the assumption of its young age.

The main aim of this thesis was to carry out time series multicolour photometry of Herbig Ae star V351 Orionis using five Johnson filters (UBVRI) to observe pulsations in this star. Specifically to measure frequencies of oscillation of the star using Fourier analysis and then to make comparisons with values of frequencies from previous research work in order to determine the frequency evolution of this star. The other related objective was to determine amplitudes of oscillation with a high relative accuracy in different colours and as an additional idea to attempt mode identification to see if there are any systematic changes and whether we can model the change. V351 Ori was selected from a list of targets which are pulsating pre-main sequence Herbig Ae/Be stars and candidates based on its visibility and its high amplitude value. We observed this star over three weeks in January and February 2013 at Sutherland, for a total of 23 nights and 85 Hrs of observations, with 370 data points taken in filter V and almost the same data points in other filters. We used a 0.5-m telescope equipped with modular photometer which is fairly conventional single-channel design to observe and the data was reduced using a FORTRAN program called LUCY.

The frequency analysis and least square fitting gave one prominent frequency of pulsation (15.687 cycles/day) which is similar to previous theoretically calculated frequencies. We also found the amplitude of oscillation which is also similar to these theoretically found values. We also found additional frequencies which are similar with previous works. But these frequencies we have got are not found in all filters. In addition to this, we also got new frequencies which were not described in previous papers and theoretical models.

The light curve of the star shows the δ Scuti pulsation and also shows a variation which seems to be variation due to dust obscuration. The pulsation frequency found was used to undergo mode identification. From the plots found, it does not seem simple to identify which best identification to choose for different l values since the error bars are large and sometimes outside the lines. This specially happened in 'Delta Scuti Mad model'. The observed value also seems to match with theoretical values of l = 0, 1 and 2. However, it seems that conclusive results on mode identification cannot be given only from the results we have got. To say which observed amplitudes ratios are most consistent with the theoretical models that have values l = 0, 1, 2 and 3, it seems that more observation, specially spectroscopic, for a greater number of nights might be needed for a better result in mode identification. Actually the mode identification result seems to give a value l = 0 for Warsaw New-Jersey model which implies that the star has a radial mode of pulsation. However, to talk about non radial pulsation we need more observations, as suggested above. The detail of pulsation frequencies found and the attempt we made on mode identification and its results are reported in this thesis.

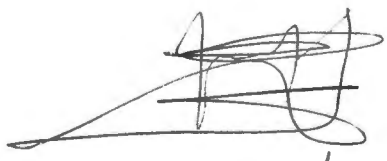

15/12/2014

Acknowledgements

First and foremost, I owe my deepest gratitude to my dearest supervisor, Prof. Thebe Medupe who has been a wonderful advisor with his great intuition on scientific support. From the instant I approached him for being my advisor, he has gone out of his way to help me very generously. This thesis would not have come to the final stage without his support, useful advice and constructive feedback. I have learnt a lot from his guidance, most importantly to plan and carry out research in the future.

I would like to show my gratitude and thanks to the National Astrophysics and Space Science Programme (NASSP) for giving me the opportunity to join the programme and providing all the support and secure funding for two years.

I would also like to thank Mr. Daniel Nhlapo for the required assistance he gave me during my first observation and introducing me with the world of telescopes. My sincere thanks also goes to Mr. Noha Sithole for the useful discussions which have been very helpful for me before going to telescope observation. I would also like to thank Mr. Moabi Matsididi for always being willing to discuss astronomy and computer related sciences and for his very easy-going personality.

I want also to thank Mr. Oyi Abedigamba and Mr. Getachew Mekonnin for assistance they made for any questions I was asking while I stacked with some research related issues.

I am grateful to my former home institution Kotebe University College for the help to complete the required administrative procedures and additional support while doing my research in the two years. I express my sincere thanks to Dr. Solomon Belay, Director of Entoto Observatory for supporting me by writing recommendations and even technical assistance related with my home institution.

I am also very grateful to Mr. Francois van Wyk for assisting me on the 0.5m telescope and keeping up with my seemingly never-ending questions. Observations could not have been done easily without his help. He is really helpful and generous man who made my stay in the observatory easy. God bless you.

Finally, I would like to mention about the pillar of my life, my parents who always pray for my success and health: my mother Emahoy Workinesh Tekle and my sister Atsede Feleke. It will always remain the best fact of my life that I am lucky to have them and dream about them. Thanks for believing in me and supporting my decisions.

Dedicated To My Sweet Parents

Contents

List of Figures

List of tables

Abbreviations

The following abbreviations are used in the text:

AA – Astronomy & Astrophysics

AAS – Astronomy & Astrophysics Supplement

ApJ – Astrophysical Journal

ApJS – Astrophysical Journal Supplement

APS – American Physical Society

Ap&SS – Astrophysics & Space Science

ASPC – Astronomical Society of the Pacific Conference

ASP – Astronomical Society of the Pacific

CCD – charge coupled device

CoAst. – Communications in Asteroseismology

COROT – Convection Rotation and Planetary Transits

CTT – Classical T Tauri

DFT – Discrete Fourier Transform

FAMIAS– Frequency Analysis and Mode Identification for Asteroseismology

HAeBe – Herbig Ae/Be

HELAS – Helio-and Asteroseismology

HJD – Heliocentric Julian Date

HR-diagram – Hertzsprung-Russell diagram

IAUS – International Astronomical Union Symposium

IR – infrared

IRAS – Infrared Astronomical Satellite

LMC – Large Magellanic Cloud

MNRAS – Monthly Notices of the Royal Astronomical Society

MNSSA – Monthly Notes of the Astronomical Society of South Africa

MOST – Microvariability and Oscillations of Stars

NASSP – National Astrophysics and Space Science Program

OB – O and B spectral type

PMS – Pre-Main Sequence

PNNV – Planetary Nebula Nucleus Variable

PSC – Point Source Catalogue

SAAO – South African Astronomical Observatory

SAST – South African Standard Time

SED – Spectral Energy Distribution

SIMBAD – Set of Identifications, Measurements and Bibliography for Astronomical Data

SPB – Slowly Pulsating B stars

UBVRI – Ultraviolet, Blue, Visible, Red and infrared

UT – Universal Time

WET – Whole Earth Telescope

WTT – Weak-lined T Tauri

YSO – Young Stellar Objects

ZAMS – Zero-Age Main Sequence

List of Publications

Papers Published in Refereed Journals:

- Kepler observations of the open cluster NGC 6819

  Balona, L. A.; Medupe, T.; Abedigamba, O. P.; Ayane, G.; Keeley, L.; Matsididi, M.; Mekonnen, G.; Nhlapo, M. D.; Sithole, N., 2013, MNRAS, **430**, 3472B

Chapter 1

Introduction

Variable stars are those that show change in brightness and spectra. Their variability may be due to geometric processes such as rotation, eclipse by a companion star (even by unseen planet), or intrinsic processes such as in pulsating stars, cataclysmic stars like eruptions on a star (flares), an accretion disk (dwarf novae), major explosions on a star (novae), or to the total disruption of a star (supernova). Variable stars have continued to be discovered and observed sporadically, occasionally through deliberate, systematic measures but more often by chance. The study of these stars is one of the most popular and dynamic areas of modern astronomical research. Variability is a property of most stars, and as such it has a great deal to contribute to our understanding of them. Once a star varies, however, more possibilities appear. We can determine a number of other parameters that we can not determine for non-pulsating stars. For example, eclipsing binaries offer the possibility of determining absolute values of stellar radius and mass. In each case, variable stars provide unique information about the nature and evolution of the stars, and the processes that go on within them. This information can be used to deduce even more fundamental knowledge about our universe in general. If a star pulsates, the pulsation amplitude may be as small as a few parts in a million, or it may be a factor of a thousand or more. The pulsation period can range from a second or less, to years, decades, or centuries (Gautschy & Saio 1995). In a sense, variable stars are 'speaking' to us. Variable star astronomers seek to learn their language, and understand what they are saying.

Stars are not quiet places. They are noisy; they have seismic waves such as sound waves in them. Those sounds cannot get out of a star, of course; sound does not travel in a vacuum. But for many kinds of stars – the pulsating stars – the sound waves make the star periodically swell and contract, get hotter and cooler. With our telescopes, we can see the effects of this: the periodic changes in the star's brightness; the periodic motion of its surface moving up-and-down, back-and forth. Thus we can detect the natural oscillations of the star and "hear" the sounds inside them (Aerts et al. 2010). Asteroseismology uses astronomical observations – photometric and spectroscopic ones – to extract the frequencies, amplitudes and phases of the sounds at a star's surface. Then we use basic physics and mathematical models to infer the sound speed and density inside a star, throughout its interior, and hence the pressure. Therefore, it is fair to say that when we observe the frequencies, amplitudes and phases of a pulsating star that are caused by sounds in the star, and we shift those by many octaves up into the audible region and play them through a speaker, we are experiencing the real music of the spheres.

The basic data for asteroseismology are the pulsation frequencies. From the pulsation frequencies, we can determine the pulsation mode of a star. Before the frequencies can be used for detailed modelling, it is imperative to know what pulsation mode gives rise to each frequency through the method of mode identification. A pulsation mode in stars is defined by three quantum numbers : n, l and m. These numbers are pulsational spherical index (l), which represents the total number of nodal lines on the surface of the star, the radial order (n), which represents number of nodal points along the radial direction as the wave propagates inside the star, and the azimuthal order (m), which is the number of nodal lines parallel to lines of longitudes on the surface of the star. Pulsational modes are very important since the amount of information about the stellar interior depends on the number of identified modes.

This thesis intends to bring a contribution to the study of pulsation and identification of mode of pulsation in the star. Our focus is on a variable Herbig Ae star V351 Ori, which is a pulsating star of δ Scuti type. The purpose of this thesis was to monitor the brightness variation of V351 Ori in order to perform mode identification and to detect any changes there might be in the light curve of this star. Although Balona et al. (2002) performed mode identification on this star, we were hoping to obtain better data by using CCD camera and observing the star over a longer period. Unfortunately, the time we started our observation coincided with the time when the UCT CCD was being decommissioned. We therefore resorted to using the Modular photoelectric photometer attached to the 0.5 m telescope. As it is shown later in the thesis, our data was more noisy than that of Balona et al. (2002).

This thesis is written in the following order. The first chapter gives some basic notes on star formation and evolution of stars, specifically, PMS stars. Literature on photometric and spectroscopic observations of PMS stars and Herbig Ae star V351 Ori (the target star) will be reviewed. The physics of pulsation and mode identification in stars is also given in this chapter. The second chapter deals with the selection criteria for our target star, the telescope we used with its control system and data acquisition, and finally the details of observations we have made. The reduction of data and plots of light curves through the reduction process is given in chapter 3. Chapter 4 discusses analysis and results of the observation. The fifth chapter gives concluding remarks and suggestions for future work related to the research.

1.1 Formation of Stars

The Big Bang did not produce a universe full of stars but of diffuse gas. Stars have been forming continuously since our galaxy took shape over 10 billion years ago. The key to understanding star formation is the correlation between young stars and clouds of gas. Where we find the youngest groups of stars, we also find large clouds of gas illuminated by the hottest and brightest of the new stars. This leads us to suspect that stars form from such clouds, much as raindrops condense from the water vapour in a thunder cloud. Indeed, the giant molecular clouds can give birth to entire clusters of new stars (Seeds and Backman 2011). A star forming region in constellation Ara is given in Figure 1.1 as an example.

Our universe is constantly renewing itself. Literally billions of stars have been born, lived out their lives, and died since our Galaxy formed. We do not see this activity when we gaze at the night time sky because the time scales on which stars play out this cosmic drama are enormously long by human standards. The magnificent emission nebulae and the ultraluminous, short-lived stars that power them are direct proof that star formation is a continuing process and there is no reason to suppose that galactic star formation has recently and abruptly ceased. Stars are constantly forming all across the Milky Way. In fact, star-forming regions are observed in all corners of the universe (Chaisson 1998).Typical molecular gas clouds must contract by a factor of a million in linear dimensions to form a star. Because of this dramatic (and rapid) reduction in size, any small initial rotation of the star-forming cloud is enormously magnified by conservation of angular momentum during collapse. In this way a modestly rotating gas cloud produces a rapidly rotating object – a disk – in addition to a small, stellar core at the end of gravitational collapse. Probably most of the material of a typical star is accreted through its disk, with a small amount left behind to form planetary systems (Hartmann 2009). Planets are also believed to form out of these discs. This could explain the disappearance of the discs once PMS star reaches the main sequence.

As it contracts, a single fragment forms out of a collapsing cloud, heats up, and begins to behave like a star. The term protostar can be used for this stage (Seeds and Backman 2011). The cloud contracts in such a way that the protostar grows deep inside a surrounding cloud of cold, dusty gas. These enveloping clouds have been called cocoons because they hide the forming protostar from view. When most of the material in a protostar's cocoon has fallen inward or been driven away, the protostar will no longer be quiet or hidden. The locations in the Hertzsprung-Russell (HR) diagram of protostars that have become detectable at visible wavelengths because their cocoons have disappeared is called the birth line. Once a star crosses the birth line and becomes visible, it continues to contract and move toward the main sequence at a pace that depends on its mass. Stars in this late stage of formation are sometimes called Young Stellar Objects (YSOs) or pre-main-sequence stars, to distinguish them from earlier protostellar stages.

Fig 1.1 A region of star formation about 1400 pc (4000 ly) from Earth in the southern constellation Ara, the Altar, (European Southern Observatory).

1.2 Pre-main sequence (PMS) stars

The pre-main-sequence (PMS) evolutionary phase is the short time span between the birth of a star from interstellar clouds and the onset of hydrogen burning on its arrival on the main sequence. Gravitational contraction is the main energy source during this stage. The universe we see is a snapshot of millions of stars, seen at various random stages of their evolution. The PMS stage lasts only a few million years, so stars spend only a small fraction of their lifetime in it, although every star passes through this stage once. One of the challenges in studying these stars is the fact that they are usually found within clouds of gas and dust, which will obscure or hide them at visible wavelengths. Radio observations have therefore been useful, and new sub-millimeter and mid-IR facilities such as the Atacama Large Millimeter Array and the James Webb Space Telescope, respectively, are ideally suited for studying star formation. A PMS star could also be an eclipsing or rotating variable, if it had a close companion. It could even be a pulsating variable, if it was located in an instability strip (Percy 2007).

PMS stars interact with the circumstellar environment in which they are still embedded; hence they are characterized by a large degree of activity, strong near or far-infrared excesses and very often by emission lines. PMS stars can be classified in to two major groups: T-Tauri and Herbig Ae/Be objects. Members of both groups show photometric and spectroscopic variabilities on time scales from minutes to years, indicating that stellar variability begins in the earliest phases of stellar evolution, prior to the arrival on the main sequence. The fact that stars move across the instability region during their evolution to the main sequence suggests that at least part of their variability can also be due to pulsations. This could also be due to obscuration due to circumstellar dust. One of the most fascinating problems in modern astrophysics is how stars and planets form out of the interstellar medium. PMS stars are of considerable interest since they usually have disks around them. These disks are possible sites of planet formation (Waters and Waelkens 1998). How these disks evolve in to planetary systems is one of the fundamental questions in astronomy.

1.2.1 Evolution of PMS stars

In the classical theory of pre-main sequence evolution, stars of every mass follow essentially different kinds of behaviour. Beginning as fully convective objects, they contract homologously until a central radiative core grows and, eventually, hydrogen ignites and stops further contraction (Palla & Stahler 1993).The general outlines of pre-main-sequence evolution have been understood for a long time, though many important details remain uncertain. One of the principal uses of pre-main-sequence evolutionary theory is to estimate the ages of young stars, providing the most reliable "clocks" we have for determining the time scales of star formation and disk evolution (Hartmann 2009).

The pre-main-sequence phase of stellar evolution marks both an end and a beginning. On the one hand, it represents the last period of a star's youth, before the object enters a protracted epoch of hydrogen fusion. It is also true that the star, as it begins pre-main-sequence contraction, is no longer buried within an opaque dust cloud (Stahler & Palla 2004). After the rapid dynamical contraction, the protostar reaches hydrostatic equilibrium and is said to have entered its pre-main-sequence phase. The contraction continues during most of the pre-main-sequence phase, on a thermal (or Kelvin-Helmholtz) time scale. Consequently, protostars with masses above about 10 $M_{\odot}$ move so fast from their Hayashi track to the main sequence that they are unobservable in their pre-main-sequence phase as they remain embedded in a thick circumstellar shell of infalling material (Aerts 2010). These stars can only be observed as infrared, accreting protostars or as main-sequence or post-main sequence objects (Palla & Stahler 1993). Pre-main sequence stars with masses between $\sim$ 2 and 10 $M_{\odot}$ end their contraction phase before they reach the main sequence. Such pre-main sequence stars are termed Herbig Ae/Be stars .

In pre-main-sequence stars with masses between 0.5 $M_\odot$ and 2 $M_\odot$, as soon as the contraction process stops, the star lights up in the HR diagram as an optically bright source called a T-Tauri star. Observations of both Herbig Ae/Be stars and T-Tauri stars suggest that they undergo active surface phenomena such as a stellar wind and differential rotation. Once the hydrogen is burning in full equilibrium and completely dominates the energy production, the star reaches a state of thermal equilibrium and is said to be born on the zero-age main sequence (ZAMS).The stars spend about 90 % of their life on the main sequence, burning Hydrogen into Helium on a nuclear time scale. The circumstellar remnant material vanishes within a thermal time scale and the star forgets its formation history. Protostars with a mass below some 0.08 $M_\odot$ never reach the ZAMS because they become degenerate before having reached a high enough central temperature to burn hydrogen in equilibrium. Such objects are called brown dwarfs (Aerts 2010).

1.2.2 T-Tauri Stars

The largest group of pre-main-sequence stars are the T-Tauri stars. They are found in regions of gas and dust along the Milky Way where stars are being formed. Often, they are found in loose groups called associations, parts of which may be gravitationally bound. The most famous of these is the Orion association, but there are other associations along the Milky Way. Most of these associations have spectral types O or early-type B and are referred to as OB associations, because they contain these hot, luminous stars with very short lifetimes. There are also T-Tauri stars in young clusters such as NGC 2264. T-Tauri stars are defined by the appearance of their spectrum which shows: the Balmer and Ca II H and K lines in emission; Fe λ4063 and 4132 in emission; forbidden S II λ4068 and 4076 lines, usually in emission and Li λ6707 strong (Percy 2007). T-Tauti stars, named after the first star of their class to be identified (located in the constellation of Taurus), are characterized by unusual spectral features and by large and rapid irregular changes on luminosity, with time scales in the order of days (Carroll & Ostlie 2007).

These stars have optical emission lines which arise from hydrogen, along with neutral and singly ionized metals. Additionally, all T-Tauri stars have significant flux in the X-ray region. The presence of cool regions on their surfaces suggests that, as in the Sun, bundles of concentrated magnetic field are penetrating the stellar surface. These stars also display activity related to convection and winds. All of the characteristics peculiar to T-Tauri stars naturally disappear in the course of pre-main sequence contraction (Stahler & Palla 2004). T-Tauri stars are slowly contracting to the main sequence, so they lie just above it in the HR diagram. Their variability and the spectral peculiarities appear to be connected with vigorous stellar activity on their surfaces. This may be due to their rapid rotation (which is connected with their youth) and, in some cases, the effects of continued accretion of matter. It should be realized that their rotation is rapid compared with that of the sun, but not rapid compared with the O, B, and A type stars.

There are several T-Tauri subtypes, or relatives, recognized today: classical T-Tauri stars (CTTS) with evidence of an accretion disc; weak-lined (WTTS) or 'naked' T-Tauri stars, which have little or no spectroscopically visible accretion disc (though there may be a cool, outer 'debris disc' still present); and FU Orionis stars, which are T-Tauri stars that exhibit significant brightenings, followed by slow declines. Most references to T-Tauri stars are actually to classical T-Tauri stars. These evolve into WTTS, which then evolve smoothly into sun-like rotating variables, after their accretion disc is gone. T-Tauri stars were initially defined as F, G, and K stars, lying above the main sequence. More recently, it has been possible to identify T-Tauri properties in M stars. We now know that the essential feature of a classical T-Tauri star (Figure1.2) is the accretion disc (or the remains of the accretion disc). Gas and dust slowly approaches the star via the accretion disk. It may be channelled on to the star by magnetic field lines, producing hot spots on the star. As a result, the star is a rotating variable; the typical period is 1 - 10 days. After the T-Tauri stage, the star may have cool spots, like the sun, and continue to be a rotating variable.

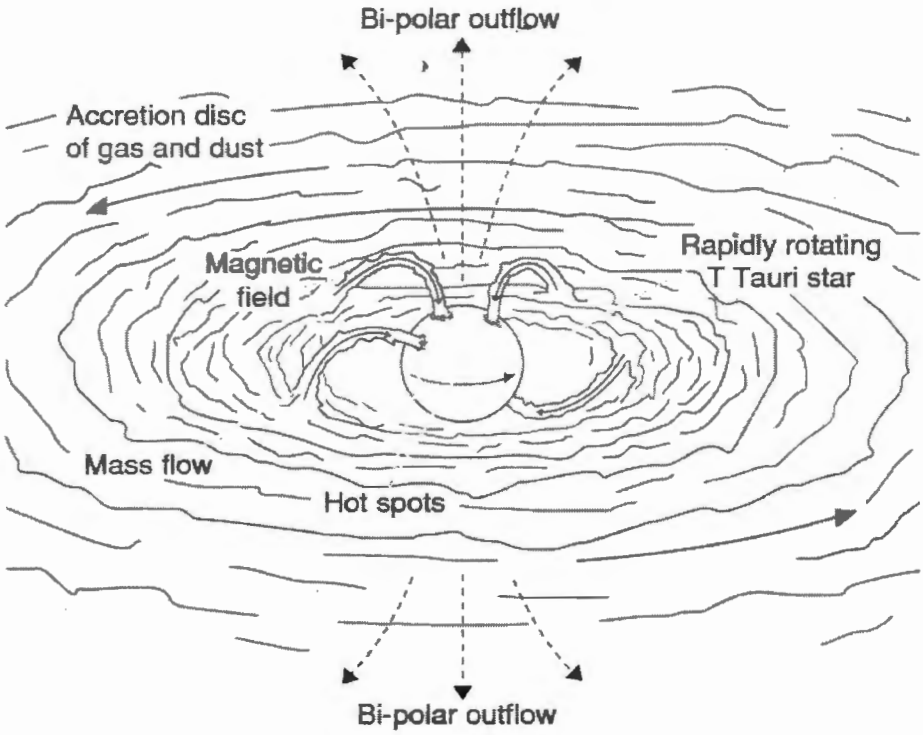

Figure 1.2: Schematic model of a T-Tauri star. The star in the centre is surrounded by gas and dust that is accreting towards the star. The gas and dust can be channelled to the star by magnetic field lines and form hotspots (Percy 2007).

1.2.3 Herbig Ae/Be Stars

The other groups of PMS stars which are relevant to this thesis are the higher-mass analogues of T-Tauri stars called Herbig HAeBe stars. These are objects which are believed to be intermediate-mass (2 – 10 $M_{\odot}$) stars still in their phase of pre-main sequence (PMS) contraction (van den Ancker et al. 1998).

The HAeBe stars were first discussed as a group in a paper by Herbig (1960) that started this field. Recent millimeter interferometric maps show that rotating disks are present in HAeBe stars. These stars also show a very rich variety of physical processes, involving the simultaneous infall and outflow of matter in a complex circumstellar environment. The Infrared Space Observatory (ISO) data also give support to the exciting hypothesis that the environment of HAeBe stars can be the site of planet formation. Aircraft and satellite observations of Herbig Ae/Be stars in the mid-infrared reveal sharp emission features.

To decide whether a star belongs to the Herbig Ae/Be (HAeBe) group or not has been a topic of great discussion, with various criteria being used in the literature for the classification. In general, to be undoubtedly considered as HAeBe star, a candidate should present the following characteristics (Viera et al. 2003): spectral type A or earlier, with emission lines; located in an obscured region; fairly bright nebulosity in its immediate vicinity; present an anomalous extinction law; show infrared excess; be photometrically variable and display line profiles of Mg II (λ 2800) in emission. The first three criteria were proposed by Herbig (1960) to define pre–main sequence stars of intermediate mass. The last four are an extension proposed by The et al. (1994) to encompass the large set of new candidates. However, very few stars satisfy all of them.

The presence of infrared excess due to thermal reradiation, usually explained by the presence of an accretion disk or an almost symmetric circumstellar halo is a feature common to all HAeBe objects. The emission lines are associated with their youth, though (like the classical Be stars) rapid rotation may play a role. Herbig Ae and Be stars were not originally thought to be variable, but careful monitoring has shown that they exhibit some of the same forms of variability as classical T-Tauri stars. No Herbig Ae/Be star is known to be rotationally variable. This is not surprising, since A and B type stars do not have solar-type magnetic fields because they do not have an outer convective zone.

Two Herbig Ae/Be stars - V628 Cassiopeiae and T Orionis – are assumed that to be eclipsing variables (Percy 2007). Herbig Ae/Be stars share certain key features with the T-Tauri class, and others with even more massive and luminous O and B stars. The study of Ae/Be stars is less advanced than that of their low-mass counterparts. The main impediment here is the relative scarcity of the objects. The number of stars produced in the range of interest, from 2 to 10 $M_{\odot}$ is only 3 percent of those from 0.5 to 2 $M_{\odot}$. Exacerbating the problem is the shorter contraction time at larger masses. On the other hand, the higher luminosity does facilitate discovery; the number of known sources now exceeds 100 (Stahler & Palla 2004). Within the HR diagram, Herbig Ae/Be stars fall close to, but below, the intersection of the birth line and the zero-age main sequence. Yet another difficulty is presented by the fact that Herbig Ae/Be stars tend to rotate quite rapidly. Of course, the faster rotation in Herbig Ae/Be stars is itself of interest. The typical equatorial speed for Ae/Be stars is about 150 km /s (Stahler & Palla 2004).

1.2.3.1 Photometric and Spectroscopic Observations of Herbig Ae/Be Stars

Photometric asteroseismology has as its goal the precise measurement of stellar intensity for the purpose of determining pulsation frequencies. It also is useful in mode identification (Aerts et al. 2010). Spectroscopy is an important observational tool for all fields of astrophysics. For stellar astronomy, it allows for spectral classification, for the derivation of the atmospheric parameters such as the effective temperature and gravity, for estimates of the abundances of the chemical elements in the stellar atmosphere, for the derivation of the amount of mass loss and circumstellar material through emission line and P Cygni line modelling, etc. It also allows the detection of binarity, or, more generally, multiplicity of the studied object whenever a time series is available.

Spezzi et al. (2012) presented a photometric multi-wavelength study of three star-forming regions, spanning the age range 1 – 14 Myr located in the Large Magellanic Cloud (LMC). Spezzi et al. (2012) also reliably identified about 1000 pre-main-sequence (PMS) star candidates actively undergoing mass accretion and estimated their stellar properties and mass accretion rate and found that the typical mass of PMS stars in the LMC is higher than for galactic PMS stars of the same mass, independently of their age. Higher mass accretion measured in the LMC might be a consequence of its lower metallicity with respect to our Milky Way. The results showed clear evidence that circumstellar discs have been eroded by photo-evaporation caused by nearby massive stars. The photometric and spectroscopic studies of the pre-main sequence stars are also very important for understanding of the early stages of stellar evolution. Depending on the initial mass, the young stars pass, through different periods of stellar activity. The most prominent manifestations of this activity are changes in the star brightness with different periods and amplitudes (Semokov 2011).

Manoj et al. (2006) studied the temporal evolution of emission-line activity in intermediate-mass PMS stars by compiling multi-epoch spectroscopic and photometric observations for a large sample of HAeBe stars. The result showed that, on average, the Hα emission line strength decreases with increasing stellar age in HAeBe stars, suggesting that the accretion activity gradually declines during the PMS phase. The results also implied that in most Hae/Be stars the Hα emission has weakened considerably by the time the star is ~ 3 Myr, indicating that the accretion activity in the mass dropped significantly. Furthermore, a relatively good correlation between the strength of the emission line and near-infrared excess due to inner disks in Herbig Ae/Be stars, indicated that the disks around Herbig Ae/Be stars cannot be entirely passive. Some of the the observed spectra are shown in Figure 1.3.

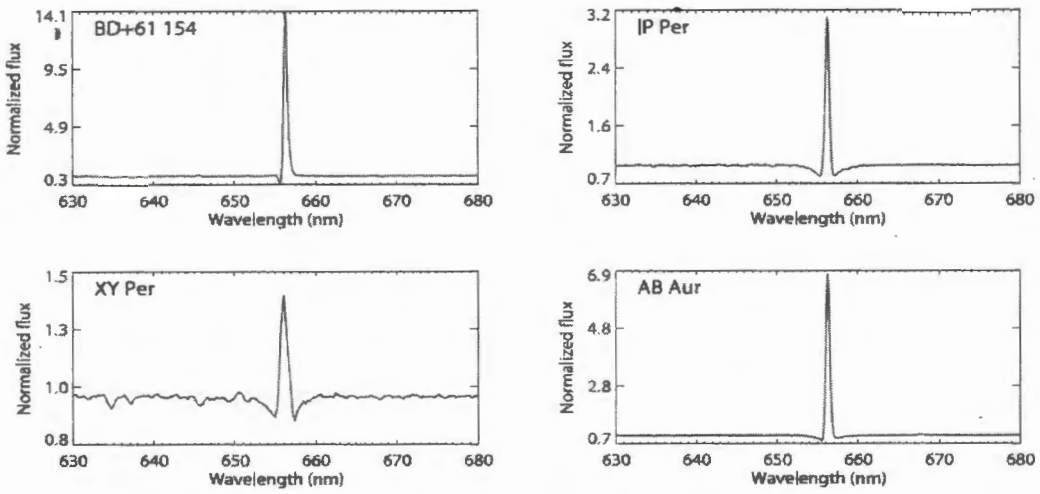

Figure 1.3 Spectra observed in four of the HAe/Be stars (Manoj et al. 2006).

A-type stars also show intense surface activity (including winds, accretion, pulsations) whose origin is still not completely understood, and infrared excesses related to the presence of circumstellar disks and envelopes (Marconi & Palla 2004). Disks display significant evolution in the dust properties, likely signalling the occurrence of protoplanetary growth.

The stars that are indisputably pre-main sequence, those with the signature of circumstellar shells and dust disks, can vary in brightness by a magnitude or more. How can one hope to study δ Sct pulsation with photometric variations two orders of magnitude less than this? The answer is that the variability of the light caused by variable transparency of the circumstellar material, and the variability caused by pulsation are on sufficiently different time-scales that the associated frequencies are separated in the Fourier Transform (Kurtz 2002). It is also shown that for instance, not all HAeBe stars inside the instability strip pulsate with detectable amplitudes, as shown by Kurtz & Muller (2001).

A spectroscopic and photometric survey of 250 PMS binaries were conducted by Guenther et al. (2001). Taking 739 spectra in this survey, 14 % of the stars were found to be spectroscopic binaries. The results of multicolour photometric and low resolution spectroscopic observations of some Herbig Ae/Be candidate stars reported by Miroshnichenko et al. (1999) show near infrared excess and Algol-type variability, which is not common in these stars. After the release of the Infrared Astronomical Satellite (IRAS) mission results, a number of new HAeBe candidates were found in the IRAS Point Source Catalogue (PSC). Summarizing these and other new results, The et al. (1994) published a catalogue of 287 early-type stars which exhibit characteristics which suggest that they are possible PMS stars. The authors called this sample "The Herbig Ae/Be stellar group". From a study of the observational characteristics of HAeBe's and related objects they concluded that there was no unique set of observational characteristics which could help to unambiguously distinguish a PMS star of intermediate mass.

van den Ancker et al. (1998) studied the photometric behaviour of a sample of 44 candidate HAeBe stars using a uniform data-set, provided by the Hipparcos astrometric satellite. The results show that most (> 65%), and possibly all HAe/Bes show photometric variations at the level of at least a few hundredths of a magnitude. They also suggest the Herbig stars with the smallest infrared excesses in their sample do not show large photometric variations and patchy dust clouds are only present during the PMS evolution of a star, and either vanish or become more homogeneous when a star has reached the ZAMS. Placing emphasis on the composition and geometry, Waters & Waelkens (1998) reviewed the wide range of observed properties of Herbig Ae/Be stars and tried to combine this rich data set into a consistent picture of their circumstellar environment and evolutionary status. They commented that HAe/Be stars show a very rich variety of physical processes, involving the simultaneous infall and outflow of matter in a complex circumstellar environment. The issue of geometry is still controversial.

A catalogue of optical and infrared photometry covering the epoch 1980-84 for a sample of 53 PMS stars and other emission line stars was presented by Kilkenny et al. (1985). Vieira et al. (2003) presented a catalogue of 108 Herbig Ae/Be candidate stars. The study suggested that most of the time a Herbig Ae/Be star will present a double peak Hα line profile (Figure 1.4) and 84 candidates can be associated with some of the more conspicuous star forming regions. The study found explains no correlation among Hα line profiles and spectral type or *v sin i* except for stars with P Cygni profiles, where there is a correlation with *v sin i* .

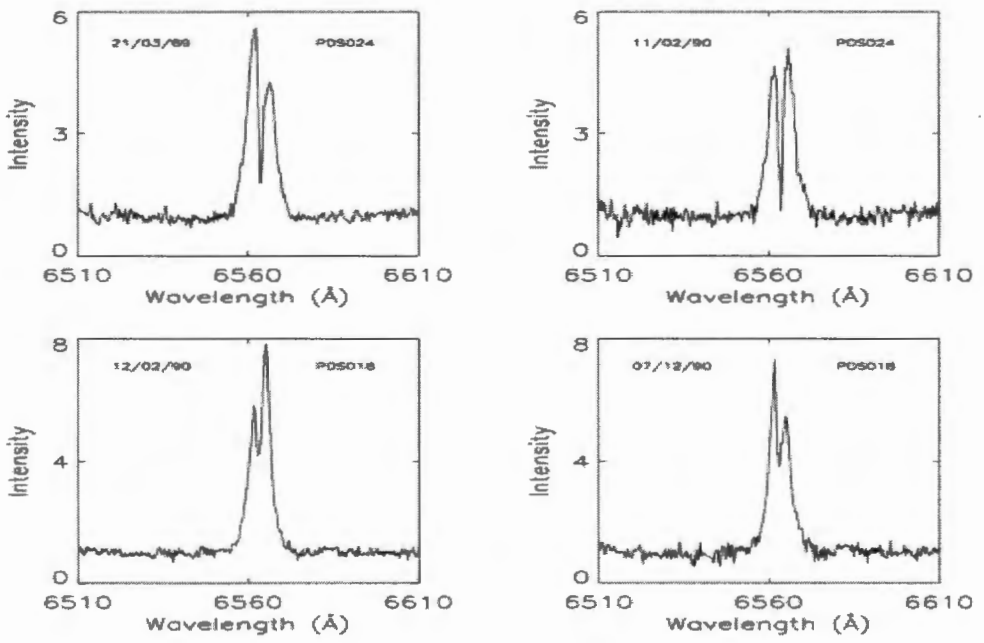

Figure 1.4: Hα line profiles observed in Herbig Ae/Be stars in two different epochs. The flip over of the red and blue peaks are said to be caused by the presence of a density structure (cometary bodies) in the circumstellar disk (Vieira et al. 2003).

Variations in Hα profile on HAe/Be stars can be explained by planetesimal bodies orbiting the star and interaction of the wind with the circumstellar environment, respectively. Another interesting variation observed in double-peaked profiles of Figure 1.4 is the flip over of the blue and red peaks, probably caused by the presence of a density structure (cometary bodies) in the circumstellar disk. During the evolution of HAe/Be stars the circumstellar disk or envelope is cleared by planetesimal or cometesimal bodies and stellar winds. In this evolutionary stage the disk (envelope) contribution to the Hα emission is very weak and the Hα is almost totally formed at the stellar chromosphere.

Sometimes the remote and cool shell is responsible for a central absorption. The following objects have Hα line profiles that might be explained by this evolutionary scenario (Figure 1.5): PDS031S, PDS179, PDS201A, PDS281). Some of the stars presented a line profile (weak emission inside the absorption well) that can be explained by an evolutionary process where the shell is almost absent (evolved HAe/Be stars).

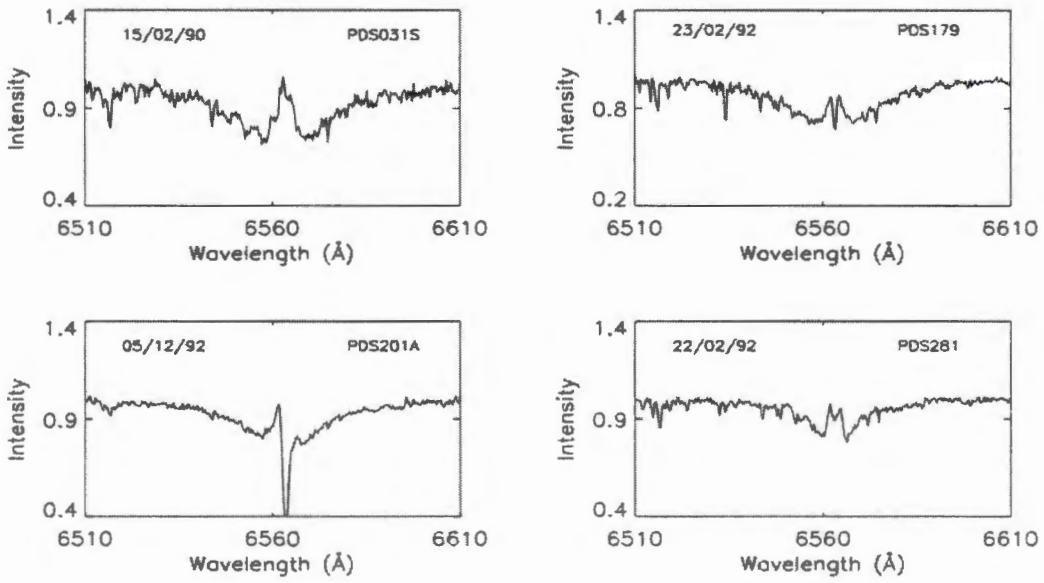

Figure 1.5: Hα line profiles of the presumably evolved HAe/Be objects. Such line profiles of weak emission inside the absorption well can be explained by an evolutionary scenario where the shell is almost absent. On each panel the star name is written on the top right and the date of observation on the left (Vieira et al. 2003).

Grinin et al. (1994) observed Algol-like minima accompanied by variations in the Hα profile in Herbig Ae/Be stars of UX Ori and HD 100546, which can be explained by inhomogeneities or clumps orbiting the star in an edge on disk. Fundamental astrophysical parameters (distance, temperature, luminosity, mass, age) of a sample of Herbig Ae/Be candidates in star forming regions were computed by van den Ancker et al. (1997) combining Hipparcos parallaxes with data from literature. It was also stressed that the time scale for the evolution of the central star and the circumstellar material are probably not well coupled.

Structure and evolution of PMS stars with masses from 1 to 6 $M_{\odot}$ was calculated numerically (Palla & Stahler 1993) and the calculations implied that Herbig Ae and Be stars are substantially younger than previously believed. The upper boundary to their distribution in the HR diagram is well matched by their theoretical birth line. There is also a good prospect for measuring evolutionary period changes in pre-main-sequence δ Scuti stars. Breger & Pamyatnykh (1998) discussed observed period changes in δ Scuti stars and calculated expected evolutionary changes. They concluded that the rate of evolutionary period change for pre-main-sequence stars is 10 to 100 times greater than that for post-main-sequence. They discuss the well-known problem of non-evolutionary period changes in δ Scuti stars and are optimistic that the expected changes for pre-main-sequence stars will be large enough to be detectable, even in the presence of non-evolutionary changes of the order seen in well-studied post-main-sequence stars. This prospect of putting observational constraints on the theoretical evolutionary time-scale makes the study of δ Scuti pulsation in pre-main sequence stars important.

For determining distance and mass of pulsating stars a purely photometric method is described in which radial velocity observations are not needed (Barcza 2003). From multicolour photometry the variation of angular diameter is determined in a conventional way by using the surface brightness of the theoretical atmospheric models ATLAS of Kurucz (1997). Photometric observations of the Herbig Ae star HD104237 (Kurtz & Muller 1999) confirm that it is a δ Scuti star with two periods, the highest amplitude one having a value of 43 min. These imply high-overtone modes which have not yet been investigated theoretically.

The δ Scuti pulsational character of HD104237 is clear from the light curve of Figure 1.6 and amplitude spectrum of this star where another peak is apparent with an alias ambiguity is shown in Figure 1.7. The top panel of the figure has the highest peak of 33.28 /d. If the spectrum is pre-whitened by the highest peak, the central panel is obtained where there is still some power left. The second highest peak is at 36.61/d, although it cannot be selected confidently in preference to its +1/d alias. There is some indication of further frequencies, suggesting that a more intensive observing campaign is highly desirable.

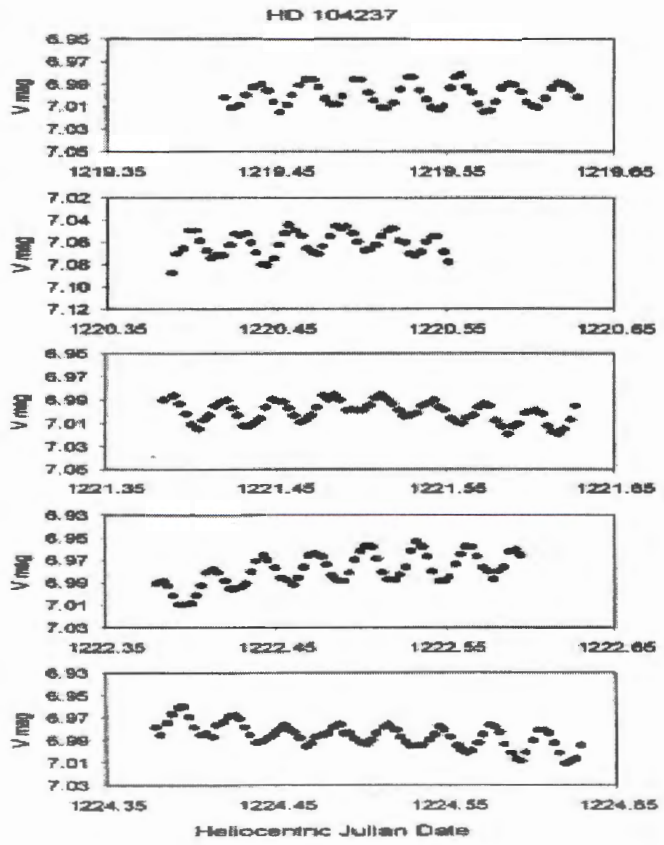

Figure 1.6 Light curves of HD104237 corrected only for mean extinction. Some of the low-frequency variation is intrinsic and is typical of Herbig Ae stars, caused by variable wind and dust (Kurtz & Muller 1999).

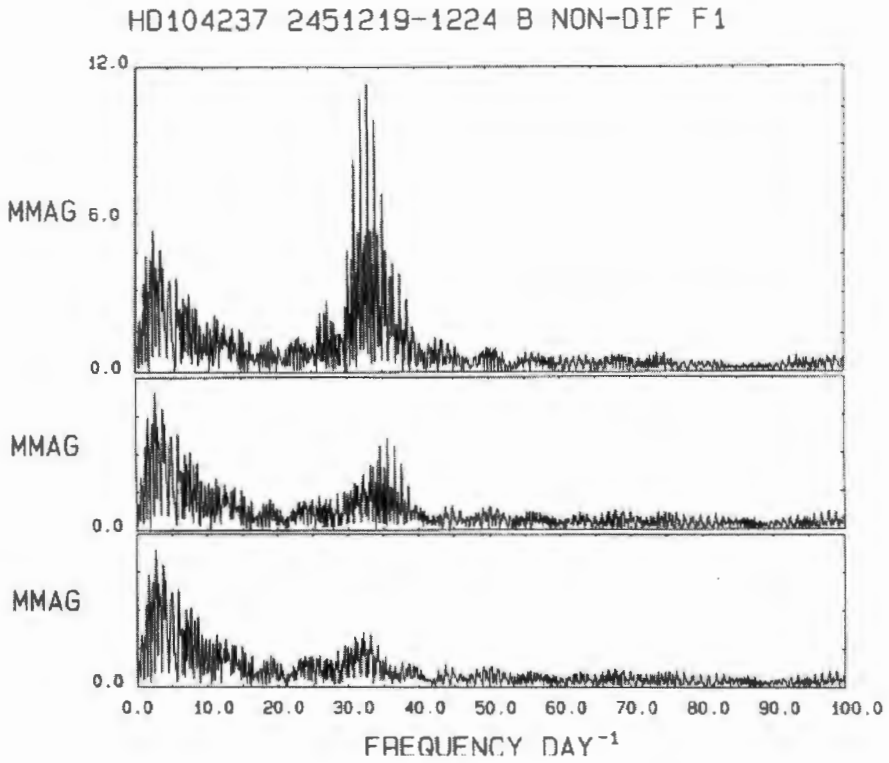

Figure 1.7: Periodogram of HD104237. The top panel is the amplitude spectrum of the light curves shown in Figure 1.6. The central panel is the amplitude spectrum of the residuals after pre-whitening by the highest peak. The bottom panel is the amplitude spectrum of the residuals after pre-whitening by the two highest peaks (Kurtz & Muller 1999).

Donati et al. (1997) were studying potential magnetic fields (detected unambiguously) in pre-main-sequence T-Tauri and Herbig Ae/Be stars using high-precision spectropolarimetric observations. They discovered radial velocity variations with a peak-to-peak amplitude of 1.3 km /s and a period of about 37 min in the star HD104237. The β Pictoris phenomenon has also been observed. This results in Herbig Ae star UX Orionis in a double peaked Hα profile observed (Grinin et al. 1994) at maximum light, which changed to single-peaked at deep minimum. This is a consequence of obscuration of part of the circumstellar gas by an optically thick dust cloud was also observed. Grinin et al. (1994) believe that, such as in the case of the star β Pictoris, violent comet-like activity takes place in the young proto-planetary disk of UX Ori, which causes the observed variability.

For a complete understanding of the physical processes causing the photometric variability of pre-main sequence systems, simultaneous optical and near-IR observations are required, to disentangle the emission from the stars and that from their associated circumstellar disks. Some stars appear to show a correlation between the optical and near-IR variability trends, which suggests a common physical origin such as spots and/or variable extinction (Eiroa et al. 2002). The optical and near-IR variability is uncorrelated in the rest of the objects, which suggests it originates in distinctly different regions. In general, the optical variability qualitatively follows the predictions of stars spots or variable extinction.

Planet formation has been known for many years to be tied to the spatial distribution of gas and dust in disks around young stars. To constrain planet formation models, imaging observations of protoplanetary disks are required. Doucet et al. (2006) undertook a mid-infrared imaging survey of Herbig Ae stars. The results show how important imaging data are in tightening constraints on the disk model parameters. Doering & Meixner (2009) also reported near-infrared photometric measurements of Herbig Ae/Be candidate stars obtained with direct imaging and aperture photometry. As a result, one extended source that has been identified as a protoplanetary nebula was detected.

1.3 Stellar Pulsations In Stars

1.3.1 Physics of a pulsating star

A *Pulsating star is* a type of star in which brightness variations are caused by changes in the area and temperature of the star's surface layers. Astronomers use the word pulsation for vibration or oscillation of a star. The Milky Way Galaxy is estimated to contain several million pulsating stars. Considering that our Galaxy consists of several hundred billion stars, this implies that the stellar pulsation must be a transient phenomenon (Carroll & Ostlie 2007).

Every physical object has natural patterns or modes of vibration, each with a corresponding period - the time required for one vibration. We commonly observe this in musical instruments like a bugle and violin strings. Therefore, it is tempting to call pulsation 'the music of the spheres'. Recent evidence suggests that all stars pulsate (if we measure them carefully enough), although the presence of concentrated populations of pulsating stars on the HR diagram implies that pulsations are more important at particular stages of stellar evolution (Percy 2007). Being a fascinating phenomena in its own right, stellar pulsation is used to constrain theories of stellar evolution and to study the mechanisms of stellar interiors. Stars are, to a first approximation, spherical. The simplest form of pulsation is radial pulsation - a simple, spherically symmetric 'in-and-out' expansion and contraction. So again it is tempting to say 'stars that breathe'. Another form of pulsation is non-radial pulsation where the star changes shape, not volume. The two main non-radial modes are (i) p (pressure) modes, in which the motion is primarily radial and the restoring force is pressure and (ii) g (gravity) modes, in which the restoring force is buoyancy or gravity.

The radial oscillation of a pulsating star is the result of sound waves resonating in the star's interior. A rough estimate of the pulsation period, Π , may be easily obtained by considering how long it would take a sound wave to cross the diameter of a model star of radius R and constant density ρ , i.e.,

$$\Pi=\frac{2R}{v_s} \tag{1.1}$$

where v_s is the adiabatic sound speed given by:

$$v_s=\sqrt{\frac{\gamma P}{\rho}} \tag{1.2}$$

where γ is the adiabatic index and

P is pressure

Using the (unrealistic) assumption of constant density for hydrostatic equilibrium, the pressure may be found as follows:

$$\frac{dP}{dR}=\frac{-GM_r\rho}{r^2}=\frac{-G(4/3\,\Pi r^3\rho)\rho}{r^2}=\frac{-4}{3}\Pi G\rho^2 r \tag{1.3}$$

This is readily integrated using the boundary condition that P = 0 at the surface to obtain the pressure as a function of r,

$$P(r)=\frac{2}{3}\Pi G\rho^2(R^2-r^2) \tag{1.4}$$

Where G = gravitational constant

R= radius of the star

r = any radius of the star less than R

M_r = total mass of the star within r

Thus the pulsation period is roughly,

$$\Pi = 2\left(\int \left(\frac{dr}{v_s}\right)\right) = 2\int \left[\frac{dr}{\sqrt{(2/3\,\gamma\,\Pi G\rho(R^2 - r^2))}}\right] \text{ or}$$

$$\Pi = \sqrt{\frac{3\Pi}{2\gamma G\rho}} \tag{1.5}$$

where the integration goes from 0 to R.

Quantitatively, this shows that the pulsation period of a star is inversely proportional to the square root of its mean density. Some stars have been observed to pulsate for hundreds of years. In many other cases we have good light curves going back over a century, thus we know that stellar pulsation is a relatively stable phenomenon in many stars. That means that energy must be fed into the pulsation via what are known as driving mechanisms (Aerts et al. 2010).

This mechanism should convert radiant energy into energy of motion in a timely way, overcoming friction and building up the motion. Such a mechanism can exist in a star: it is the thermodynamic effect of partial *ionization zones* in a star. A driving mechanism for the changes in luminosity of many types of pulsating variables located in instability strip is called

κ *mechanism.*

For Cepheid variables, RR Lyrae stars, δ Sct stars, β Cep stars – for most of the pulsating variables seen in Figure 1.8 – the driving mechanism is connected with the opacity. The opacity fluctuations are responsible for the 'bump' often seen in the temperature eigenfunctions in the region of the hydrogen ionization zone of A stars (Medupe, et al. 2009).

In those zones of the star where the gases are partially ionized, part of the work done on the gases as they are compressed produces further ionization rather than raising the temperature of the gas. With a smaller temperature raise, the increase in density with compression produces a corresponding increase in the Kramers opacity. Similarly, during expansion, the temperature does not decrease as much as expected since the ions now recombine with electrons and release energy. Again, the density term in the Kramers law dominates, and the opacity decreases with decreasing density during the expansion. This layer of the star can thus absorb heat during compression, be pushed outward to release the heat during expansion, and fall back down again to begin another cycle. Partial ionization zones are the pistons that drive the oscillations of stars; they modulate the flow of energy through the layers of the star and are the direct cause of stellar pulsation (Carroll & Ostlie 2007).

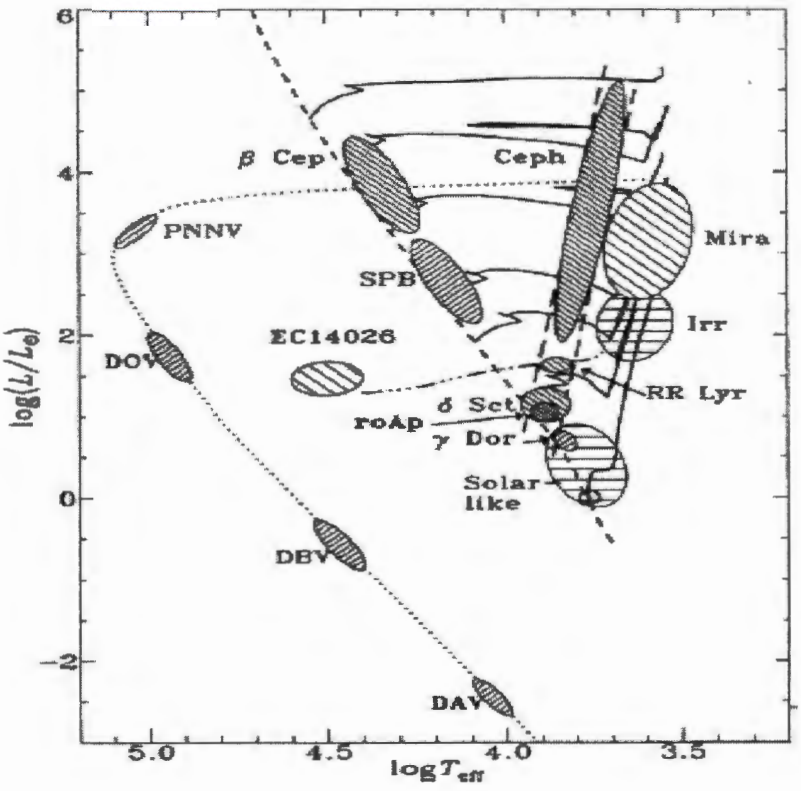

Figure 1.8: A pulsation HR diagram showing many classes of pulsating stars for which asteroseismology is possible (Aerts et al. 2010)

Pulsating stars are not generally found uniformly over the HR diagram. Instead, most pulsating stars occupy a narrow, vertical band on the right hand side (larger shaded region) of the HR diagram both above and below the main sequence. This region in which stars pulsate is called the *instability strip* (Figure 1.8).

The main instability regions are the Cepheid strip, including its intersection with the main sequence (dashed line), the region of the coolest stars (Miras and their relatives), and the region of the Beta Cephei and SPB stars. There are also instability regions along the white dwarf cooling track (dotted line) at the bottom of the diagram, including the nuclei of planetary nebulae (PNNV) and pulsating white dwarfs (DOV, DBV and DAV). If the pulsating variables have spectral type A–F with pulsation periods between 18 min – 8 hr and light amplitudes ranging from thousandths of magnitude to some tenths, we call them *δ Scuti* stars. These stars have masses in the range of 1.5 - 2.5 $M_{\odot}$.

1.3.2 Pulsations in Herbig Ae stars

As newly born protostars contract towards the main sequence, either radiatively as the Herbig Ae/Be stars or convectively as the T-Tauri stars, the higher mass stars enter or cross the classical instability strip. Such pre-main-sequence stars tend to be highly variable, both in photometry and spectroscopy, on time scales of minutes to hours. Part of this variability is certainly due to activity and interaction with the circumstellar environment. On the other hand, part of the shorter period variability may be due to oscillations. Since the interior structure of pre-main-sequence stars is different from that of evolved stars in the instability strip, their oscillation spectra may allow us to distinguish between the two evolutionary stages for stars with the same effective temperature and luminosity (Aerts et al. 2010).

After the discovery of the first two pulsating PMS stars in the young cluster NGC 2264 (Breger 1972), it took more than 20 years until another PMS pulsator was found. Kurtz & Marang (1995) observed the Herbig Ae field star HR 5999 and detected δ Scuti-like pulsations (Figure 1.9, Figure 1.10, for 5, and 1 night observations respectively is given). These measurements enabled for the first time the examination of the internal structure of a PMS star using asteroseismology and the placing of constraints on the pulsation models (Marconi & Palla 1998). Since then, several detections of pulsations in Herbig Ae field stars (e.g., Donati et al. 1997; Marconi et al. 2000), as well as in members of young clusters have been published. The PMS pulsators have the same spectral types and luminosities as the classical δ Scuti stars. Hence, it is expected that their pulsation is driven by similar mechanisms, i.e., the κ -mechanisms.

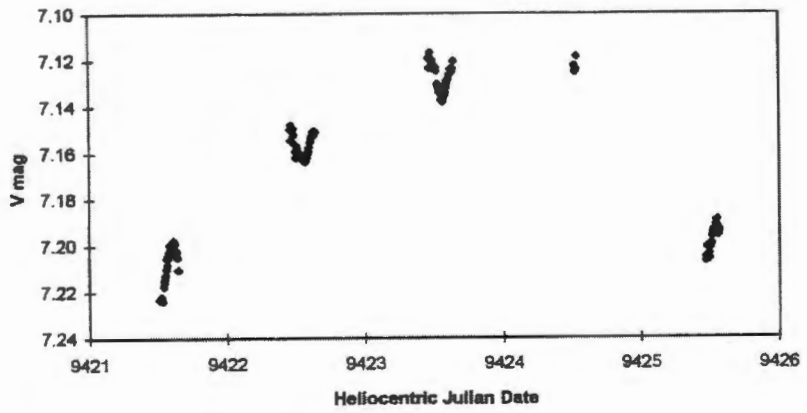

Figure 1.9: The light curve of HR 5999 for five nights. The long-term variation over several days is probably caused by variable dust obscuration in the disc around the star. The δ Scuti period variations are visible on a much shorter time scale (Kurtz & Marang 1995).

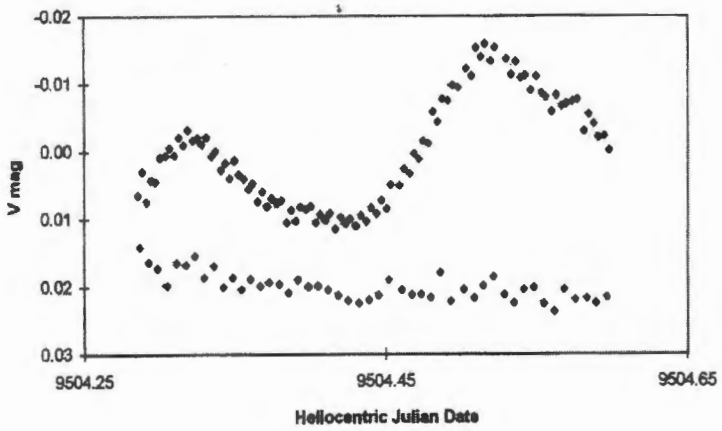

Figure 1.10: The light curve of HR 5999 for one night (with comparison star HR6000). The δ Scuti variability of HR 5999 is easy to see. The upward trend in the data is probably a result of the variable obscuration of dust in the disc Kurtz & Marang (1995).

The evolutionary stage of a star with given effective temperature (T_{eff}), luminosity, and mass may be ambiguous, as the evolutionary tracks for pre - and post - main-sequence stars intersect several times (Breger & Pamyatnykh 1998). Thus, the PMS nature of a star has to be assessed by other means than the position in the HR diagram. Marconi & Palla (1998) obtained the first theoretical instability strip (Figure 1.11) for PMS intermediate-mass pulsators by computing an extensive and detailed set of non-linear convective models for the first three radial modes, along the PMS evolutionary tracks by Palla & Stahler (1993). Marconi & Palla (1998) also pointed out that the interior structure of PMS stars entering the instability strip differs significantly from that of more evolved main-sequence stars (with the same mass and temperature).

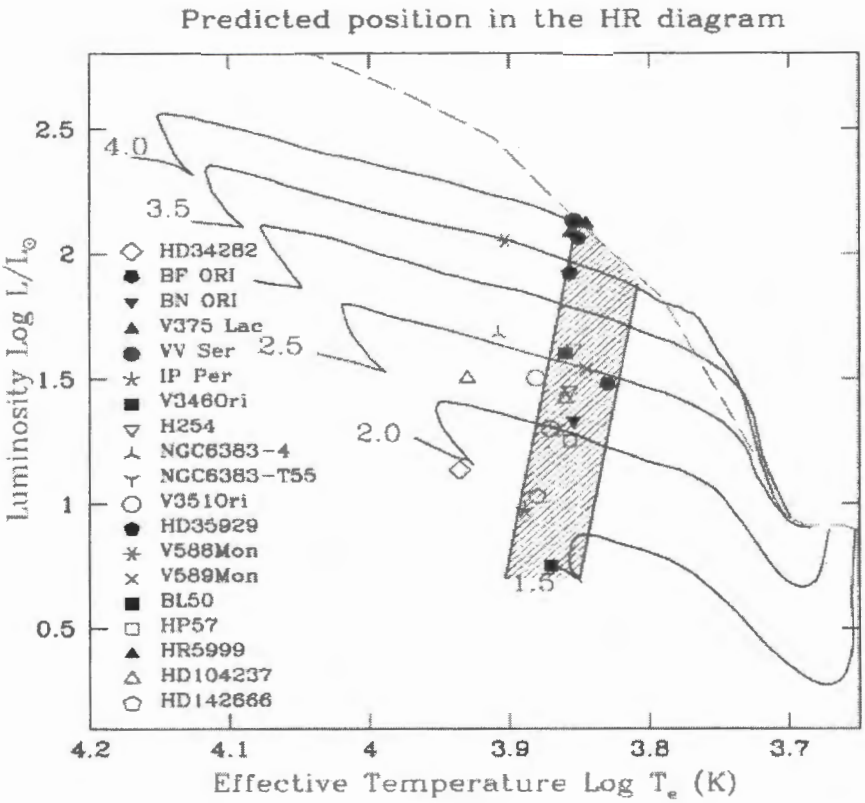

Figure 1.11: The position of PMS Scuti stars in the HR diagram as predicted on the basis of the comparison between the observed periodicities and linear non-adiabatic radial pulsation models. The hashed region is the theoretical instability strip for the first three radial modes (Marconi & Palla 1998).

It is also worth noticing that it was suggested (Breger & Pamyatnykh 1998) that PMS stars could in principle be used to search for mode frequency changes due to evolution of the stellar inner structure.

As of 2007 36 pulsating PMS stars have been found to have δ Scuti pulsations, of which 30 are confirmed PMS pulsators and 6 remain pulsating PMS candidates because their periods could not be determined accurately enough yet (Zwintz 2008). This allows to investigate the location of the empirical PMS instability region and to compare its boundaries to those of the classical (post- and main-sequence) instability strip. As for asteroseismology from space, two satellites have the possibility to observe PMS stars: Microvariability and Oscillations of Stars (MOST) and Convection Rotation and Planetary Transits (COROT). MOST is equipped with a 15 cm telescope and a CCD camera. Ruoppo et al. (2007) aimed at developing a theoretical approach for the interpretation of observed frequencies, both from the already available ground-based observations and from this more accurate and extensive COROT result.

Ripepi et al. (2006) presented the status of the observational and theoretical studies of δ Scuti pulsations in PMS intermediate mass stars and discussed the prospects for future investigations of these objects from the ground and from space. The result, show that most of the well observed pulsating Herbig AeBe candidate shows frequencies which cannot be reproduced by radial mode analysis only, the presence of non-radial modes in this class of stars is also indicated.

The Kepler mission has been also extremely important in the study of stellar pulsation. This mission has observed, and is still observing, the light variations of over 150000 stars in a large field of 105 square degrees in the direction of Cygnus and Lyra. For example, using photometry from the Kepler Input Catalogue, Balona et al. (2013) determined the distance and age of NGC 6819, many different types of variables in the field, including eight δ Scuti stars and at least three γ Dor variables and several eclipsing binaries of various types. Balona et al. (2013) also discovered 64 oscillating red giants, of which 39 are previously unknown.

To select our star, we have used different sources and criteria. Table 1.1 consists of the list of stars which we considered to select our target star. From this list a variable star of δ Scuti type V351 Ori is selected as our target based on the selection criteria mentioned in chapter two. According to the sources, if the type of star is simply 'star' in the remark part as shown in Table 1.1, it means that it is not variable star or it is simply observed and no detail information about the star is given or is candidate star.

Table 1.1 A List of pulsating and candidate Herbig Ae/Be stars used to select our target star. '--' represents that information in not provided from the resource used.

Sources: Kilkenny et al. (1985), van den Ancker et al. (1998), Kurtz (2002), Marconi & Palla (2004), Manoj et al. (2006), Zwintz (2008).

	Name	RA	Dec	Magnitude				Spectral type	Remark
				V	J	H	K		
1	HR 5999/ HD144688/V856 Sco	16 08 34.3	-39 06 18	6.98	5.91	5.22	4.39	A7III/IVe	Variable star of δ Sct type
2	RS Cha	08 43 12.21	-79 04 12.30	6.07	5.99	5.88	5.85	A7 Vc	Eclipsing binary of Algol type (detached)
3	HD 142666/V1026 Sco	15 56 40.02	-22 01 40.01	8.8	7.35	6.74	6.08	A8 Ve	T-Tau Type star
4	*HD 35929*	*05 27 42.79*	*-08 19 38.45*	*8.1*	*7.21*	*6.97*	*6.67*	*F2III D*	*Emission line star*
5	HD 261331/V588 Mon	06 39 05.90	+09 41 03.40	9.75	9.28	9.12	9.08	A7III/IVD	Variable star of δ Sct type
6	BN Ori (HD 245465)	05 36 29.34	+06 50 02.17	9.6	8.6	8.3	8.23	A7D	Variable star of Orion type
7	BF Ori	05 37 13.26	-06 35 00.58	9.65	9.11	8.56	7.9	A5 II-IIIev C	Variable star of Orion type
8	V346 Ori	05 24 42.80	+01 43 48.26	10.2	9.7	9.18	8.56	A5 III:C	Variable star with rapid variations
9	HD 261446/V589 Mon	06 39 28.45	09 42 04.076	10.3	9.55	9.36	9.33	F2IIID	Variable star of δ Sct type
10	HD 104237/DX Cha	12 00 05.1	-78 11 34.6	6.6	5.81	5.25	4.59	A4V	Variable star of δ Sct type
11	HD 38238/V351 Ori	05 44 38.79	+00 08 40.40	8.91	7.9	7.5	6.85	A7IIIe	Variable star of δ Sct type
12	BL50	--	--	--	--	--	--	--	Candidate,pulsation not yet found
13	HP57	--	--	--	--	--	--	--	Candidate,pulsation not yet found

Continued...

Table 1.1 continued.....

	Name	RA	Dec	Magnitude				Spectral type	Remark
14	HD 34282	05 16 00.477	-09 48 35.416	9.84	9.26	8.48	7.68	AO D	Star ~ Candidate
15	V375 Lac	22 34 40.9	+40 40 05.0	12.94	11.29	10.31	8.92	A7e	Variable star of Orion type
16	VV Ser	18 28 49.0	+00 08 39.0	11.82	8.67	7.44	6.32	A2e	Variable star of Orion type
17	IP Per	03 40 46.966	+32 31 53.735	10.36	9.14	8.41	7.59	A6 D	Variable star with rapid variations
18	H254	--	--	--	--	--	--	--	Candidate,pulsation not yet found
19	WW Vul	19 25 58.7	+21 12 31.0	10.68	9.09	8.18	7.28	A3e	Variable star with rapid variations
20	PX Vul	19 26 40.3	+23 53 49.0	11.83	9.32	8.55	7.91	FoVe	Variable star of Orion type
21	PDS 2	01 17 43.50	-52 33 30.763	10.75	10.01	9.68	9.31	F2D	T-Tau star type
22	UX Ori	05 04 29.988	-03 47 14.29	10.53	8.71	8.04	7.21	A3D	Variable star with rapid variations
23	CQ Tau/HD 36910	05 35 58.466	+24 44 54.095	10	7.93	7.06	6.17	F3D	Variable star of Orion type
24	V1247 Ori	05 38 05.249	-01 15 21.67	9.82	8.88	8.2	7.41	A5III C	Variable star of δ Sct type
25	HD142527	15 56 41.889	-42 19 23.274	8.34	6.5	5.72	4.98	F6IIIe C	Star ~ Candidate

Continued ...

Table 1.1 continued ...

	Name	RA	Dec	Magnitude				Spectral Type	Remark
				V	J	H	K		
26	B Pic	05 47 17.1	-51 03 59.5	3.86	3.67	3.54	3.53	A5V	Star ~ Candidate
27	IC 348254	03 44 31.2	+32 06 22.1	10.6	--	--	--	F0/A8IIII-IV	--
28	NGC 22642	06 39 05.9	+09 41 03.4	9.73	9.23	9.12	9.08	A7III/IV	Variable star of δ Sct type
29	NGC226420	06 39 28.5	+09 42 04.1	10.32	9.55	9.36	9.33	F2III	Variable star of δ Sct type
30	NGC638327	17 34 37.0	-32 36 17.9	12.6	11.01	10.43	9.75	A5IIIp	Eclipisng binary
31	NGC638355	17 34 48	-32 37 24	12.83	11.23	10.99	10.90	--	Star in a cluster
32	NGC638354	17 34 55.1	-32 35 30.9	12.34	11.10	10.82	10.76	F0 Ve	Star in a cluster
33	NGC653013	18 04 00.2	-24 15 02.6	13.35	--	--	--	--	Star in a cluster
34	NGC653028	18 04 09.9	-24 12 21.1	13.23	12.21	12.04	11.95	--	Star in a cluster
35	NGC653038	18 04 13.9	-24 13 28.0	12.17	10.92	10.63	10.48	A0/A5	Star in a cluster
36	NGC653053	18 04 20.7	-24 2455.7	13.07	11.39	11.01	10.89	A1III	Star in a cluster
37	NGC653057	18 04 21.8	-24 15 46.9	13.67	11.97	11.7	11.56	--	Star in a cluster
38	NGC653078	18 04 30.8	-24 23 42.1	13.97	--	--	--	--	Star in a cluster
39	NGC6530159	18 04 42.3	-24 18 03.5	13.59	12.69	12.54	12.54	--	Star in a cluster
40	NGC6823230	19 43 06.8	+23 16 37.8	14.60	--	--	--	--	--
41	NGC6823279	19 43 09.1	+23 17 49.6	14.50	--	--	--	--	--
42	*IC 4996201*	20 16 22.0	+37 39 31.0	15.21	--	--	--	A5	--
43	IC 4996171	20 16 30.0	+37 39 32.8	15.03	--	--	--	A4	--
44	IC 49961085	20 16 43.9	+37 42 26.5	15.30	--	--	--	--	--

1.4 Mode Identification in Stars

There is one area of stellar pulsation which, in spite of many successes, is still in its infancy. This is the deduction of physical stellar parameters from a study of the pulsations (asteroseismology). The key to unlocking this harvest is mode identification (Balona 1998). On the other hand, Handler (2008) reviewed methods available to perform mode identification from time-series photometric measurements and suggested that photometric mode identification methods have now matured to a point where they can be widely applied to different classes of pulsators. Successes have been obtained for pulsating white dwarf, γ Doradus, δ Scuti, SPB and and β Cephei stars. In several classes, interesting astrophysical information has been obtained as a 'by-product', such as that white dwarfs pulsate in g-modes rather than in r modes, constraints on the frequency of surface convection of δ Scuti stars were found, and T_{eff} and log g determinations were made for some stars.

The choice of the most suitable sets of filters for mode identification is a crucial point in planning observations; at one wavelength the geometry variation should be significant, and the temperature variation should be well constrained in combination with a second filter. Handler (2008) further suggested that if possible, photometric mode identification should go hand in hand with spectroscopic observations to provide the largest possible set of information to the asteroseismologist. The basic data for asteroseismology are the pulsation frequencies. Before the frequencies can be used for detailed modelling, it is imperative to know what pulsation mode gives rise to each frequency. Determining this is called mode identification. The frequency of pulsation is a measure of the sound travel time along the ray path for p modes, and that is determined by the variable sound speed and the length of the ray path itself.

It is thus critical to know the ray path, and that is specified by the pulsation mode geometry. Mode-identification techniques assign values to the discrete spherical harmonic quantum numbers (l, m) of each of the detected oscillation modes. The amount of astrophysical information that can be derived from the observed pulsations depends on the number of successfully identified modes. Therefore, a great effort is put into mode identification in any seismic analysis.

Essentially two types of diagnostics are in use to identify the modes. One of them is based on time series of multicolour photometry, and the other relies on time series of line-profile variations detectable from high-resolution spectroscopy. The introduction of high-resolution spectrographs with sensitive detectors had a large impact on the field of empirical mode identification. Spectroscopic data indeed offer a very detailed picture of the pulsation velocity field. On the other hand, it requires moderate to large telescopes equipped with sophisticated instrumentation to be available for extended observing time spans. It remains a challenge to obtain spectra covering the overall beat period of the multiperiodic oscillation, with a high resolving power (typically above 40000) and with a high signal to- noise ratio (typically above 200 and preferably much higher than that) for a good temporal resolution, i.e. , for a ratio of the integration time to the oscillation periods below a few per cent. The latter condition is necessary in order to avoid smearing out the oscillations during the cycle. Also, the methodology to derive the full details of the pulsational velocity field (at least six unknowns) is complicated. For this reason, multicolour photometric observations, which can only lead to an estimate l , but which can be obtained from small telescopes, are still of utmost importance for mode identification. These kinds of data are especially more suitable for studying long-period pulsations because small telescopes are available on longer time scales. The most reliable results are obtained from the exploitation of simultaneous multicolour photometry and line-profile data (Aerts et al. 2010).

1.4.1 Mode Identification from Multicolour Photometry

This was a method we used in this thesis. A pulsating star changes in temperature and in surface area over its pulsation cycle, both of these contributing to variations in its bolometric luminosity. Photometric observations measure the intensity of the starlight reaching us – usually through various filters, and never bolometrically; no photometer can measure the entire electromagnetic spectrum. Therefore, in all observational cases we are measuring the starlight and its variations over some wavelength range.

The intensity change is much greater in the blue than it is in the red – just because of the shape of the black body curve. That effect alone means that most pulsating stars will have larger photometric variations in the blue than in the red. In addition to this basic effect, the light variations at different wavelengths depend on the geometry of the temperature variations – hence on the spherical harmonic of the pulsation mode – and on the change in surface area, also dependent on the pulsation mode. Both the pulsation amplitude and phase as a function of wavelength are affected by the geometry of the temperature changes and the surface area; thus observations of the pulsation amplitudes and phases in different photometric pass-bands can constrain mode identification. In the best cases the spherical degree l can be uniquely determined – an important step for asteroseismology (Aerts et al. 2010)

The mode-identification method that uses photometric amplitudes and phases is based on the time variations of the stellar magnitude measured with different filters of a photometric system. One considers only the oscillation frequencies that are found in all the different filters for the mode identification; when the amplitude is too small in one or more filters of the system being used, then there is too little information for that mode. For reasons given above the amplitudes of a mode can be markedly different in the different filters. This is illustrated for two stars in Figure 1.12.

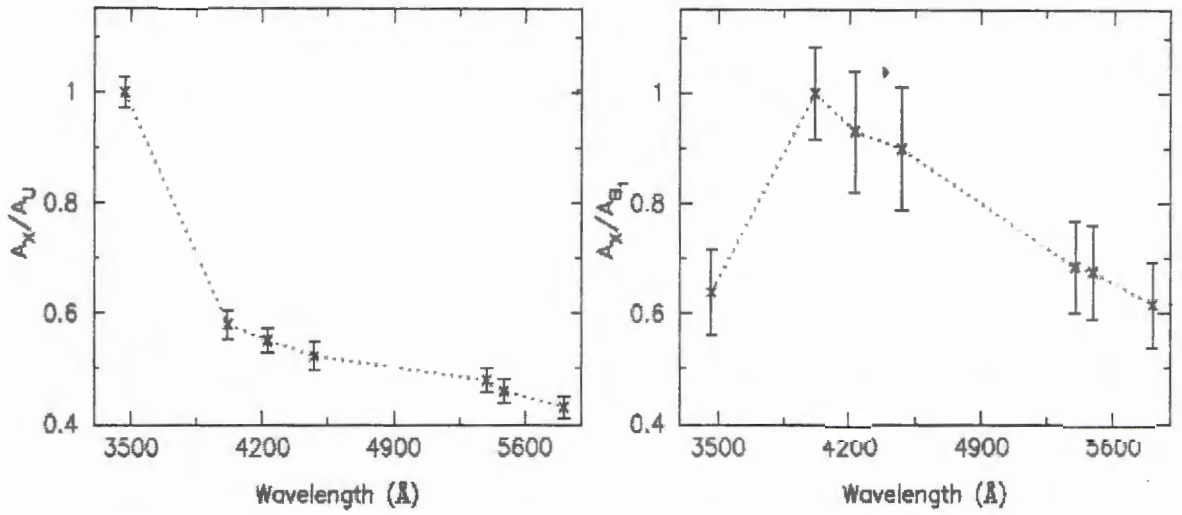

Figure 1.12: Observed amplitude ratios from long-term monitoring of the $l = 0$ mode of the B2 β Cep star HD71913 (left) and for the $l = 1$ mode of the F2 γ Dor star HD12901 (right) in the Geneva 7-band photometric system with filters X=UB1BB2V1VG (Aerts et al. 2010).

Amplitude ratio depends on the kind of oscillation mode – more particularly on the degree l of the mode as illustrated in Figure 1.13 . Similarly, the difference in phase behaviour of the light curves in the different photometric bands is connected to the degree of the mode. This implies that, for a certain oscillation mode whose frequency is detected with sufficient signal-to-noise in all the filters of the photometric system, the comparison of the amplitude and phase values for the different filters allows one to derive the mode degree. This can be seen for the case of the amplitude ratios by comparing Figure 1.12 and Figure 1.13. In Figure 1.13 the computations were done in the adiabatic approximation and assumed Z = 0.02. Comparison of these predictions with the observations shown in Figure 1.12 allows the identification of the mode degree l. In these examples, $l = 0$ for HD71913 and $l = 1$ for HD12901.

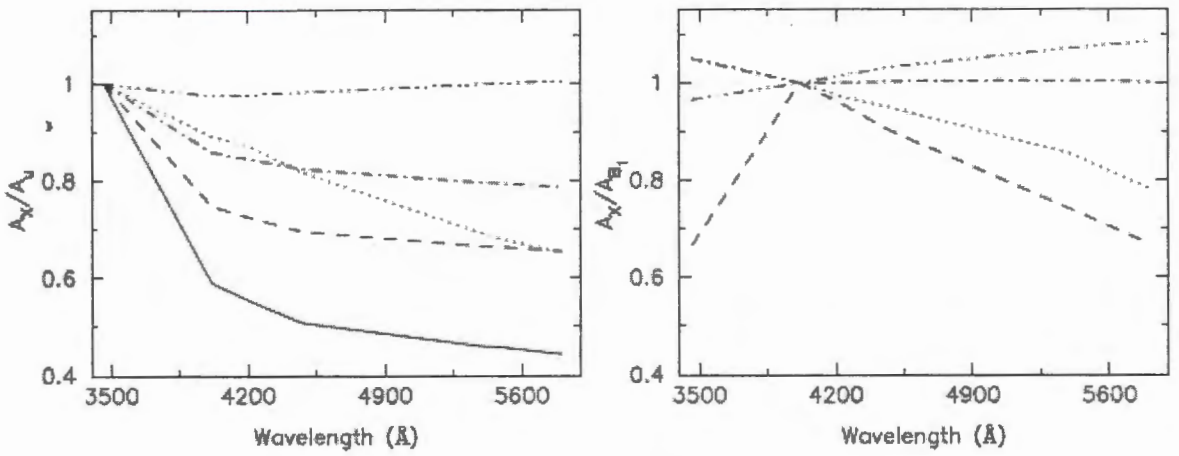

Figure 1.13: Theoretically predicted amplitude ratios for various degrees l of a typical B2 star for the dominant p-mode frequency of HD71913 (left) and of a typical F2 star for the dominant g-mode frequency of HD12901 (right). The line style coding is as follows: *solid line* for $l = 0$ (not applicable in the right panel), *dashed* for $l = 1$, dashed-dot for $l = 2$, *dotted* for $l = 3$ and *dash-dot-dot-dotted* for $l = 4$ (Aerts et al. 2010).

For our work in identifying modes, a software package FAMIAS (Frequency Analysis and Mode Identification for Asteroseismology; Zima 2008) which was developed in the framework of the FP6 Coordination Action in Helio- and asteroseismology (HELAS) is used. This package allows mode identification from multi-colour photometry or high-resolution spectroscopy with the methods discussed above. FAMIAS is applicable to pulsators hotter than the Sun. This includes: γ Dor, δ Sct stars, Slowly pulsating B (SPB)-stars and β Cep stars.

Mode identification is performed by fitting a pulsation model to photometric amplitudes measured in various filters such as the Johnson ones. One such pulsation model is the one presented in Watson (1988). According to this, the pulsation amplitude of a pulsating star is given by:

$$m(\lambda,t)=-1.086\,\epsilon\,Y_l^m(\theta_0,\phi_0)(T_{1\lambda}+T_{2\lambda})\exp(i(\omega t+\Psi_T))+(T_{3\lambda}+T_{4\lambda}+T_{5\lambda})\exp(i\omega t) \quad (1.6)$$

where $\epsilon \ll 1$ is an amplitude parameter and θ_0 and ϕ_0 are the inclination angles of the pulsation axis with respect to the observer. $Y_l^m(\theta_0,\phi_0)$ is spherical harmonic function.

$T_{1\lambda}$ = $b_{l\lambda}\frac{\partial \log(F_\lambda)}{\partial \log(T_{eff})}B$ = The temperature term

$T_{2\lambda}$ = $\frac{\partial b_{l\lambda}}{\partial \log(T_{eff})}\frac{B}{2.3026}$ = limb-darkening variations due to surface temperature variations

$T_{3\lambda}$ = $b_{l\lambda}(2+l)(1-l)$ = The variation in the actual geometry of the star. It includes surface normal variations and the projected surface area variations

$T_{4\lambda}$ = $-b_{l\lambda}$ p*C $\frac{\partial \log(F_\lambda)}{\partial \log(g)}$ = This is the pressure term. C= C(l, s), s is dimensionless frequency.

$T_{5\lambda} = \frac{-\partial b_{l\lambda}}{\partial \log(g)}$ p*C/2.3026 = This term accounts for limb-darkening variations due surface gravity variations

The function P_l is the Legendre polynomial of degree l. A measure of the variation in the atmospheric gas pressure as surface gravity varies is given by $p^* = [\frac{\partial \log(g)}{\partial \log(P_s)}]$ equivalent at $\tau = 1$.

In the above equations B is a measure of the ratio of local fractional temperature amplitude to local fractional radius amplitude and Ψ_T is phase difference. These five terms are calculated from a model atmosphere grid in T_{eff} and log g. Usually, as in the case of FAMIAS, the models are calculated using ATLAS9 model atmosphere program (Kurucz 1993). After the terms are calculated the above pulsation amplitude equation is used to determine normalized theoretical pulsation amplitudes in Johnson UBVRI or any other filters system by convolving the terms with the filter response function. These amplitudes are normalized to the value of 1 in Johnson B. Then the normalized theoretical amplitudes are fitted to the data, changing the values of l and the best fit is made. This is how l is determined. The input required is the T_{eff}, log g, mass, microturbulence and metallicity.

In order to determine the ratio of relative temperature to radius perturbations :

$B = \frac{\delta T}{T} / \frac{\delta r(R)}{R}$, a relation between $\frac{\delta T}{T}$ and $\frac{\delta r(R)}{R}$ needs to be established.

In the adiabatic case, the following equation applies:

$$\frac{\delta T}{T}=\nabla_{ad}\frac{\delta P}{P} \qquad (1.7)$$

The non radial pressure perturbation is related to radius perturbation at the stellar surface in the following way:

$$\frac{\delta P}{P}=C(l,\sigma)\frac{\delta r(R)}{R} \quad \text{at the surface,} \qquad (1.8)$$

where the perturbed gravitational potential is neglected, and C depends on l and dimensionless frequency (σ) in the following way:

$$C(l,\sigma) = \frac{l(l+1)}{\sigma^2}-4-\sigma^2 \ . \qquad (1.9)$$

The term C gives us a measure of whether the radial or the horizontal component of the oscillations dominates. It is clear that for pure radial oscillations C is negative, implying that pressure variations always act in opposition to the radius variations. Hence a star pulsating in pure radial modes is compressed at minimum radius, and rarefied at maximum radial perturbations. The situation for a non-radial pulsator is different because here C can have a positive (horizontal motions dominate), zero, or negative sign where the radial motions dominate the horizontal ones.

Therefore, adiabatic oscillations near the surface of a star relate $\frac{\delta T}{T}$ and $\frac{\delta r(R)}{R}$ as:

$$\frac{\delta T}{T}=\nabla_{ad}C(l,\sigma)\frac{\delta r(R)}{R} \qquad (1.10)$$

Hence Watson (1988) defines

$$B=\nabla_{ad}C(l,\sigma) \quad , \qquad (1.11)$$

The energy equation for non-adiabatic oscillations is complex; it therefore results in a complex relation between $\frac{\delta T}{T}$ and $\frac{\delta P}{P}$. This introduces an amplitude parameter R_{ad} and the phase difference Ψ_T between the temperature and radius perturbations so that the following relation can be obtained (Medupe 2002):

$$\frac{\delta T}{T}=R_{ad}\nabla_{ad}\exp(i\psi_T)C(l,\sigma)\frac{\delta r(R)}{R} \quad . \qquad (1.12)$$

R_{ad} and Ψ_T can be considered free parameters that can be determined from a fit to multicolour photometric data as was done from two-colour diagrams by Medupe and Kurtz (1998) in their study of α Cir, and Watson (1988). R_{ad} = 1 for adiabatic oscillations and $R_{ad} \rightarrow 0$ for strongly non-adiabatic oscillations.

1.5 V351 Ori (HD38238)

V351 Orionis (V351 Ori, HIP 27059, HD 38238) belongs to a group of young Herbig Ae/Be stars with spectral type A7IIIe that showed photometric and spectroscopic variabilities over various time scales (Choudhury et al. 2011) caused by variable obscuration of the star by circumstellar dust. There are several peculiarities of the star that easily justify the definition "remarkable" that was given by van den Ancker et al. (1996). The photometric variability manifests itself in the form of unpredictable Algol-like dimmings (Koval'chuk and Pugach 1998). Algol-like dimmings are due to variations in the column density of circumstellar dust in the direct line of sight toward the star. According to Palla & Stahler (1993), the age of the star would be between 1 and 2 million years. V351Ori is located between the main sequence and the birth line, at the evolutionary track of a star with a mass between 2.5 and 3.0 $M_{\odot}$ (van den Ancker et al. 1996).

V351 Ori is located on to the region of the Orion belt (Figure 1.14), where the Orion complex and the region of star formation are found. Though the star is not clearly visible, the idea is to show where the star is in general with respect to constellation Orion. In addition, the unstable pattern of light variations and the apparent indications of accretion of matter onto the star (van den Ancker et al.1996) are consistent with the assumption of its young age. However, Kovalchuk & Pugach (1998) thought V351 Ori is a post main sequence star since profile of its Hα emission line points to an outflow of matter rather than its accretion on to the star. However, recent research shows that it is indeed a PMS star (Choudhury et al. 2011) due to presence of dust shell. Comparison with the predictions of linear non-adiabatic radial pulsation models put stringent constraints on the stellar parameters and indicate that the distance to V351 Ori is intermediate between the lower limit measured by Hipparcos (210 pc) and that of the Orion nebula (450 pc) (Ripepi et al. 2003a).

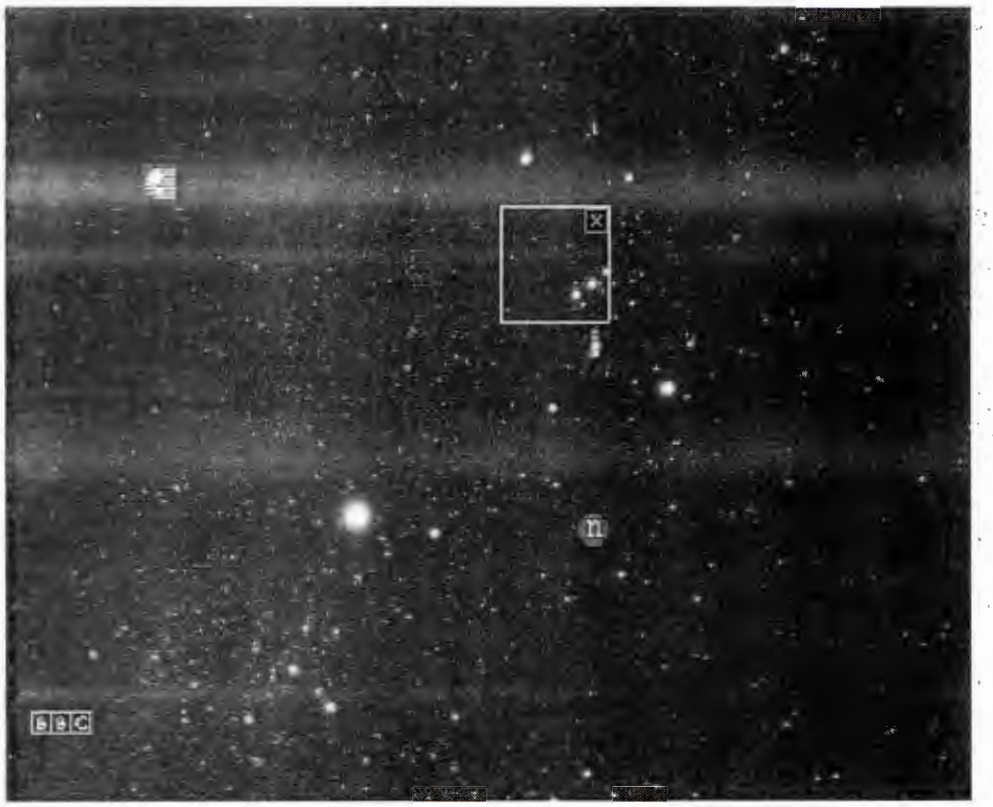

Figure 1.14: Location of V351 Ori (at the centre of the rectangle) in the region of Orion belt (Image credit:www.sky-map.org).

Using photometric observations, Marconi et al. (2000) presented that V351 Ori has pulsational periods that fall in the expected range of δ Scuti type variability which corresponds to a pulsation period of 0.058 ± 0.002d. V351 Ori pulsates in a mixture of several radial modes, at least four, values mentioned in Table1.1 (Marconi et al. 2001).

Ripepi et al. (2003b) suggests that there is a possibility that nonradial pulsation modes are also present. Marconi et al. (2001) have succeeded in matching four frequencies with a single pulsation model with mass = 1. 8 $M_{\odot}$, luminosity L = 13. 87 $L_{\odot}$, and effective temperature T_{eff} = 7350 K. The Hα profile in V351 Ori generally has the inverse P Cygni profile typical of accretion (Balona et al. 2002). Inverse P Cygni profiles are signatures of the accretion of circumstellar material onto the central object and are characterised by blue-shifted emissions with red-shifted absorptions or systematically enhanced red shifted absorptions. Balona et al. (2002) also estimated the effective temperature (T_{eff} = 7500 K), rotational velocity (v sin i =102 km /s), log g = 4.00 and radial velocity of 13.3 km/s ± 0.7 km/s. Using best fit pulsation models, Ripepi et al. (2003a) estimated effective temperature (Teff ~ 7425 – 7600 K) of the star using the pulsation models. V351 Ori has a microturbulent velocity of 2 km /s and peak to peak pulsation amplitude 0.02mag (Kurtz & Muller 1999). According to SIMBAD data base, V351 Ori is a variable star of δ scuti type which has ICRS coordinates α (2000) 05 44 18.79329 and δ (2000) +00 08 40.4024, galactic coordinates 204.9707-14.8212 and magnitudes : B = 9.25, V = 8.91, J = 7.950, H = 7.504, & K = 6.846. SIMBAD also gives finding chart of the star as shown in Figure 1.15.

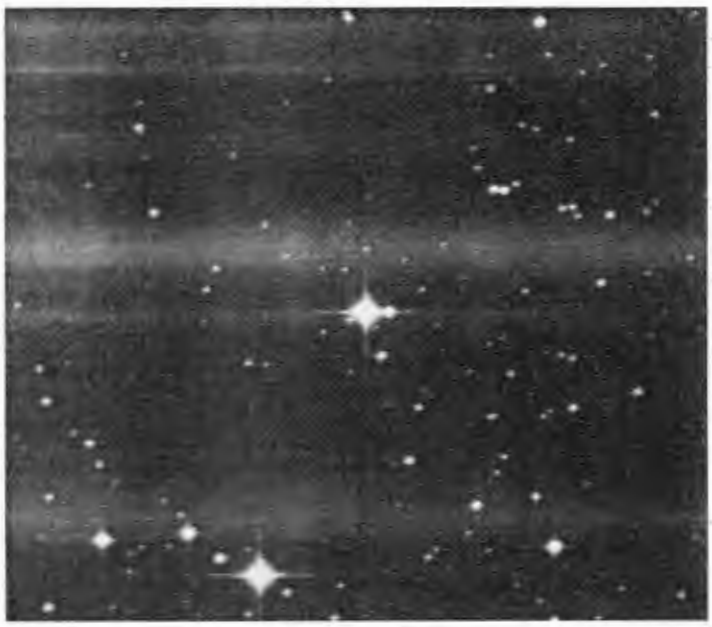

Figure 1.15: A finding chart of V351 Ori, the size is 12.9' x 12.9'. V351 Ori is at the centre of the chart (image credit: SIMBAD Astronomical data base).

1.5.1 Photometric and Spectroscopic observations of V351

In the previous section I have discussed that V351 Ori has two types of variability. The first is irregular variability caused by dust obscuration and the second is regular pulsational variability.

Choudhury et al. (2011) presented a high-resolution spectroscopic observation of V351 Ori along with optical BVRI observations. This was to investigate the patterns and time scales of temporal line profile variability in order to understand the dynamical circumstellar environment of V351 Ori. The Hα line profiles showed strong variations over all time-scales. The shape of the profiles changed over time scales of a day. Choudhury concluded that the line profile variations are caused by changes in disk wind, wind acceleration, rate of accretion, and outflow of cool gaseous material. The Hα emission line profiles in the rest frame velocity of V351 Ori and over-plot of the photospheric components are given in Figure 1.16.

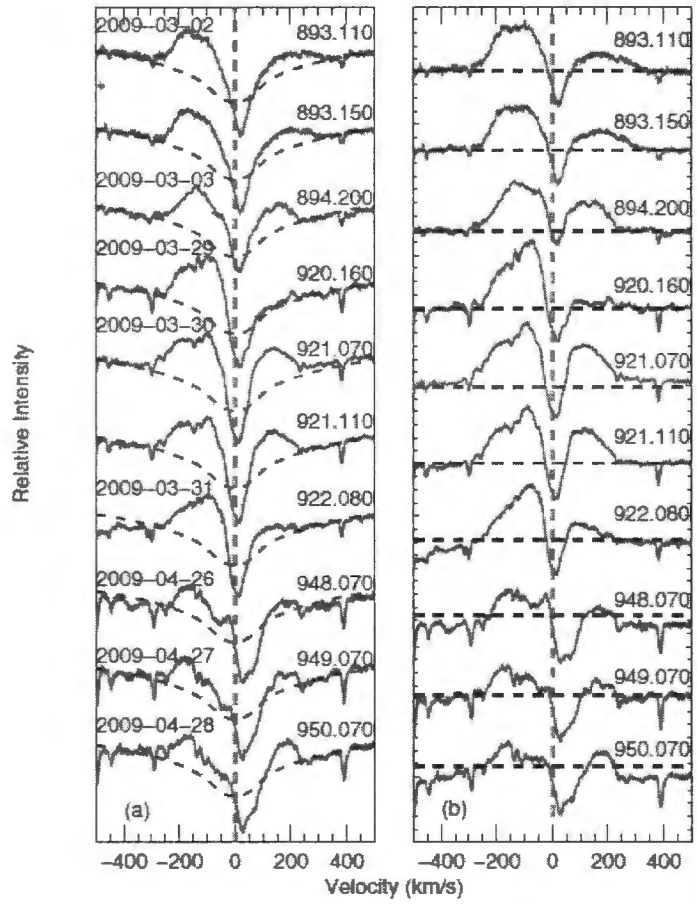

Figure 1.16: Hα line profiles (solid lines) of V351 Ori are shown in the (left). Synthetic Hα line profiles (blue dashed lines) are over plotted on each spectrum. Modified Julian days are displayed on the respective spectrum. The vertical dashed line represents the rest frame velocity of the star. Residual spectra of Hα line profiles (right) in the same epochs. Horizontal blue dashed lines represent the zero absorption levels (Choudhury et al. 2011).

Modified Julian Date (MJD) is an astronomical time convention that has the great advantage of being a continuous variable without the discontinuities introduced by the usual civil time convention of years, month, days, hours, minutes and seconds. Modified Julian Date is time measured in days from 00:00 UTC on 17 November 1858. The origin of MJD is simply Julian Date 2400000.5.

Choudhury et al. (2011) also obtained a time series optical BVRI photometric observations of the star and obtained the magnitudes $V \sim 8.89$, $B - V \sim 0.38$, $V - R \sim 0.19$, and $V - I \sim 0.41$ mag, and suggested that this might indicate that there are no significant changes in the long-term photometric behaviour of V351 Ori. However, it is also noteworthy that the photometric observation did not coincide with the spectroscopic observation. Unlike the variations in visual magnitudes, which reflect the variable stellar photosphere, near infrared variability can account for changes in both the stellar photosphere and the circumstellar environments. Ripepi et al. (2003b) presented time series observations of the Herbig Ae star V351 Ori and commented that this star is a good candidate for Whole Earth Telescope (WET) observations. The predicted position of V351 Ori in the HR diagram is presented in Fig 1.17. The box (dashed lines and open triangles) indicates the range of luminosity and effective temperature corresponding to the empirical estimates available in the literature. Also shown are the evolutionary tracks (solid lines), and the instability strip by Marconi & Palla (1998) (shaded area). The dashed line on the right is stellar birth line.

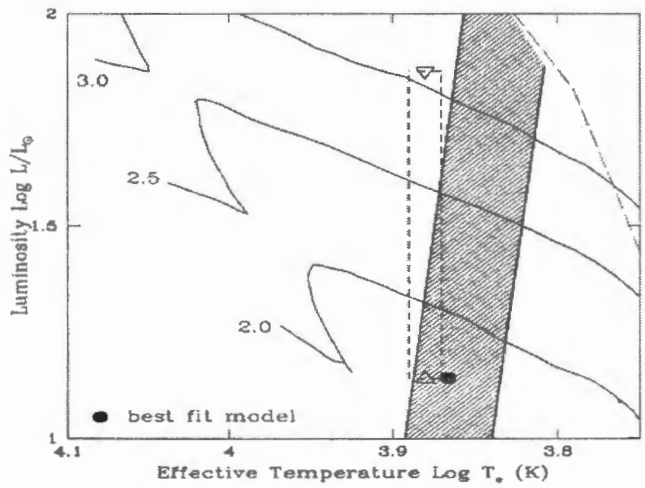

Figure 1.17: Position of the best fit model in the HR diagram for V351 Ori (filled circle). The shaded area is the δ Scuti instability strip. The dashed box indicates the range of luminosity and effective temperature corresponding to the empirical estimates available in the literature. V351 Ori clearly falls in the δ Scuti instability strip. Over plotted solid lines are evolutionary tracks of 3 $M_{\odot}$, 2 $M_{\odot}$ and 2 $M_{\odot}$ stars (Ripepi et al. 2003b).

Ripepi et al. (2003a) identified five pulsation frequencies (Table 1.4), four of which were highly significant. The periodograms are shown in Figure 1.18, where the solid line displays the S/N = 4 level, and the dotted and dashed lines represent the 99 % and 90 % significance levels. In the Figure there is another apparently significant frequency at 3.347 c/d with S/N 3.9. However, this was not considered to be relevant since the period of 7.2 hr is just the duration of the longest time series obtained at a single site, and the resulting frequency could be a spurious one. The rule of thumb is that the "background noise" level in the periodogram should be estimated, and peaks lower than 4 x this noise level should not be accepted as statistically significant (meaning they lie below the statistical 3-sigma detection threshold). As an example, S/N = 3 ("3-σ" detection) has a probability of 99.7 % being 'real' (often used as a criterion for believing a result). Signal to noise ratio (S/N) is the ratio of the amplitude of a signal above the noise level to the amplitude of the noise level itself.

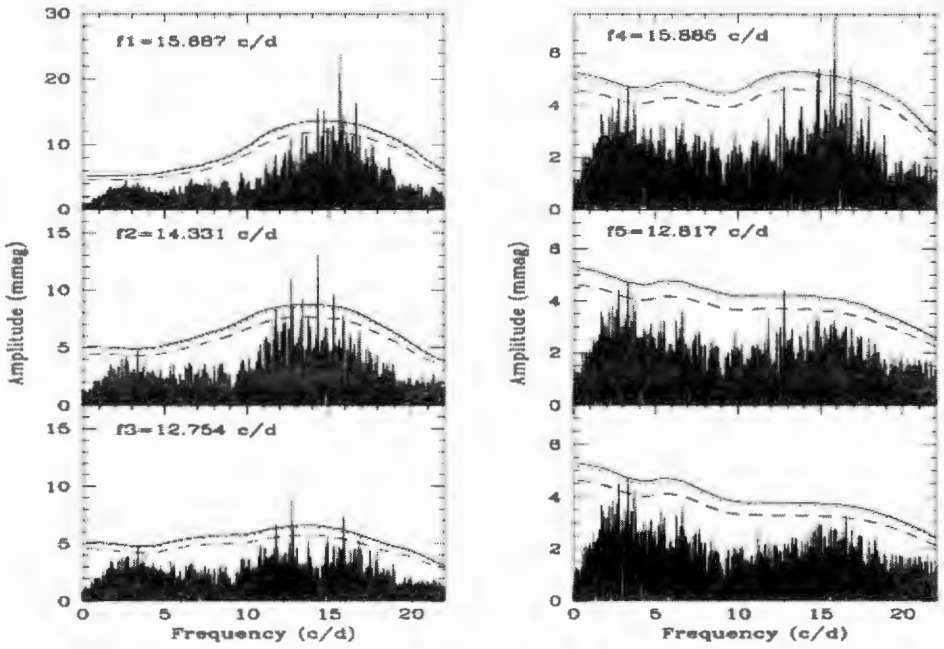

Figure 1.18: Frequency analysis of the whole photometric data set of V351Ori collected in 2001 & 2002. Each panel shows the Fourier Transform after the subtraction of a pulsating frequency. The solid line corresponds to S/N = 4. The dotted and dashed lines show the 99 % and 90 % significance level (Ripepi et al. 2003a).

Balona et al. (2002) obtained simultaneous multi-colour photometric and spectroscopic observations of V351 Ori to investigate the nature of the pulsation of V351 Ori. Optical magnitudes (e.g. V ~ 8.92, B − V ~ 0.37, V − R ~ 0.22 and V − I ~ 0.46 mag) were obtained over time-scales of minutes to weeks and did not find any significant variation within 0.05 mag. They also compared the near infrared magnitudes of V351 Ori and found that H−K excess of V351 Ori (which is an indicator of the inner disk materials) decreased continuously over the period from 1982 to 2002.

Balona et al. (2002) also found that V351 Ori pulsates in at least three modes: $f_1 = 15.675$ *c/d,* $f_2 = 14.335$ *c/d and* $f_3 = 11.877$ *c/d. A* periodogram of the observation is given in Figure 1.19. The top panel is the periodogram of the raw data. Subsequent panels show the periodogram sequentially pre-whitened by f_1 = 15.675 c/d, 0.053 c/d, 0.258 c/d and (bottom panel) f_2 = *14.335 c/d.* Finally it was concluded that there are at least two δ Scuti type periods in the light variations of V351 Ori. Different frequency values suggested by Balona et al. (2002) and other authors are compared in the tables given at the end of this chapter.

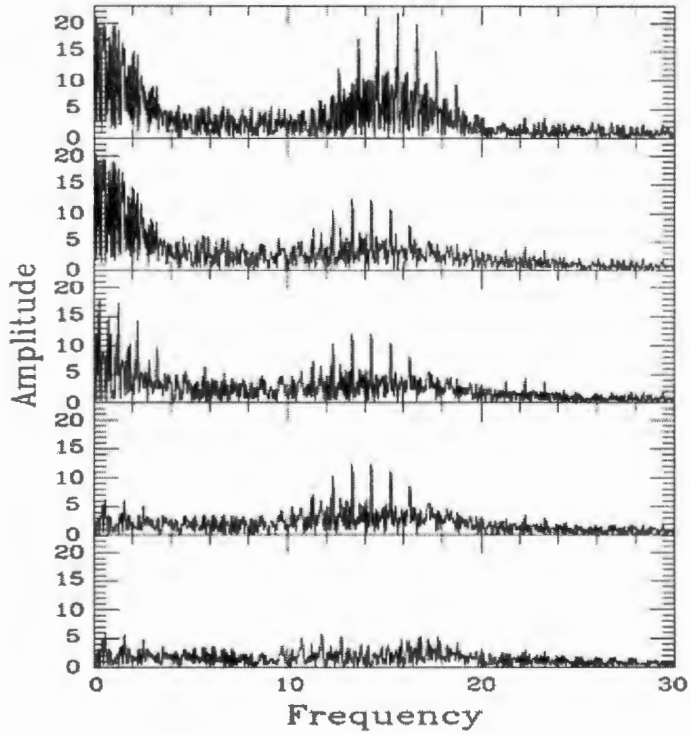

Figure 1.19: Periodograms of the mean $UBVR_CI_C$ photometric data. The amplitudes are in mmag and frequency in c/d (Balona et al. 2002).

High quality photometric observations of V351 Ori in UBV Johnson system was presented by Marconi et al. (2001) which showed pulsation in a mixture of several radial modes. A maximum amplitude of ~ 0.12 mag was found in the U and B filters. Marconi et al. (2001) also concluded that V351 Ori represents an excellent candidate for asteroseismological studies. Marconi et al. (2000) and Marconi et al. (2001) have interpreted the frequencies observed in the light curve of V351 Ori as due to pulsations in a mixture of several radial modes.

From a photometric investigation of a sample of seven Herbig Ae stars with spectral types in the range A5 to F5, located within or near the boundaries of the instability strip, Marconi et al. (2000) found that V351 Ori shows δ Scuti type pulsation. This is another characteristic of pre-main sequence stars of mass $\geq 1.5\ M_{\odot}$ as they cross the pulsation instability in their contraction towards the main sequence. Koval'chuk and Pugach (1998) carried out spectroscopic observation of V351 Ori in order to determine its evolutionary status for the first time the hydrogen abundance in the photosphere of the star by thoroughly analysing the profile of the emission line. They concluded that the hydrogen abundance (amount of hydrogen) in the stellar photosphere is ~ 40 %. A carefully reconstructed profile of the Hα emission line points to an outflow of matter rather than its accretion onto the star which could suggests that V351 Ori is a post-main sequence star.

van den Ancker et al. (1996) and Balona et al. (2002) suggested that the systematic near infrared variability of V351 Ori is caused by the clearing of dust around the star, which indicates a variable circumstellar environment around V351 Ori. This is further supported by the fact that until 1996 the V351 Ori light curve was highly irregularly variable as shown in Figure 1.20. After this period of 1996, such variability ceased to exist. van den Ancker et al. (1996) presented photometric and spectroscopic observations of V351 Ori and found that it transformed into an almost non-variable star from a strong photometric variable within a short period of ~14 years. The star showed a large variation of > 2 mag before 1985 (Figure 1.20). van den Ancker et al. (1996) also reported that the visual magnitude of V351 Ori varied by 0.16 mag between 1985 to 1990, i.e. over a time scale of years. During 1990 to 1995, the visual magnitude of the star became almost constant without any significant variation. It was also shown that the Hα profile of V351 Ori was of an inverse P Cygni type and also a high infrared excess emission was observed.

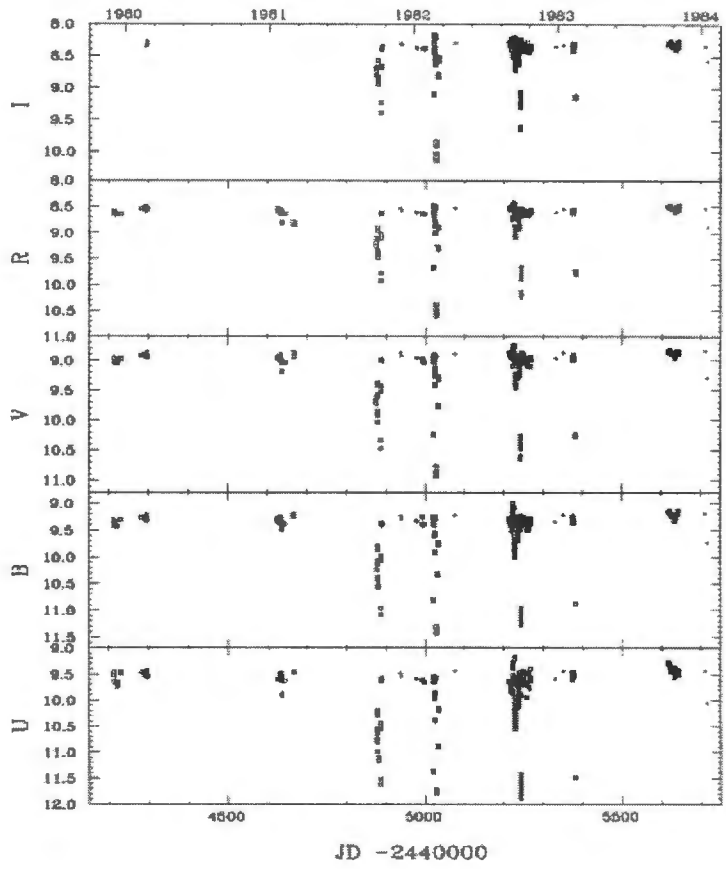

Figure 1.20: Light curves of V351 Ori in Johnson UBVR and I magnitudes. Time is in Julian days (taken from van den Ancker et al. 1996).

1.5.2 Spectral Energy Distribution (SED) of V351 Ori

The SED of HAEBE stars is characterized by the presence of (large) amounts of circumstellar matter (CSM), which can dominate the SED at IR wavelengths; there is also some evidence for a contribution from the circumstellar gas to the ultraviolet (UV) continuum (Waters and Walkens 1998). van den Ancker et al. (1996) finally suggested that it is very important to observe V351 Ori in the near infrared. If the dust clouds close to the star are indeed accreted onto the central star, one should expect a clear decrease of the infrared excess in the SED of this star. Further monitoring of V351 Ori remains necessary to see whether the dust clouds around this very interesting object start to re-occur again, in which case the star will become strongly variable once more. Spectral energy distribution of the star is given in Figure 1.21.

Taken near maximum brightness, the extinction-free SED of V351 Ori was analysed by comparing it with the Kurucz (1991) theoretical model with T_{eff} = 7650 K, and log g = 3.6, corresponding to a spectral type of A7III. For the construction of SED, the main sources of the photometry used are the simultaneous UBVRI and JHKL photometric observations by Kilkenny et al. (1985).

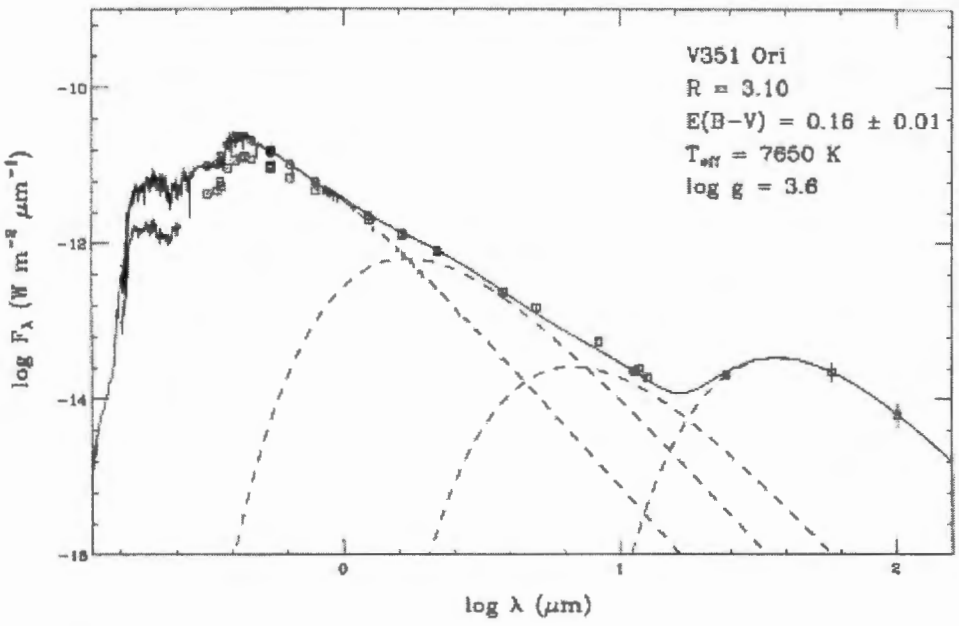

Figure 1.21: The spectral Energy Distribution of V351 Ori. Squares show observed values and circles belong to extinction-corrected ones. Also shown are the Kurucz model (left dashed line), and three Planckians fitted to the infrared excess (right dashed lines) and total model (solid line), fitted to the extinction-free SED (van den Ancker et al. 1996).

van den Ancker et al. (1996) commented that Kurucz model is very good in the optical and ultraviolet wavelength ranges with a large amount of excess radiation above photometric levels in the infrared. The excess can be explained as due to three dust shell components, radiating as black-bodies of temperature about 1700 K, 430 K and 80 K. However, the fact that SED in the near infrared can be approximated by a straight line probably indicates that the 1700 K and 430 K components are not due to two separate dust shells, but due to an extended disk or dust shell around the star.

Among the unique nature of the V351 Ori is that a flare-like event on its optical light curve which is strongest in the ultraviolet was reported by (Koval'chuk 1984) without an explanation of its cause. Since then, no appropriate explanation is given for the cause of this event.

1.5.3 Summary of Frequencies

Below follows a summary of pulsation frequency values of V351 Ori taken from different papers to make comparisons clear. Table 1.2 gives 6 identified periodicities by Marconi et al. (2001) whose corresponding frequencies are listed for filters U, B and V. Inspection of this table reveals that all the frequencies are well separated except for f_3, which is close to f_1. Table 1.3 shows frequency analysis of photometry according to Balona et al. (2002). The frequency at 0.052 cycle/day is not regarded as true periodicity since not even one cycle was completed during the run. Therefore, according to Balona et al. (2002), this frequency was assumed to be a general increase in brightness. 0.258 cycle/day is also considered as artefact of the irregular variations typical of Hae/Be stars since there was no convincing evidence for it.

Therefore, the general conclusion was that V351 Ori pulsates in at least three modes of frequency value: 15.675 c/d, 14.335 c/d and 11. 877 c/d respectively. Table 1.4 shows frequencies (from photometry and spectroscopy) derived by Ripepi et al. (2003a) in comparison with the previous work by Marconi et al. (2001), also given as M01, and by Balona et al. (2002), also given as B02 (P) for photometric result and B02 (RD) for radial velocity result. Ripepi et al. (2003b) also compared the six frequencies detected (Table1.5) with M01 and B02 and concluded that at least four frequencies (f_1, f_3, f_4 & f_6) fall in the domain of δ Scuti pulsation.

Results of Ripepi mentioned in Table 1.4 and 1.5, are from multisite observations. The difference is that the results in Table 1.4 are for longer time observation where six observatories were involved. However, results listed in Table 1.5 are for relatively shorter time scale where four observatories were involved. There is also difference in frequency values obtained.

Table 1.2: Observed frequencies of V351 Ori. Frequencies f_1 to f_6 are ordered by decreasing amplitude. The error on the individual frequencies is of the order of 0.23 per day.

Author	Frequencies (c/d)	U (d^{-1})	B (d^{-1})	V (d^{-1})	Average (d^{-1})
Marconi et al. (2001)	f_1	15.59	15.39	15.51	15.49 ±0.24
	f_2	11.89	11.92	11.86	11.89 ±0.23
	f_3	15.85	17.27	15.69	16.27 ±0.74
	f_4	31.26	32.40	30.32	31.33 ±0.88
	f_5	8.32	6.20	6.19	6.90 ±1.03
	f_6	27.08	27.14	26.09	26.77 ±0.53

Table 1.3: Frequencies derived from photometry for V351 Ori. Only f_3 and f_4 were considered to be true frequencies.

Author	Frequencies (c/d)
Balona et al. (2002)	f_1 = 0.053
	f_2 = 0.258
	f_3 =15.675
	f_4 =14.335

Table 1.4: Comparison with previous works of M01 and B02. The labels "(P)" and "(RD)" indicate if the frequency has been detected on the basis of photometric or radial velocities data. An uncertain correspondence of previous frequencies with the present work is marked by a question mark. The uncertainties on the frequencies are also indicated.

Author	Frequencies (c/d)		M01 ± 0.6 c/d	B02(P)±0.08 c/d	B02(RD) ±0.08 c/d
Ripepi et al. 2003(a)	f_1	15.687	15.49	15.675	15.682
	f_2	14.331	-	14.335	14.153
	f_3	12.754	11.89?	-	11.877?
	f_4	15.885	16.27?	-	-
	f_5	12.817	-	-	11.877?

Table 1.5: Frequencies, amplitudes and phases derived from the Fourier analysis of the data. For comparison, the frequencies found in previous works are reported. ("(?)" means uncertain correspondence between this work and Balona et al. 2002 frequencies).

Author	Frequencies (c/d)		Marconi et al. (2001)	Balona et al. (2002)
Ripepi et al. 2003 (b)	f_1	15.687	15.49	15.675
	f_2	0.145	-	0.053?
	f_3	13.337	-	14.335
	f_4	16.868	16.27	-
	f_5	2.099	-	1.900(?)
	f_6	11.780	11.89	11.877

Chapter 2

Target Selection and Observations

This chapter shows how the target star we wanted to observe was selected from a list of targets which are pulsating pre-main sequence Herbig Ae/Be stars and candidates based on its visibility from December to February and its high amplitude value. The chapter also shows the details of observations on the selected star.

2.1 Target Selection

The target star was selected based on some specific criteria. We first looked at its amplitude value, to be sure that the amplitude can be fairly detectable using the telescope we were supposed to use. The amplitude was relatively larger and the star is also brighter. Then, from the list of 44 stars (Table 1.1) which contains the pulsating Herbig stars so far known and candidate pulsating stars, we have chosen V351 Ori as our target star. In the table, we have listed the sources we have used to select the target is mentioned. The summary of detailed information on the target star is also mentioned in Appendix D.

We then used SIMBAD coordinate query to select comparison stars. We cautioned for the magnitude of the comparison stars not to be much dimmer compared to the target star and we have also checked their spectral type. We were also aware about the distance of the comparison stars from target and both comparison stars were within 15 arcmin from it. The parameters and additional information on the comparison stars is given in Table 2.1. Finally, we checked visibility curves (Appendix A) of the star to be sure that we can see it in the night we want to observe.

To determine zero-points and colour equations, which helps us to transform data to a standard homogeneous system and thus compare data from different sources, we need to observe one E-region star. We have selected this star from the list of E-region stars provided in the working station inside the dome. We chose E232 (HD24696) since its finding chart was more visible compared to others we selected. This star has RA:03 53 48.0, Dec : - 43 09 46, V-mag: 7.922 and spectral type: K0III.

2.2 Observations

In this section we discuss the methods used to collect data. All the data presented here were acquired using the 0.5 m telescope in Sutherland.

2.2.1 SAAO 0.5-m Telescope

The 0.5-m telescope which is now located at Sutherland was built by Boller & Chivens in 1967 for the Republic Observatory, then moved to the current observing site near Sutherland in 1972. Optical and additional diagrams on the telescope are given in appendix B. It has a Cassegrain focus f/18, 22.6 arcsec/mm and guide-finder 100 mm f/9.1. A PC runs the Modular Photometer using the program LUCY (all-sky photometry) or MILLY (uninterrupted observations on one object with one filter with integration times in the range 2 ms-60 sec). The details of this are given by Kilkenny et al. (1988). The Modular Photometer is the dedicated 0.5-m instrument. This photometer is of a fairly conventional single-channel design except that the filter wheel and aperture wheel are plug-in modules to facilitate maintenance and repair. The detector is photomultiplier of a Hamamatsu R943-02 GaAs tube . The focal plane aperture wheel is manually operated and contains ten circular apertures of approximate angular diameters 10, 15, 20, 25, 30, 35, 45, 60 and 90 arcsec and 8 arcmin, the latter being used for field identification. In our case 30 arc second was used. The aperture wheel has been designed so that the centres of all the apertures locate to better than 75μm when brought into the optical axis. The apertures are viewed directly or via an LCD display. No offset guiding is available.

There are ten positions for the filter wheel for 25 mm diameter or 25 mm square filters. UBV(RI)$_C$ filters are provided as standard. In addition to the colour filters, neutral density filters are provided in a four-position wheel containing: "clear" (i.e. no filter), 0.4ND, 1.0ND and 2.0ND filters, corresponding to light reductions of 0, 1, 2.5 and 5 mag, respectively.

2.2.2 LUCY: Photometric control & data acquisition

Control of the system and data acquisition is handled by a program called LUCY which presents the user with various 'menus' or boxes on the computer screen which contain information, request data input or present options for operations. The user needs to input colour equations, extinction coefficients, star names and coordinates. This information can be stored from week to week, and regular users have their own directories on the hard disk. Lists of standard stars for UBVRI and uvby photometry are stored permanently on the hard disk; coordinates, magnitudes and colours are included so that zero-points can be determined on-line.

The user also has to input 'programs' which specify the sequence of filters to be used and the integration time for each filter. A simple example of a LUCY program is given as follows:

30 1 11 1
30 1 12 1
30 0 13 1
30 1 13 0
30 1 12 0
30 0 11 0

which carries out 30 second 'integrations' of counts (column 1), which is also our case, through filters 1, 2 and 3. The second column is a code or 'flag' which tells the program to proceed immediately to the next filter (1) or to stop (0) whilst the telescope is moved (to observe the sky, say) or at the end of the program. The third column tells the program which channel (always channel 1 with the modular photometer) and filter to select and column 4 is a flag which tells the program to expect a star measure (1) or sky (0). Up to 32 lines can be entered in a program and 10 programs can be stored. When a program runs within LUCY, the results of each integration (SAST, integration time, channel and filter number and total counts integrated) are displayed on the computer screen, stored on disk and printed on the matrix printer, if requested. At the end of the program the heliocentric Julian date and air mass corresponding to mid-program and the computed magnitude(s) and colours are calculated, displayed and stored on disk. The hard disk file name contains the last four digits of the Julian date and is thus unique for each night.

A number of other features are available in LUCY, such as the macroprograms which allow sequences of stars (typically a variable with its comparison and check stars) to be run without the observer needing to type in star names or initialise the run program. For high speed photometry, a separate program, MILLY, is available which allows the observer to obtain data down to an integration time of 1 millisecond. With integration times longer than 100 milliseconds, data are recorded in ASCII format, between 100 and 5 milliseconds, data are stored in binary form which can later be converted to ASCII, but between 5 and 1 milliseconds data cannot be recorded on disk fast enough and MILLY uses a 'snapshot' mode. This saves only the most recent 16000 data points (i.e. 16 seconds worth at a 1 millisecond integration time).

2.2.3 Observations in January and February 2013

V351 Ori was observed for 15 days in January and 8 days in February, a total of 23 nights worth of data was collected. This amounted to 85 Hr of observations (see Table 2.2 for details). In total 370 data points were taken for the whole observation on our target star. Precautionary measures were taken during the course of observations to ensure good data collection. These includes checking the centring of the star inside the aperture, avoiding long time gaps while moving the telescope from target star to comparison star or vice versa, checking regularly that the dome did not cover the telescope, random checks of the sky outside the dome, and checking the temperature of the photomultiplier tube (which should be kept at about -15 ^{0}C). Using the Fortran program shown in Appendix C, a light curve of the target star and the comparison stars was drawn to make sure that the appropriate stars were measured. The light curves of all the nights are presented in chapter 3.

Some problems were encountered during observations. A continuous power cut was also a problem on one night. Malfunctioning of the telescope hand set was also a problem for about 3 days. On one of the days the temperature of the tube increased, which was reported to the technicians. It is also very important that the telescope is focused correctly, otherwise one will get poor results. It can be focused just by looking at the stars. The best focus occurs when the stars are smallest, however the best focus for one's eye is not necessarily the same as the best focus for the photometer. It must be ensured that the star is focused at the aperture hole. To do this, a moderately bright star was selected and brought to the centre of the cross hair which is visible through the eye piece. When the aperture was put in place and the telescope was focused, the star could be seen near the centre of the aperture.

Table 2.1 Information on the comparison stars and E-region star compared to the target star.

Stars	**Name**	**V-mag**	**Coordinates**		**Spectral type**
			RA	Dec	
Comparison star 1	HD 38119	8.2	05 43 24.7	+00 10 30.6	K0
Comparison star 2	HD 38311	8.71	05 44 48.6	-00 03 43.02	A0
Standard star	E232	7.93	03 53 48	-43 09 44	KOIII
Target star	HD 38238	8.91	05 44 18.8	+00 10 40.4	A7IIIe

The sky transparency can change due to, for example, dust. To correct for sky transparency changes, we observed two standard stars or comparison stars (Table 2.1), from time to time. The standard stars were selected to be as near as possible to the star that we were observing. If the transparency changes slowly it is possible to correct the results, but if it changes too rapidly (e.g. by clouds), then we need to stop observing. This happened many times. The following pattern was used to observe the target star and the comparison stars. If C stands for the observation of the standard (or comparison) star and V stands for the observation of the target star, then we used the sequence: C1,V,C2,C1,V,C2,....., where, C1 stands for comparison 1 and C2 for comparison 2.

Since the target star is fairly bright, we used an integration time of 30 seconds for each filter. This integration time is relatively large so that scintillation noise (noise due to rapid variations in the air) would not limit the accuracy of the photometry. On the other hand, sky measurements were taken in the interval between one hour and one and a half hours to ensure proper monitoring of sky brightness variations.

Table 2.2 Summary of observation log for photometry at SAAO for each day. The first column is the starting Julian day with respect to JD 2450000. The second column is duration of observation, ΔT, in hours and the third column is number of data points, N.

Date	ΔT (hours)	N				
		U	B	V	R	I
6295	3.53	14	13	14	13	13
6296	3.18	12	12	12	12	12
6297	3.50	14	14	14	14	14
6298	4.67	21	21	21	21	21
6299	5.23	20	20	22	20	20
6300	5.23	23	23	23	23	23
6301	5.00	22	22	22	22	22
6303	4.07	16	16	17	16	16
6304	5.12	22	24	23	24	24
6305	5.28	24	22	24	22	24
6306	5.00	22	22	23	23	22
6307	5.10	23	22	24	22	23
6319	4.22	14	14	14	14	14
6320	3.53	16	16	17	16	16
6321	3.13	12	8	15	8	9
6325	3.22	13	13	14	13	13
6326	2.00	7	7	8	7	7
6328	2.4	10	10	11	10	10
6329	2.8	11	11	13	11	11

Continued ...

Table 2.2 continued ...

Date	ΔT hours)	N				
		U	B	V	R	I
6344	2.1	7	7	9	7	7
6345	2.45	10	19	11	9	7
6346	2.05	8	8	9	8	8
6347	2.25	9	9	10	9	9

Chapter 3

Data Reduction

In this chapter we describe the reduction steps that we followed for all the data obtained. The program used to reduce (LUCY) and the the light curves we obtained during the daily reduction will also be presented in this chapter.

3.1 Reducing LUCY Data

The data was reduced using a FORTRAN program written By Luis Balona. The program requires inputs like name of target star (V351 Ori in this case), filter name, data file name, etc. The following steps of reduction are performed by this program: dead-time correction, sky subtraction, atmospheric extinction correction and the heliocentric time correction.

3.1.1 Dead time correction

The dead-time correction is a factor applied in the reduction procedure to correct for overlapping pulses which can occur if the star is bright. Since the star we observed is bright (V = 8.9), it is important to correct for dead-time losses . To correct for this effect, we use the following equation:

$$N_0 = N exp(-\tau N) \tag{3.1}$$

where N_0 is the observed count rate in counts per second, N is the corrected count rate also in counts per second. τ is the dead-time coefficient for the counting system. On the Sutherland 0.5m photometer we have used, $\tau = 40 \times 10^{-9}$ (40 nano seconds). N is obtained using Newton's method for finding roots of equations. By application of binomial expansion to the equation above, one can get the often used dead-time correction equation:

$$N = \frac{N_0}{1 - \tau N_0} \tag{3.2}$$

This is an alternative way of performing dead time corrected counts.

3.1.2 Sky-Subtraction

As can be seen on the visibility curve shown in appendix A, most observations were done on bright nights when the moon was up. Therefore, this had to be considered while LUCY program was written to run for each night. Different simple equations can be used to subtract the sky rate from the star plus sky rate and convert to a magnitude,

3.1.3 Atmospheric extinction correction

Since there is a loss of starlight while traversing through the earth's atmosphere, atmospheric extinction also had to be considered. The extinction coefficient was not measured on every night. Instead, we used the mean extinction coefficients which are measured at Sutherland from time to time. The magnitude corrected for extinction, m_0, is calculated using,

$$m_0 = m - E_\lambda X \tag{3.3}$$

where m is the apparent magnitude, E_λ is the extinction coefficient and X is the air mass.

However, in our data, we corrected for transparency variations by subtracting the mean magnitudes of comparison stars. In Figures 3.1 – 3.6, we present the light curves for all nights before transparency correction. To perform this, the magnitudes of comparison stars had to be interpolated to the times at which our target star was observed.

3.1.4 The heliocentric time correction

In observations like these which use different filters, one should consider a time which is representative of the observations of the star as a whole. One should give individual times for the mid-exposure of each filter, but the assumption in LUCY is that we are observing objects which do not vary in brightness by a significant amount during the time taken to observe the object through all the filters.

Therefore LUCY adopts the time which lies midway between the start of the first star observation and the end of the last star observation. For example, the time midway between SAST 19:20:26 and 19:22:09 which is SAST 19:21:17.5 = UT 17:21:17.5. The fractional geocentric JD is given by (UT-12:00:00)/24 = 0.2231. This value must be added to the heliocentric time correction for the star. This is the time measured at the sun and allows for the motion of the earth around the sun. Since light from the sun takes 8 minutes to reach the earth, the maximum value of this correction is 0.0056 days, which occurs for a star in opposition on the Ecliptic. The heliocentric correction, t, is calculated as follows:

$$t = -0.0057755r\{\cos\lambda_\odot \cos\alpha \cos\delta + \sin\lambda_\odot(\sin\epsilon\sin\delta + \cos\epsilon\cos\delta\sin\alpha)\} \tag{3.4}$$

where r is the distance of the sun in astronomical units, $\lambda_{\odot}$ is the longitude of the sun, α is the RA of the star, δ is the declination of the star and ϵ is the inclination of the rotation axis of the earth.

The amount of air along the optical path of the star is proportional to *sec z* where z is the zenith distance of the star. A small correction term is added for refraction to give :

$$X = \sec z \, [1.0-0.0012 \, (\sec^2 z-1) \,] \qquad (3.5)$$

where X is the air mass.

The FORTRAN program *lucy.f* allows full reduction of LUCY data. First of all, a file is constructed a file called *lucy.inp*. This file contains the dead-time coefficient expressed in nanoseconds, filter name, filter number, extinction coefficient and zero point. We can enter this information when prompted the program will save it as file lucy.inp.

The data acquisition program LUCY saves the night's work in files with names like L6295.dat, where the number 6295 refers to the Julian day. This file must be edited to remove bad data, and this was done before going to the next step. The program will ask for the name of this file and the date, month and year of observation for each night must be entered. Then, we can have an input file to run the reduction. The program reads the L6295.dat file, extracts the star names, star counts and sky counts and writes data in a new format in a new file. This is a temporary file which is subsequently read again in a second pass. The new file contains magnitude in all filters, HJD and air mass for the target star, comparison stars and for E-rigion star.

The reduction program does dead-time correction, extinction correction and adds the zero points. It does not calculate colour equations because the program was designed for short-period variables in which differential photometry is all that is necessary.

Finally, one wants to apply transparency curve to the variable. This is done by running the program *smoothp*. For this we need to copy files like L6295.dat to stand.in as before. It then produces a transparency-corrected data file and some statistics which contain the number observations, mean values and mean offsets of the comparison stars followed by the differential magnitude for one day for the target star, for the comparison stars and for the standard star in all filters. It also shows HJD and air mass. We did the same step for all nights and selected values off the target star (HD38238) and put them together. This is the final step in the data reduction and we separated HJD and magnitude value for each filter to make it ready for frequency analysis using FAMIAS.

3.2 Light Curves

The next section shows the light curves of V351 Ori for each night (Figure 3.1) and also for all nights in all filter types. The light curve of each night was plotted daily after observations were made. This helped us to visually see the magnitude of the target star and the comparison stars and it was possible to check that we were observing the right stars. The variability of the target is also visible from the plots.

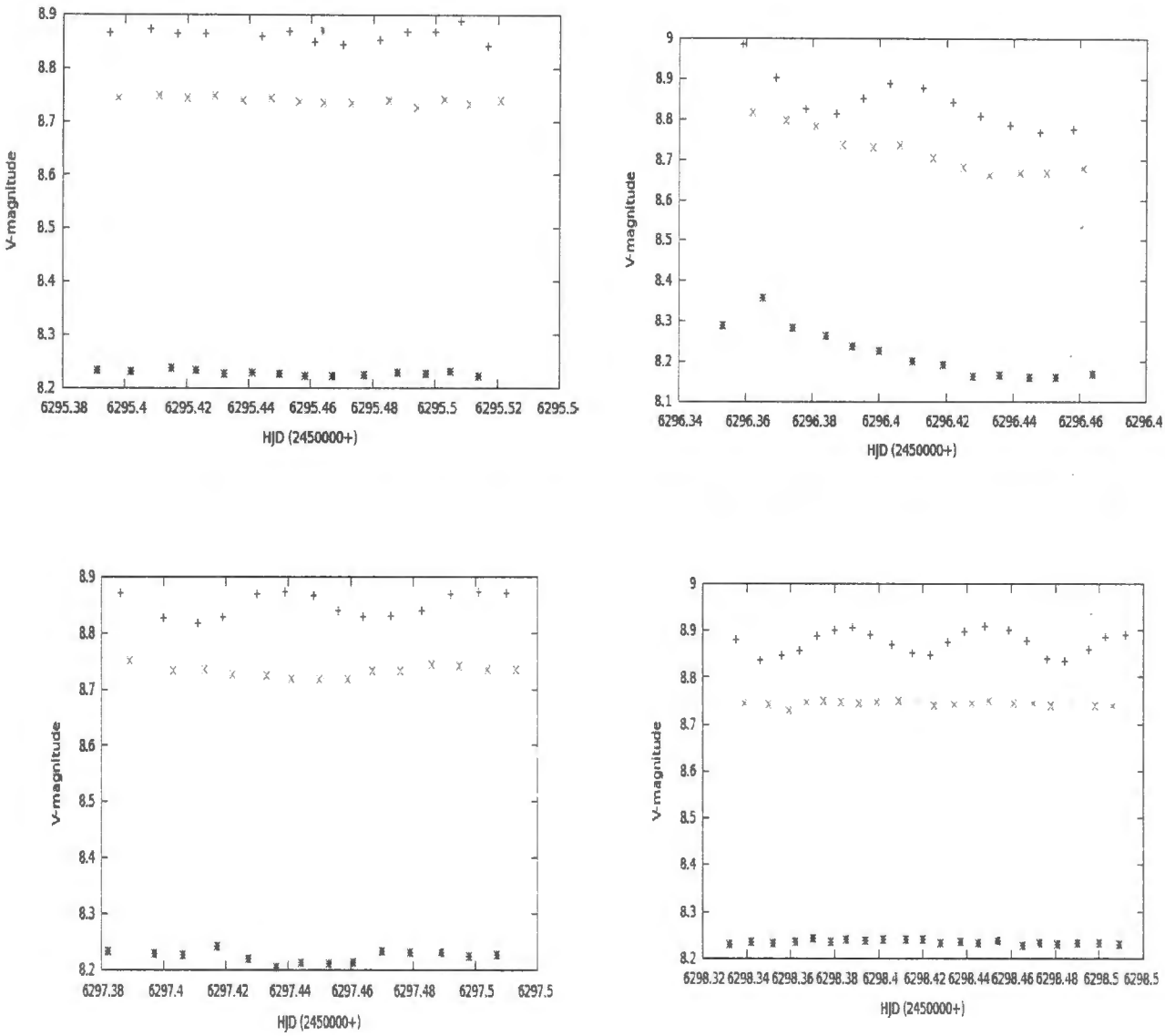

Figure 3.1: Light curves of the variable pulsating star V351 Ori (+), comparison star HD 38311 (x) and the other comparison star HD 38119 (*) in V magnitude for all nights in January and February 2013.

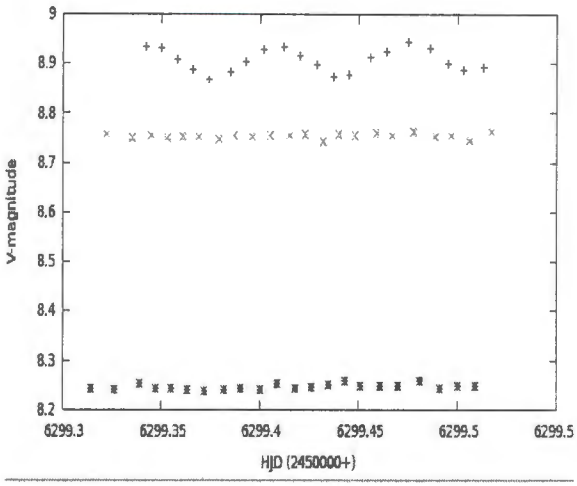

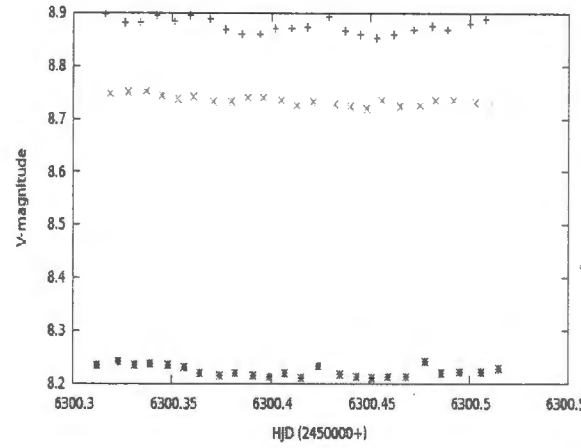

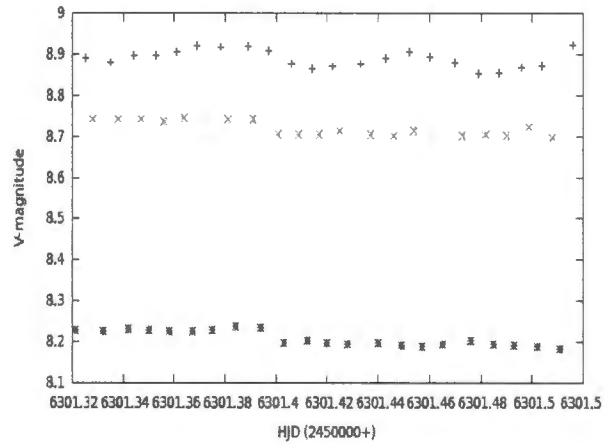

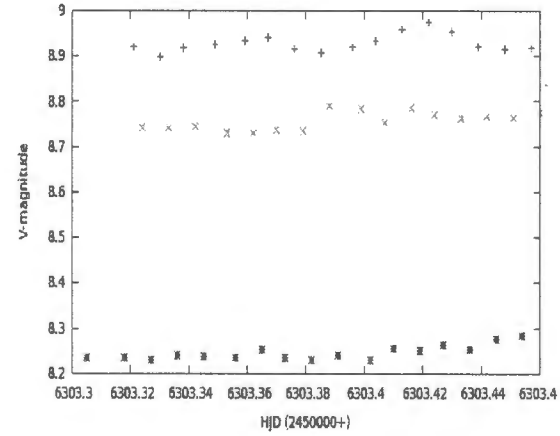

Figure 3.1: continued ...

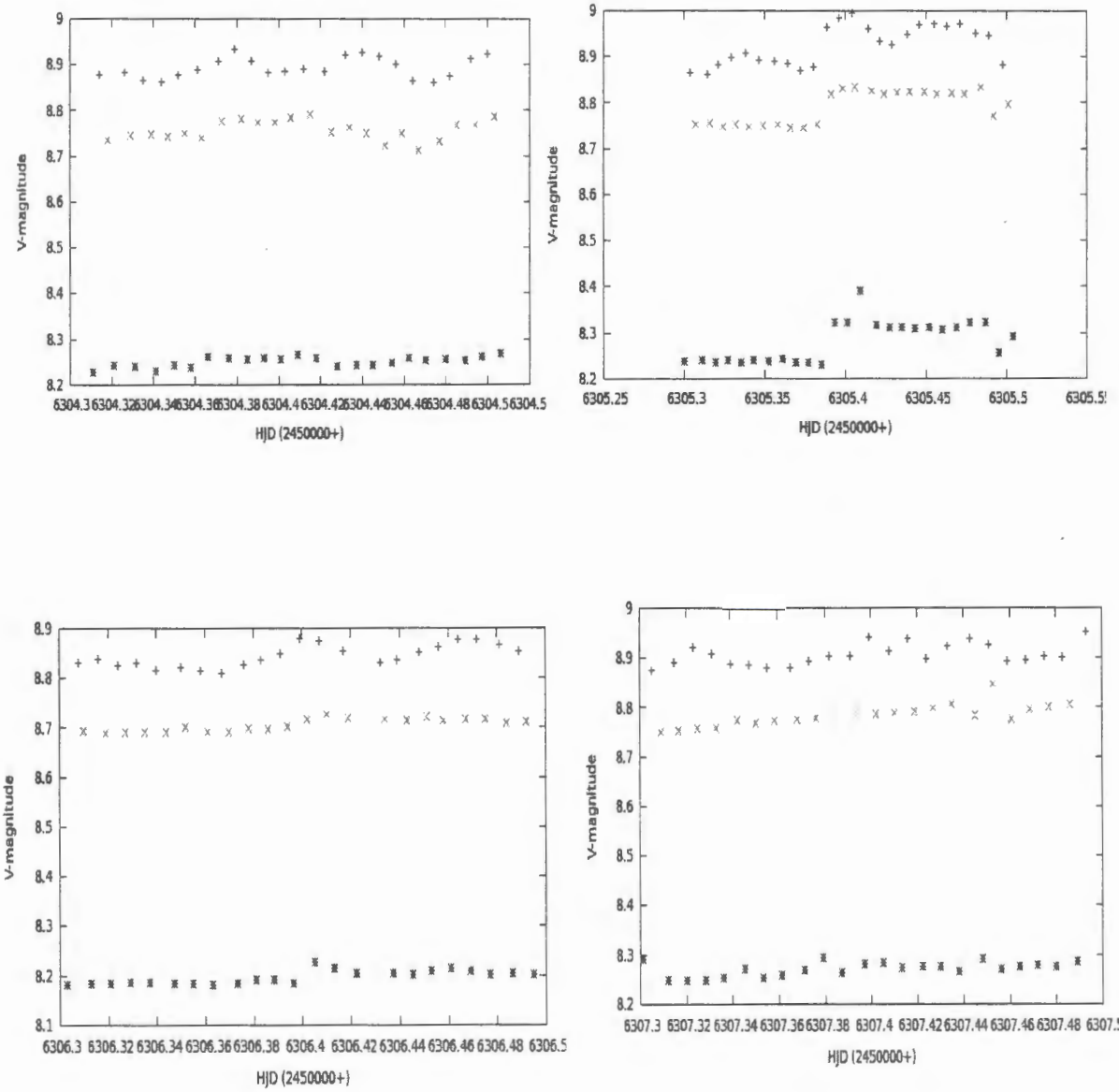

Figure 3.1: continued ....

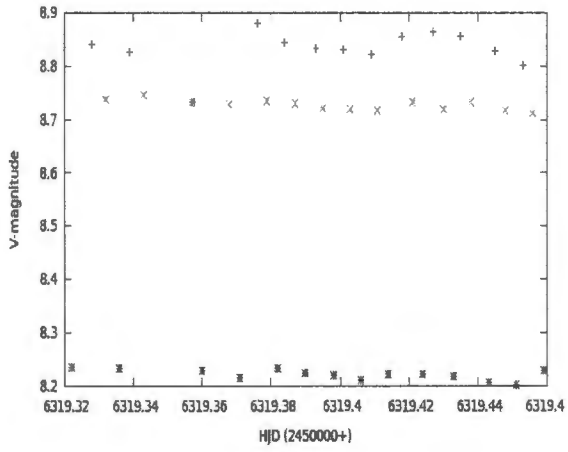

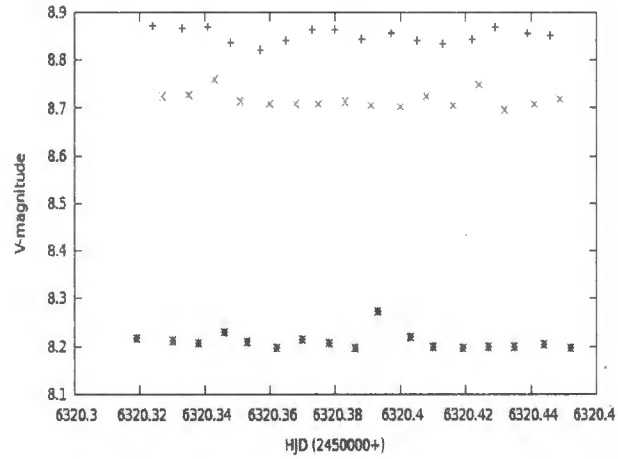

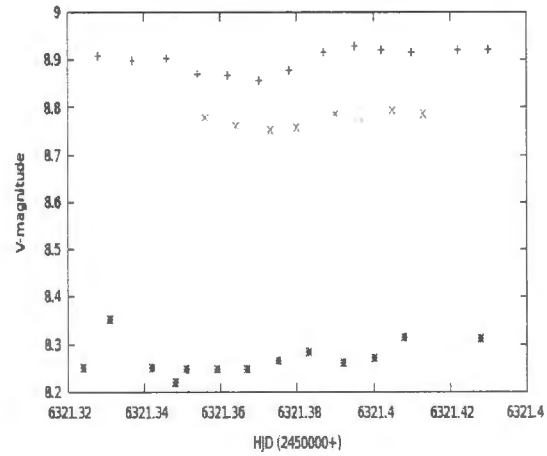

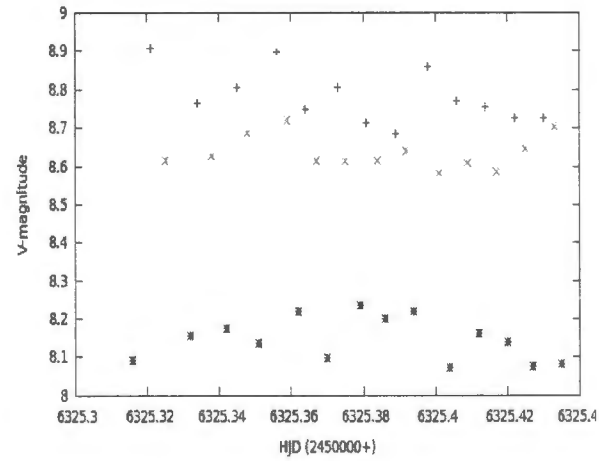

Figure 3.1: continued ....

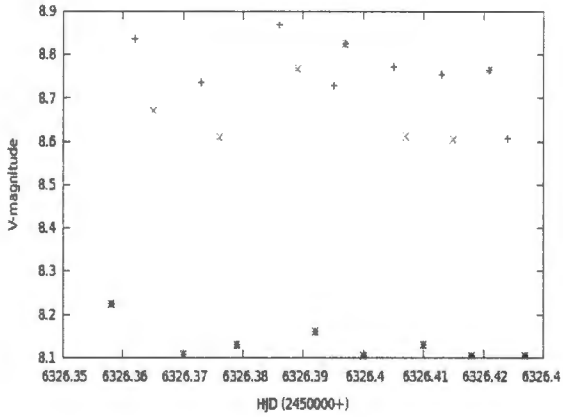

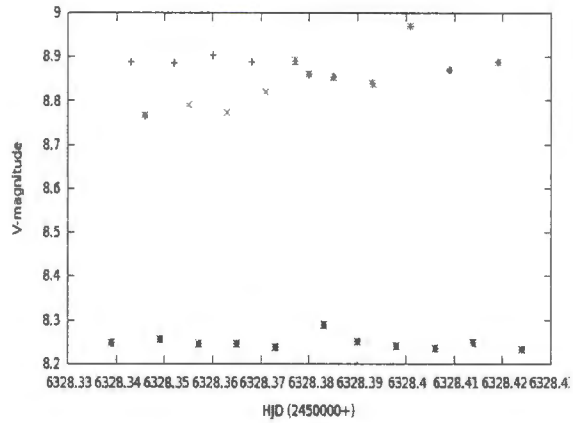

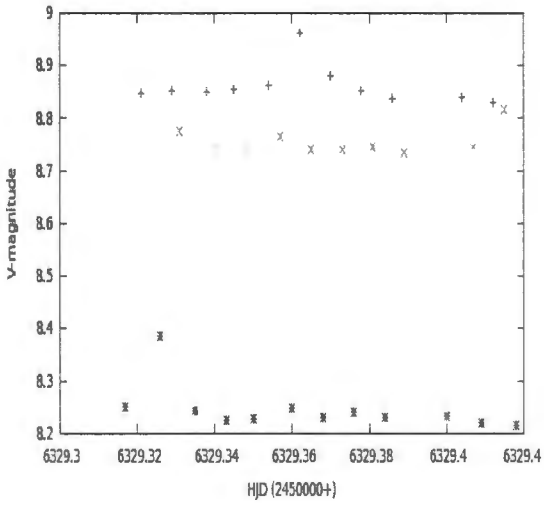

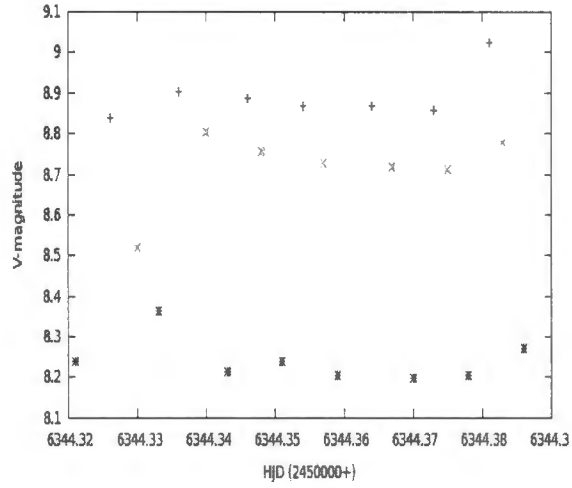

Figure 3.1: continued ....

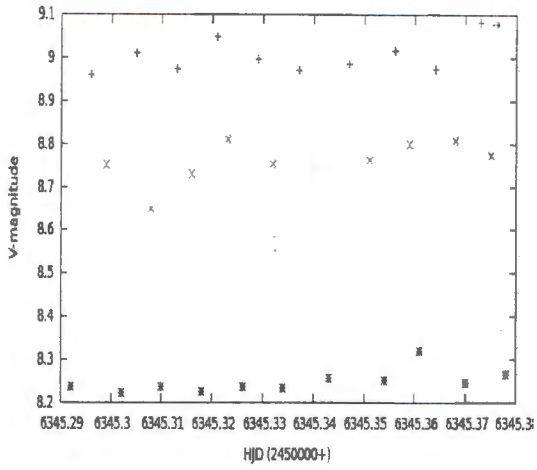

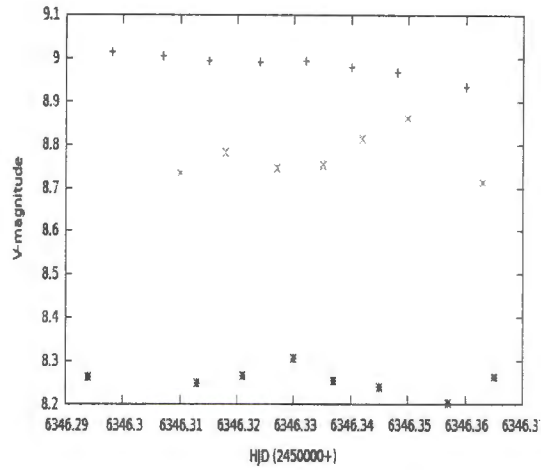

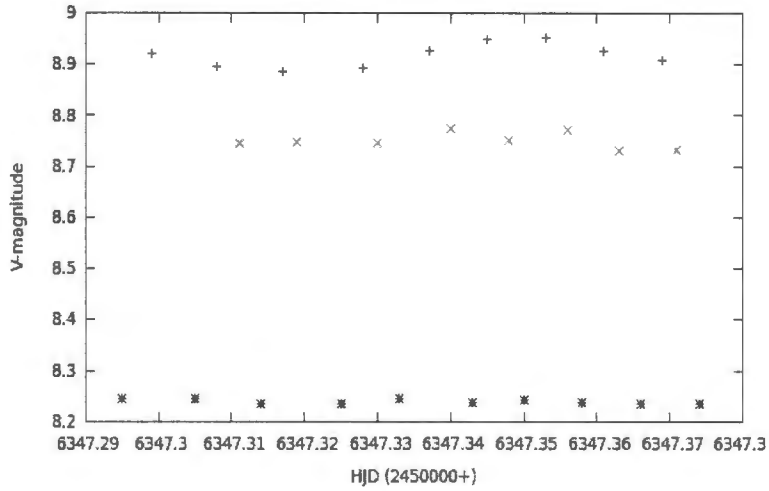

Figure 3.1: continued ….

In one of the nights the brightness of all stars (target star and comparison stars) decreased for about two hours. The next day the opposite has happened, i.e., the brightness has increased with spikes seen (for example in HJD 2456305 & HJD 2456306). This day the weather was surprisingly good. The same thing again happened in a different week for two nights. We have also seen this case on the E-region star on a different night. In the day of HJD 2456325 and HJD 2456326 (as it can be seen also from the light curves), the brightness of the target star and the comparison stars increased irregularly for some time. Specially in HJD 2456326, exceptional to the rest of the days, the temperature of the photomultiplier tube was increasing. I suspect that this might be the reason for the jumps we see in some of the light curves also. In the final week of our observation (HJD 2456344 - HJD2456347), we took an observation of about two hours only since visibility time for the target star on the sky decreased. The light curves even became some how different from the rest of previous observations. The light curve of the comparison stars seems as if the stars are variable. Actually some very thin cloud was also observed especially on the day of 2456346. These might contribute for a variability type shape on the light curve of the comparison stars in the last week of our observation.

The following light curves (Figure 3.2 – Figure 3.6) are for V351 Ori for all 23 nights in each filter. Time is in Heliocentric Julian day and the y-axis shows differential magnitude. The same light curve was obtained using FAMIAS. In Figure 3.2 (HJD 2456321) there was a power cut many times and the program (LUCY) was loosing synchronization. There was also very thin cloud that I recognized later. I don't know clearly which of these two factors might contribute for the the longer line seen on this Figure.

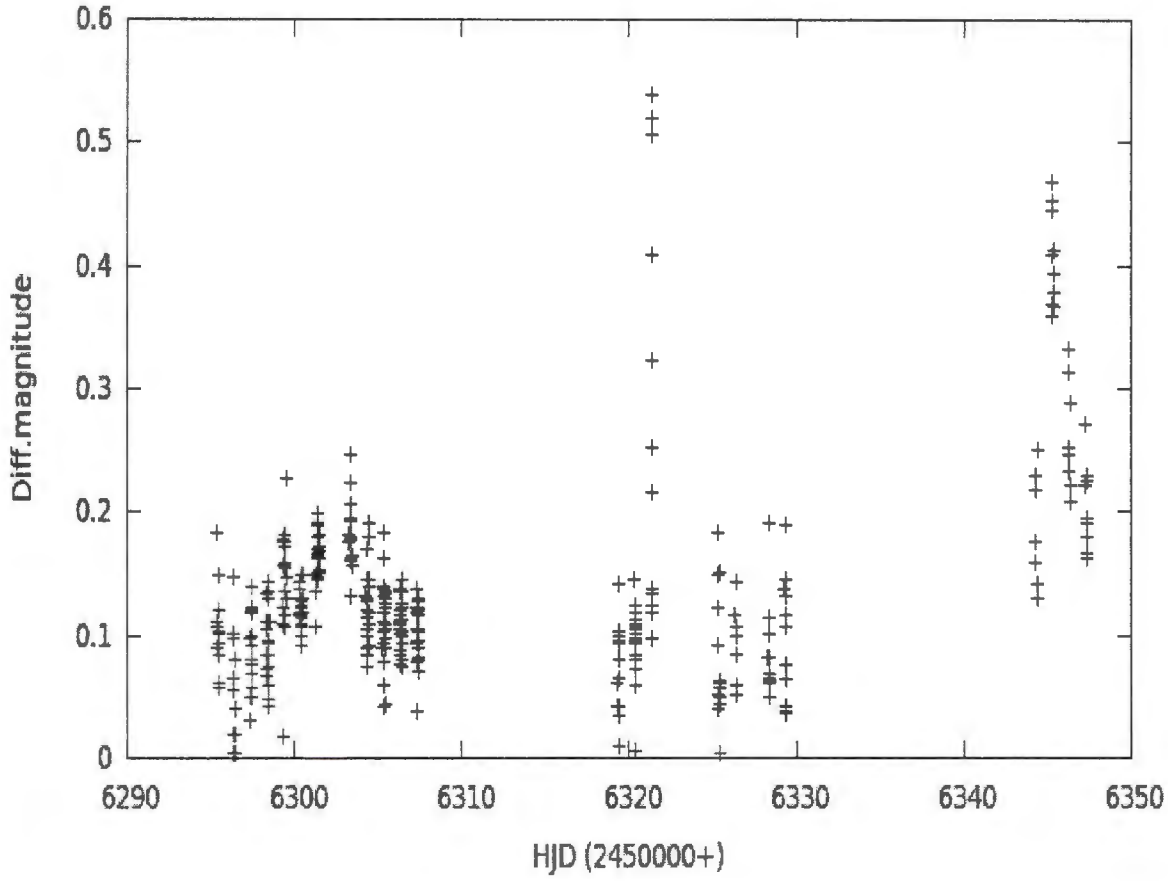

Figure 3.2 Light curve of V351 Ori in U filter for all 23 nights .

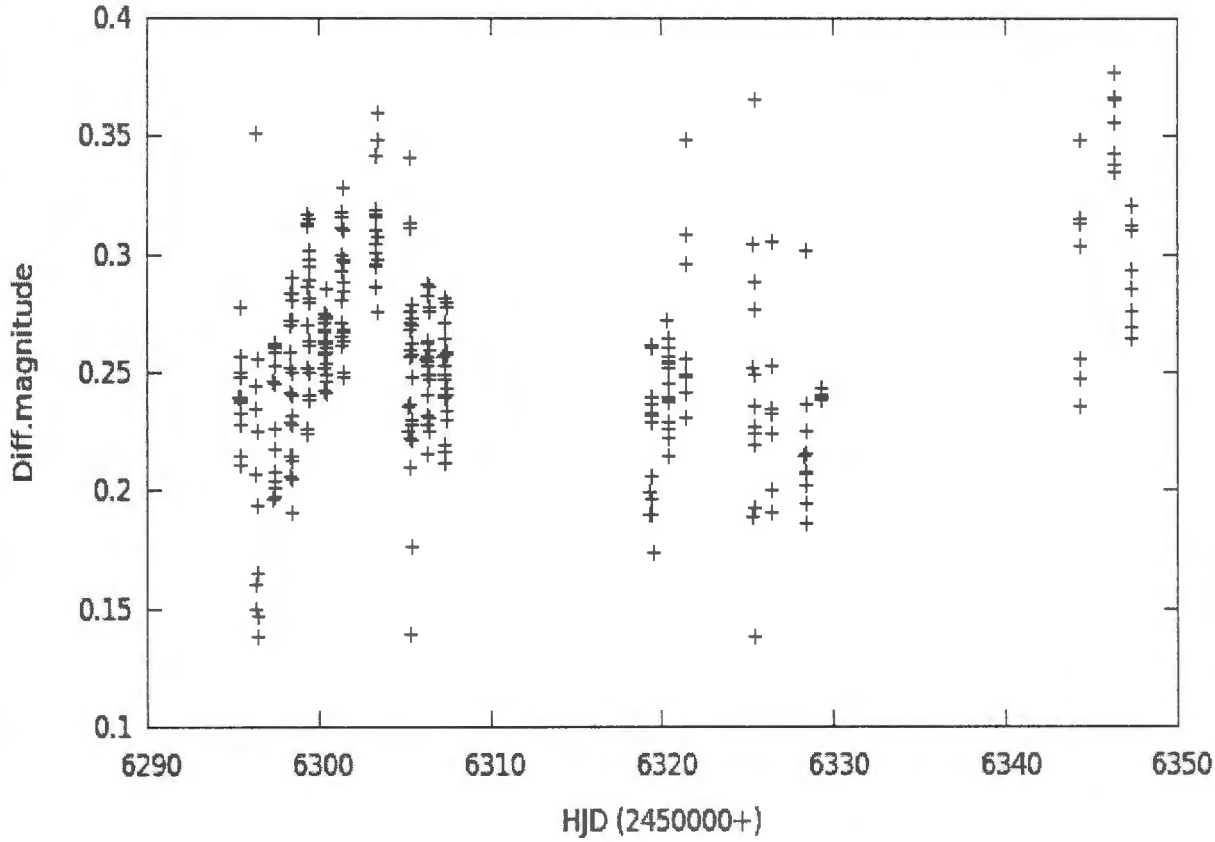

Figure 3.3: Light curve of V351 Ori in B filter for all 23 nights

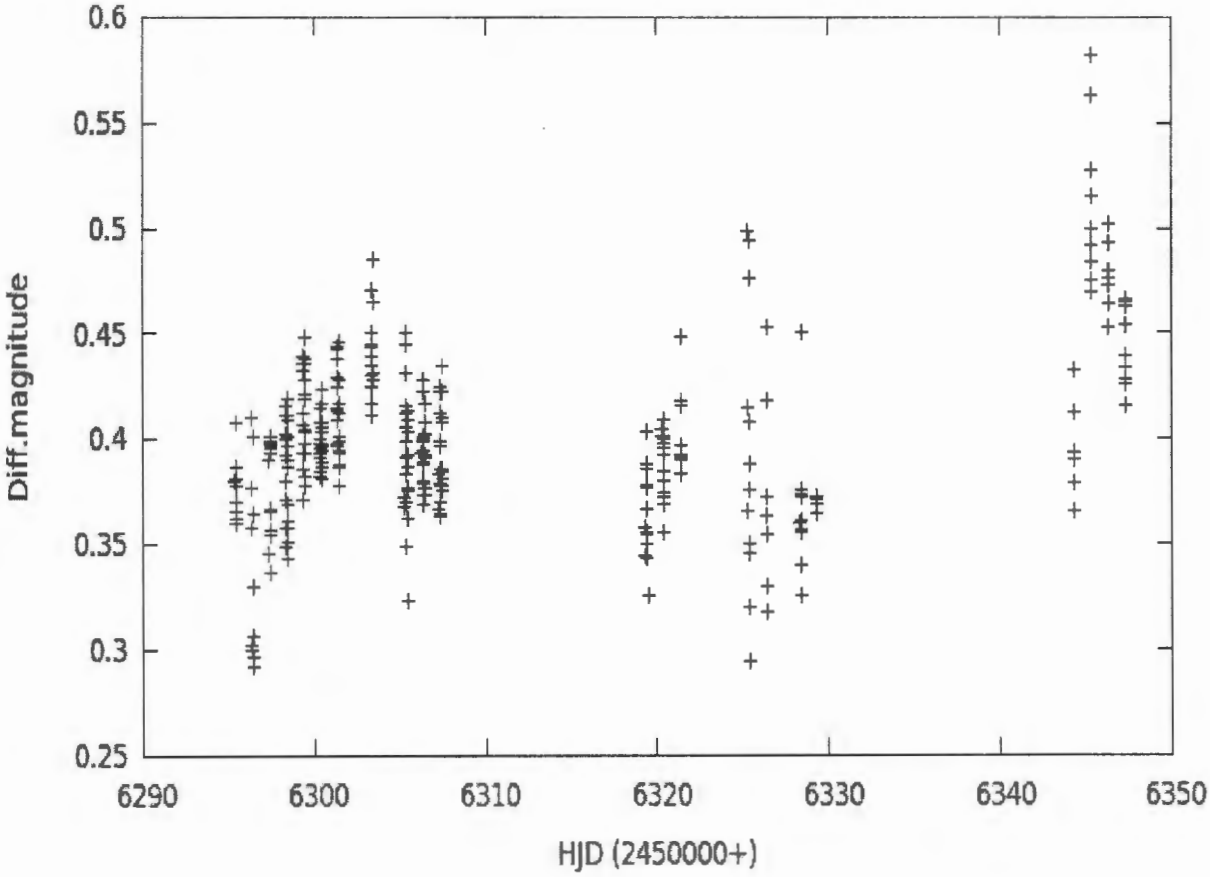

Figure 3.4: Light curve of V351 Ori in V filter for all 23 nights

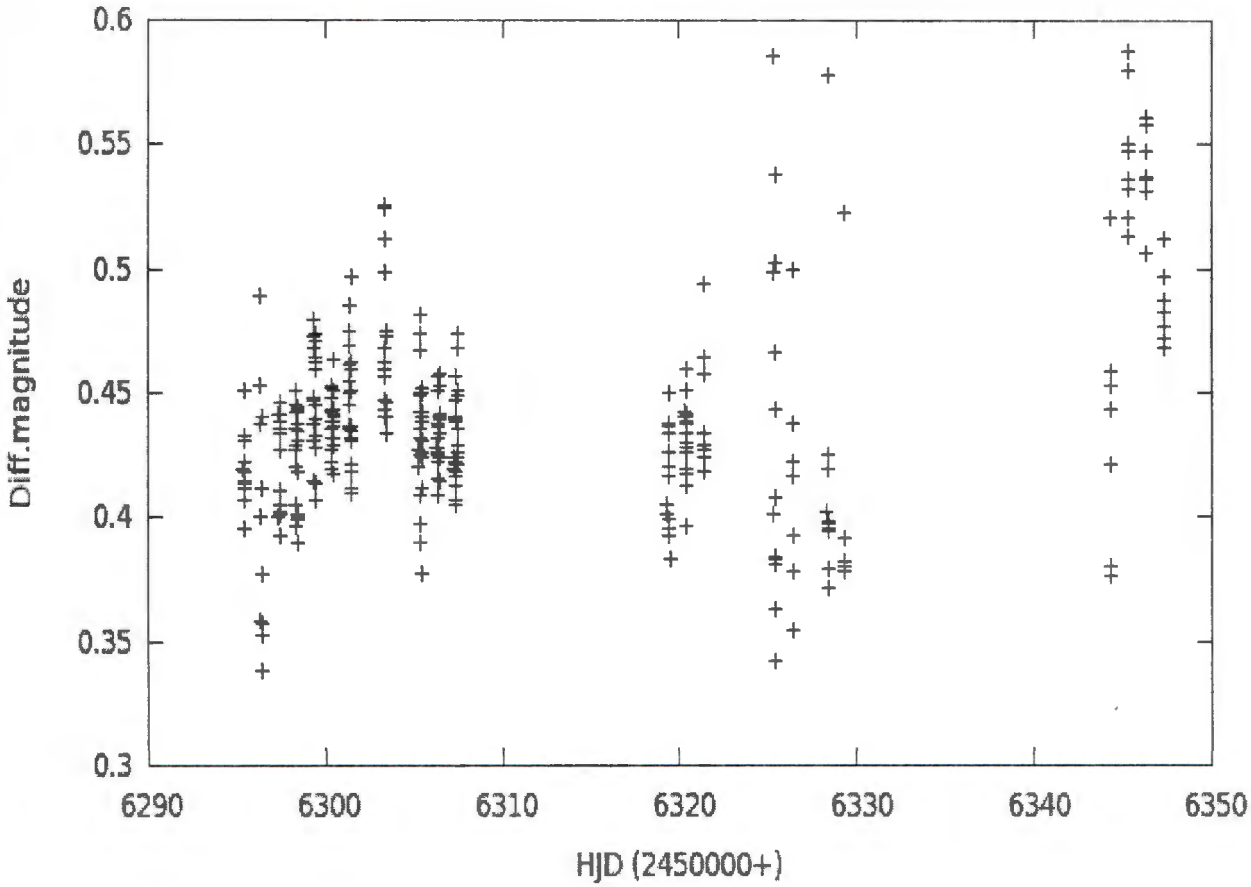

Figure 3.5 Light curve of V351 Ori in R filter for all 23 nights

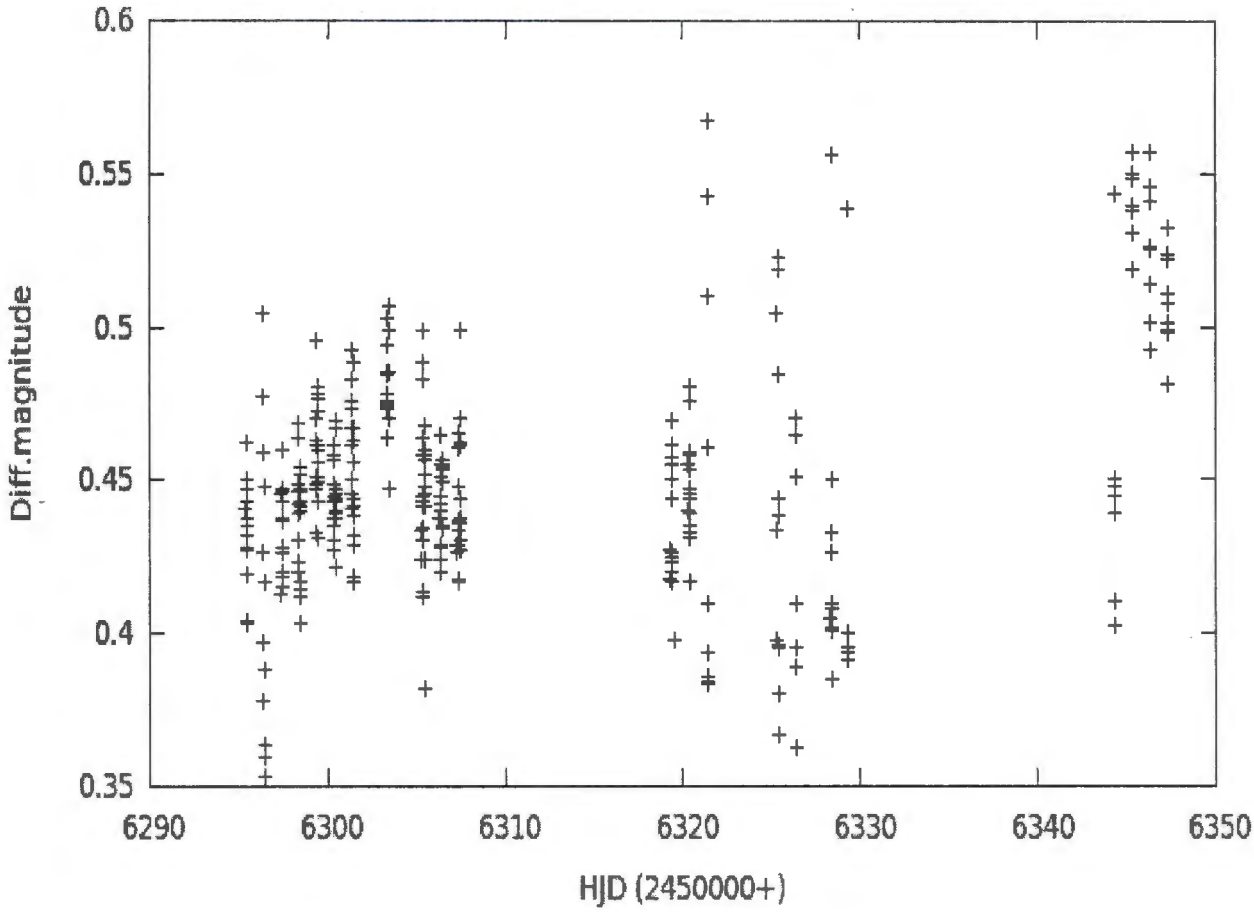

Figure 3.6 Light curve of V351 Ori in I filter for all 23 nights

Chapter 4

Analysis and Results

This chapter describes the analysis of the data reduced in chapter three. In particular, discussion of Fourier analysis and mode identification results are part of this chapter.

4.1 Fourier Spectrum and Least Squares Fitting

The data for all the nights were put together in to separate files for each filter used. We then put the data for each filter in the software FAMIAS in order to produce periodograms. With a Fourier analysis module of FAMIAS, a discrete Fourier transform (DFT) can be computed to search for periodicities. We have computed the Fourier spectrum from the minimum frequency of 10 cycles/day to the maximum value of 30 cycles/day since most predicted frequencies were in this interval and also since we couldn't get appropriate values when we take frequency interval between 0 and 30 cycles day. The spectrum is presented in Figures 4.1 - 4.5. As can be seen on each plot, the frequency value of the peak of interest having the highest amplitude is shown.

The data pre-whitened with this frequency is also computed from the pre-whitened Fourier spectrum. The summary of frequencies found, amplitude, uncertainties in amplitude, phase and uncertainties in phase for all filters are shown in Table 4.1. As can be seen from each plot, the same frequency of pulsation (about 15.6 cycles per day) is obtained in all filters which is true according to theoretical predictions given in the literature. As indicated in chapter one in Tables 1.2 up to 1.5, we can get this same frequency value in all papers which were results of photometric and spectroscopic observations.

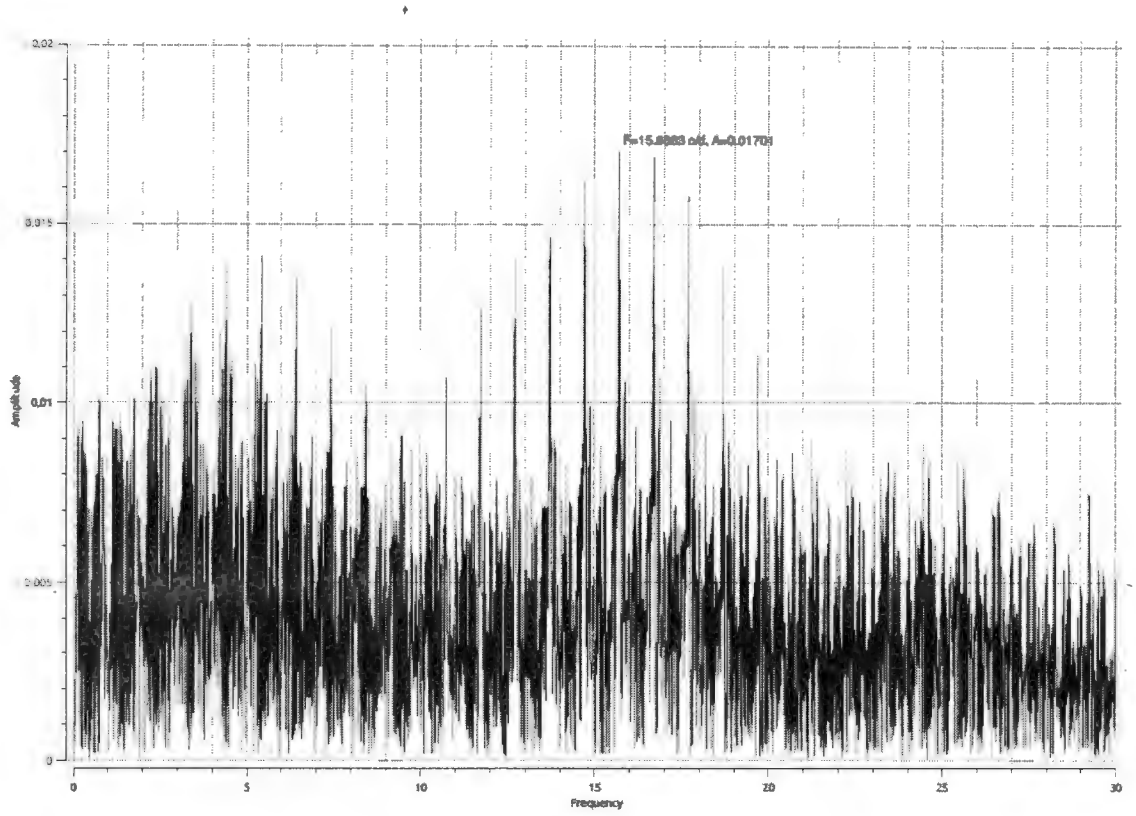

Figure 4.1: Periodogram of V351 Ori in Johnson U filter for all the nights. Frequency is in c/d and amplitude in mag. From this, we were able to detect f = 15.688 c/d with amplitude 0.017 mag. The noise level here is large (about 0.008 mag) compared to the noise level of about 0.003 mag detected by Balona et al. (2002).

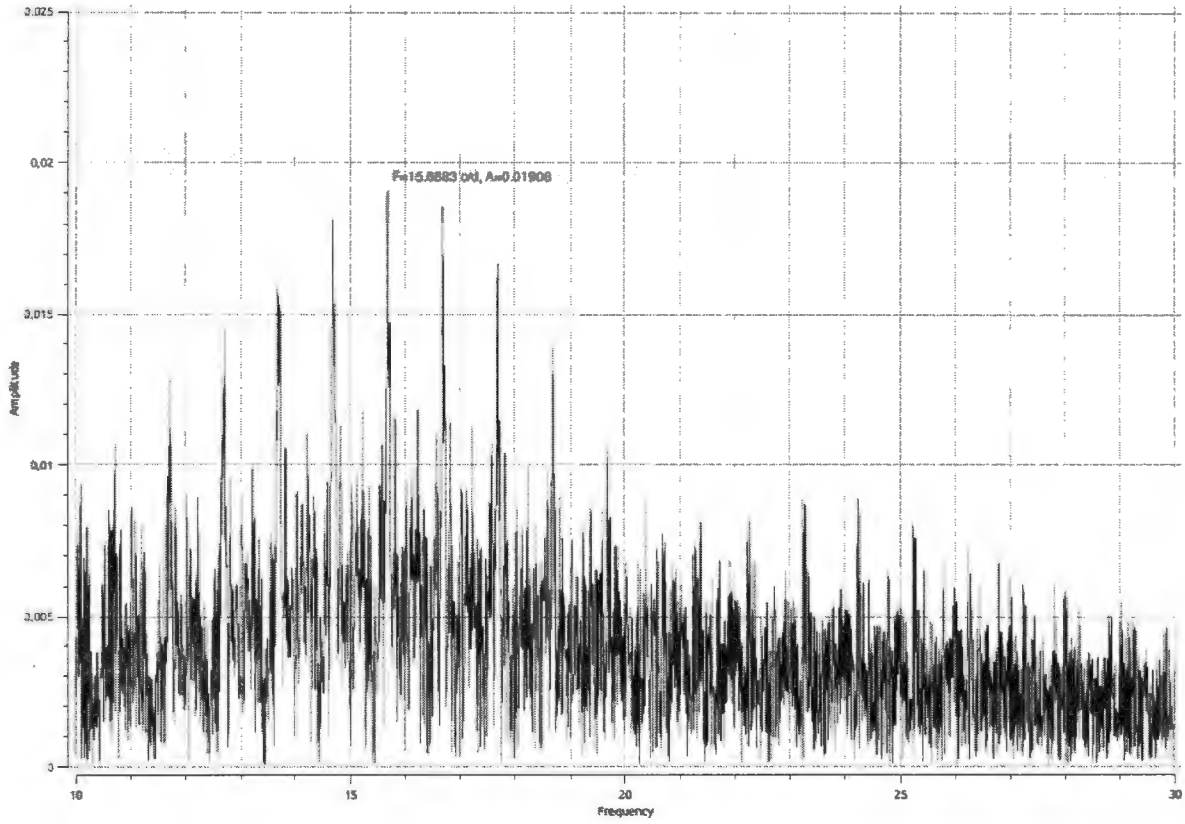

Figure 4.2 Periodogram of V351 Ori in Johnson B filter for all the nights. Frequency is in c/d and amplitude in mag. From this, we were able to detect f = 15.688 c/d with amplitude 0.0190 mag.

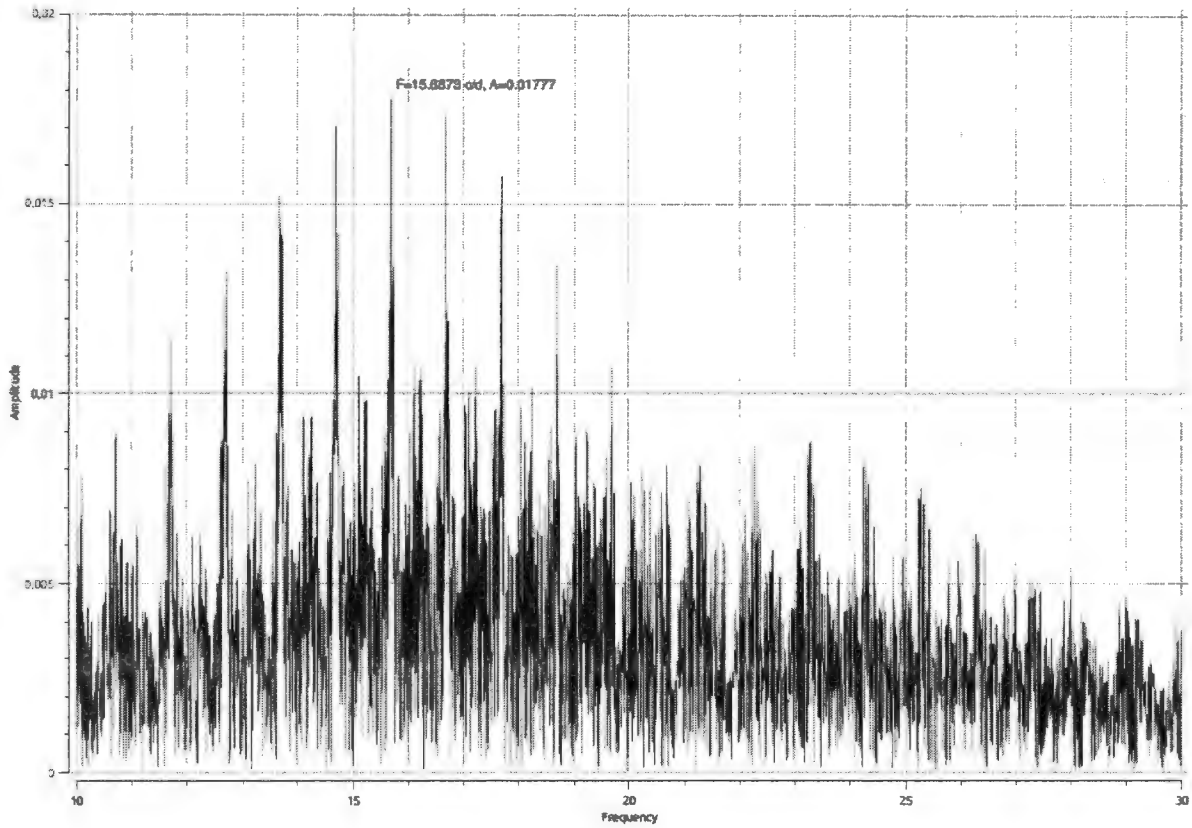

Figure 4.3 Periodogram of V351 Ori in Johnson V filter for all the nights. Frequency is in c/d and amplitude in mag. From this, we were able to detect f = 15.687 c/d with amplitude 0.0177 mag.

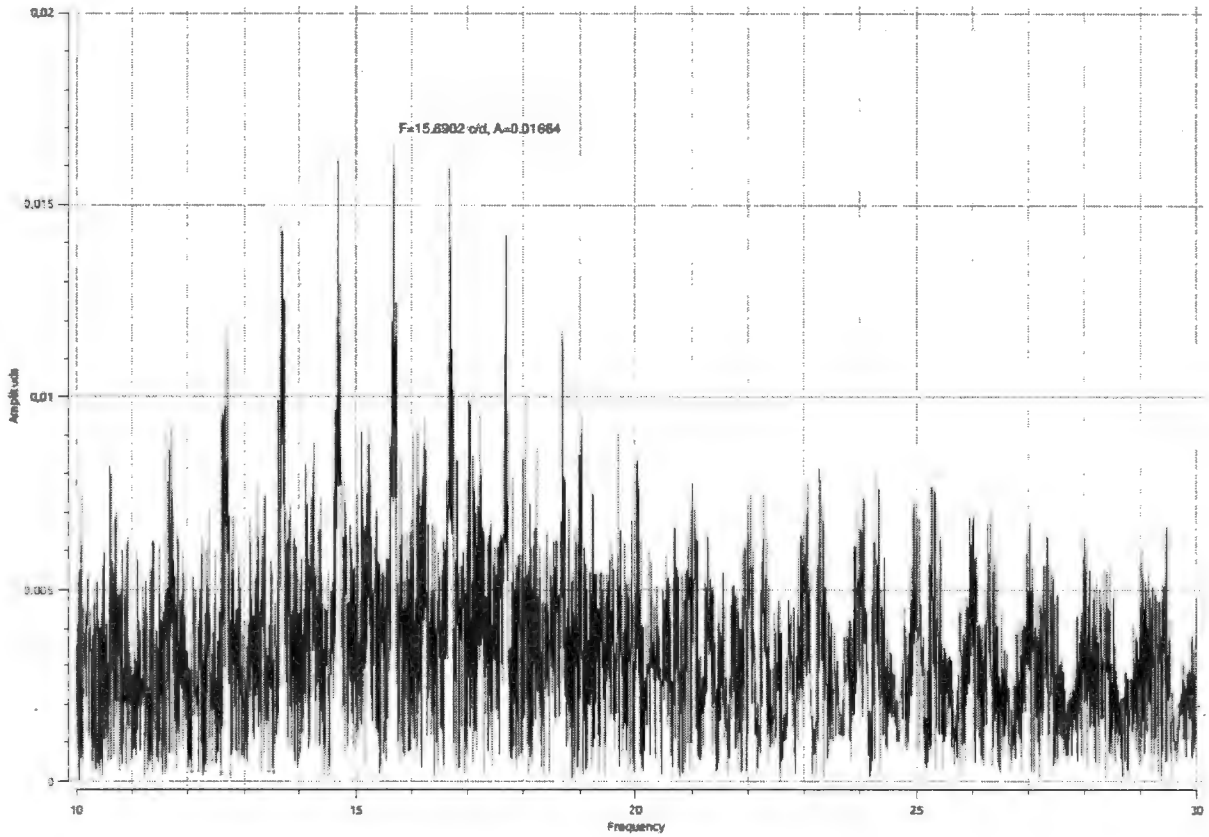

Figure 4.4: Periodogram of V351 Ori in Johnson R filter for all the nights. Frequency is in c/d and amplitude in mag. From this, we were able to detect f = 15.690 c/d with amplitude 0.0166 mag.

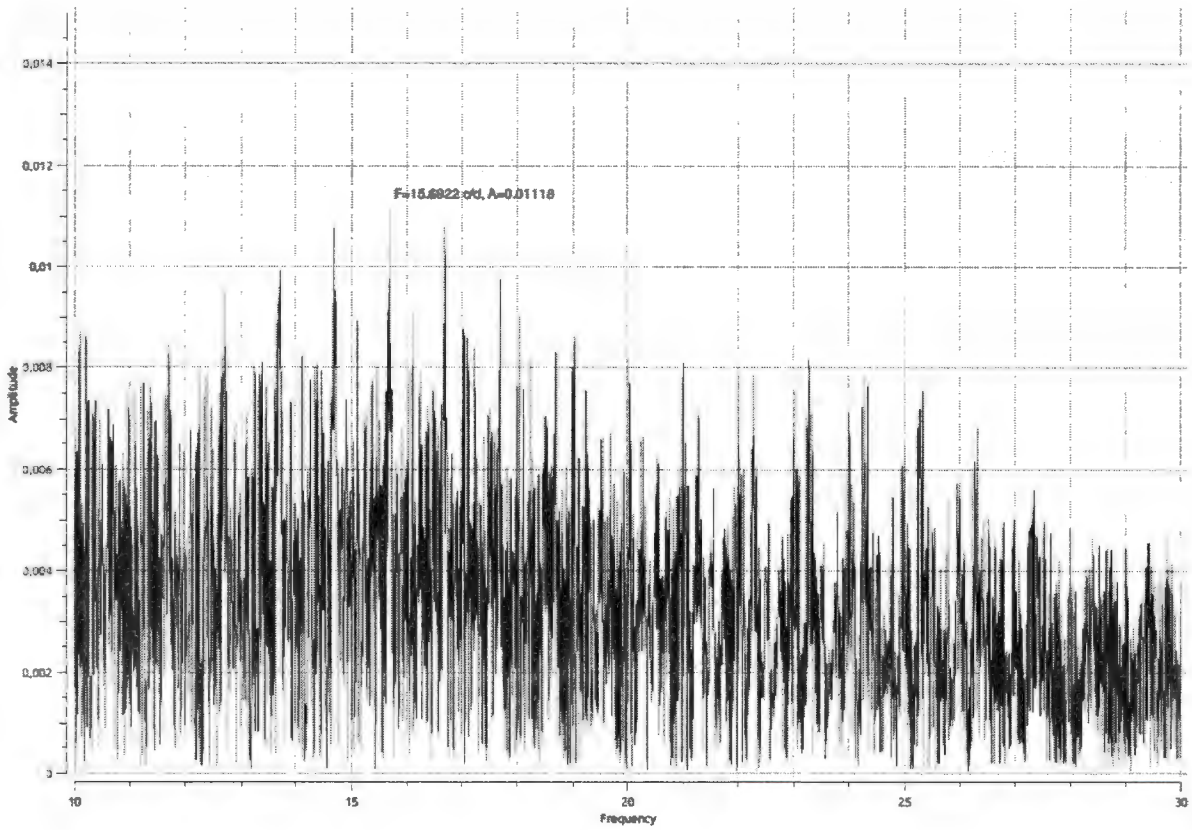

Figure 4.5: Periodogram of V351 Ori in Johnson I filter for all the nights. Frequency is in c/d and amplitude in mag. From this, we were able to detect f = 15.692 c/d with amplitude 0.0112 mag.

Table 4.1: A summary of frequencies we found in all filters. Also shown is amplitude (A) with its error, ΔA and phase (φ) with its error $\Delta \varphi$.

	f(c/d)	A (mag)	ΔA (mag)	Phase φ (radians)	$\Delta \varphi$ (radians)
U	15.686	0.0233	0.0060	0.336	0.041
B	15.688	0.0189	0.0031	0.180	0.027
V	15.687	0.0176	0.0031	0.258	0.028
R	15.689	0.0164	0.0031	0.076	0.030
I	15.692	0.0111	0.0029	0.968	0.042

We also pre-whitened the data for different frequencies in each filter. The result of pre-whitening is shown in Figures 4.6-4.10. The frequency, amplitude and phases of the pre-whitened values are also summarized as shown in Tables 4.2 – 4.6. In addition to the frequency of pulsation (15.687 c/d) which was obtained in all filters and which is also similar with theoretical models and observational results on different papers, we have got another frequency of pulsation in R filter (14. 622 c/d) with amplitude value of 9.456 mmag and (14.257 c/d) with amplitude value of 11.362 mmag. In filter I, frequency value of 14.262 c/d with amplitude value of 10.436 mmag is obtained. This frequency was also obtained in previous works like Balona et al. (2002) and Ripepi et al (2003a). The amplitude value is also almost the same.

The frequency value of 16.116 c/d seen in filter I (Table 4.6) might also be compared with frequency value of 16.27 c/d obtained by Marconi et al. (2001). Frequency 12.704 c/d found in filter V (Table 4.4) is also comparable with frequency 12.817 c/d found by Ripepi et al. (2003a). The following frequencies were also obtained which are not mentioned in literature: 15.317 c/d and 17.303 c/d in U filter, 15.842 c/d and 15.332 c/d in B filter, 17.038 c/d and 15.357 c/d in V filter, 15.112 c/d in R filter and finally 22.002 c/d in I filter.

Phase diagrams are given in Figures 4.11- 4.15. These diagrams show the various phases of the frequency values mentioned under each plot and generally used to visualize and illustrate the conditions under which the frequency is present in a certain phase and changes to another phase.

Table 4.2 Frequencies, amplitudes and phases derived from the Fourier analysis of the data in U filter.

Frequency (c/d)	Amplitude (mag)	ΔA (mag)	Phase φ (radians)	Δ φ (radians)
15.686	0.0263	0.0058	0.3207	0.0352
15.317	0.0216	0.0062	0.3629	0.0457
17.303	0.0193	0.0062	0.0949	0.0512

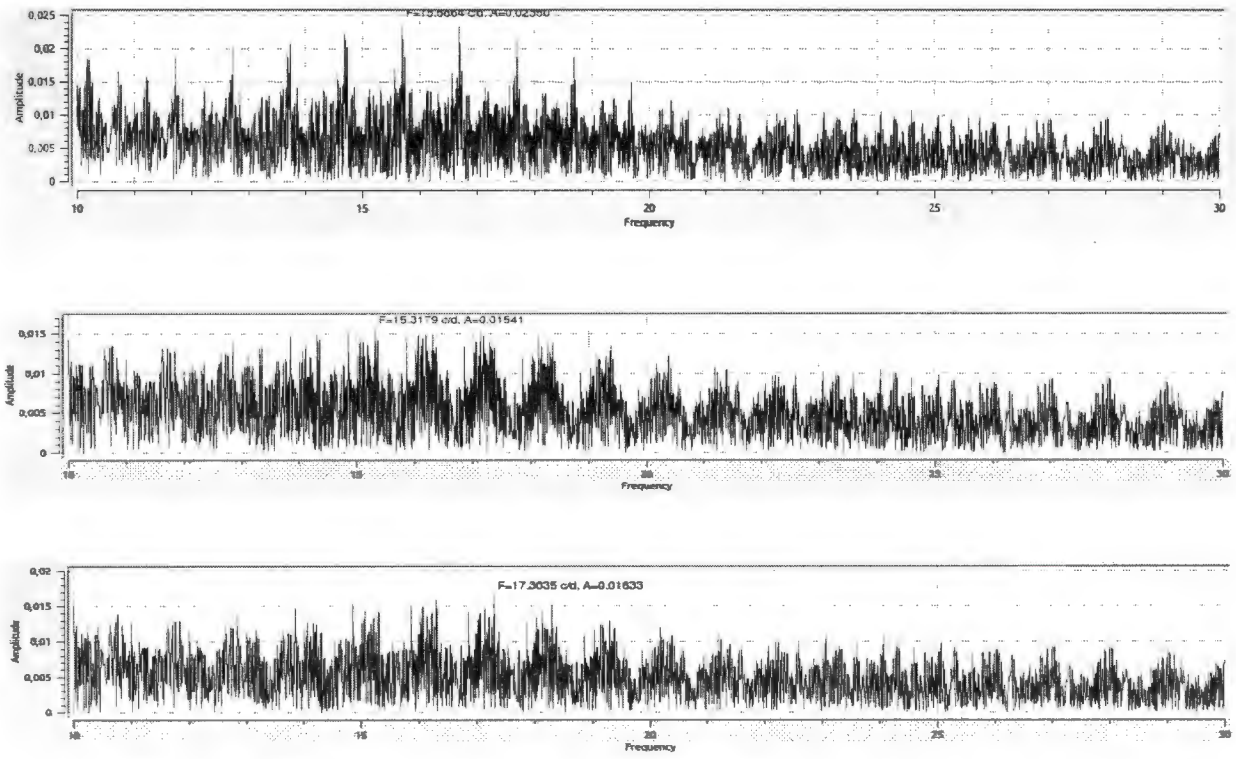

Figure 4.6 Periodograms of UBVRI photometry. The top panel is the periodogram of the unmodified data. Subsequent panels show the periodogram sequentially pre-whitened by frequencies 15.317 c/d and 17.303 c/d.

Table 4.3 Frequencies, amplitudes and phases derived from the Fourier analysis of the data in B filter.

Frequency (c/d)	Amplitude (mag)	ΔA (mag)	Phase φ (radians)	Δ φ (radians)
15.688	0.0237	0.0031	0.1523	0.0212
15.842	0.0144	0.0032	0.8234	0.0356
15.332	0.0123	0.0031	0.3272	0.0395

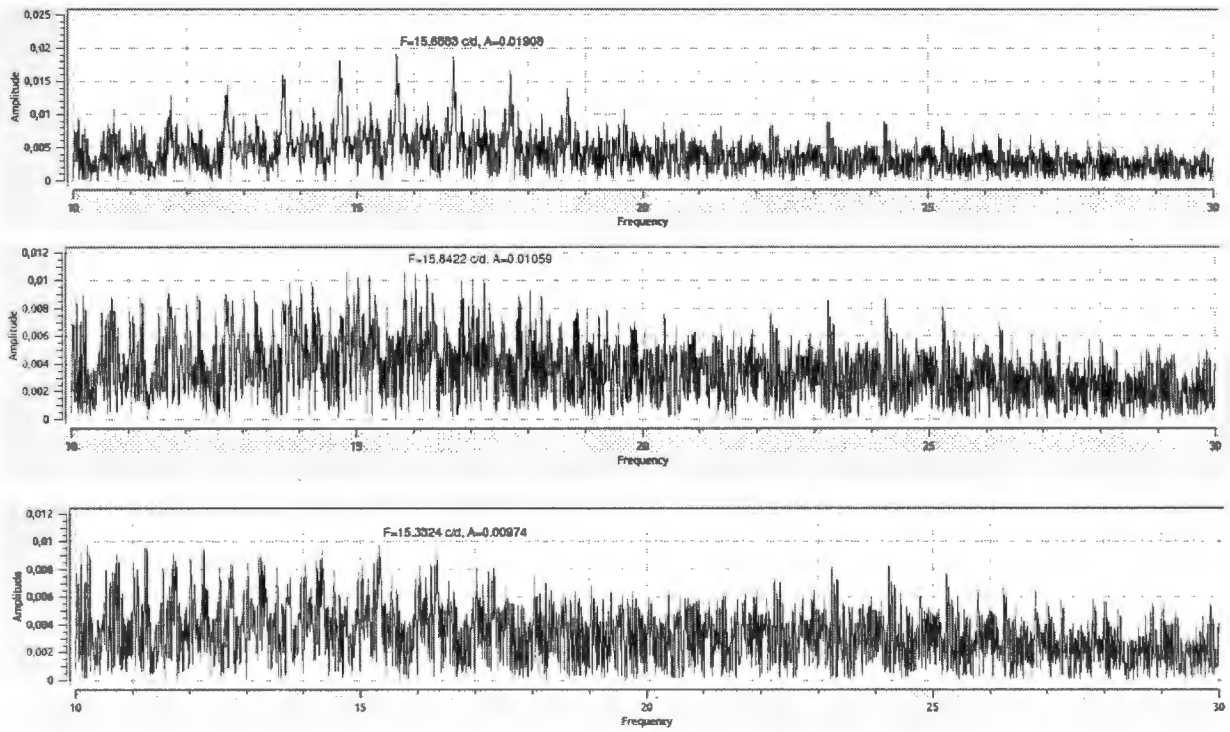

Figure 4.7 Periodograms of UBVRI photometry. The top panel is the periodogram of the unmodified data. Subsequent panels show the periodogram sequentially pre-whitened by frequencies 15.842 c/d and 15.332 c/d.

Table 4.4 Frequencies, amplitudes and phases derived from the Fourier analysis of the data in V filter.

Frequency (c/d)	Amplitude (mag)	ΔA (mag)	Phase φ (radians)	Δ φ (radians)
15.687	0.0175	0.0030	0.2349	0.0280
17.038	0.0110	0.0029	0.8527	0.0436
15.357	0.0114	0.0031	0.8211	0.0437
12.704	0.0102	0.0030	0.5253	0.0475

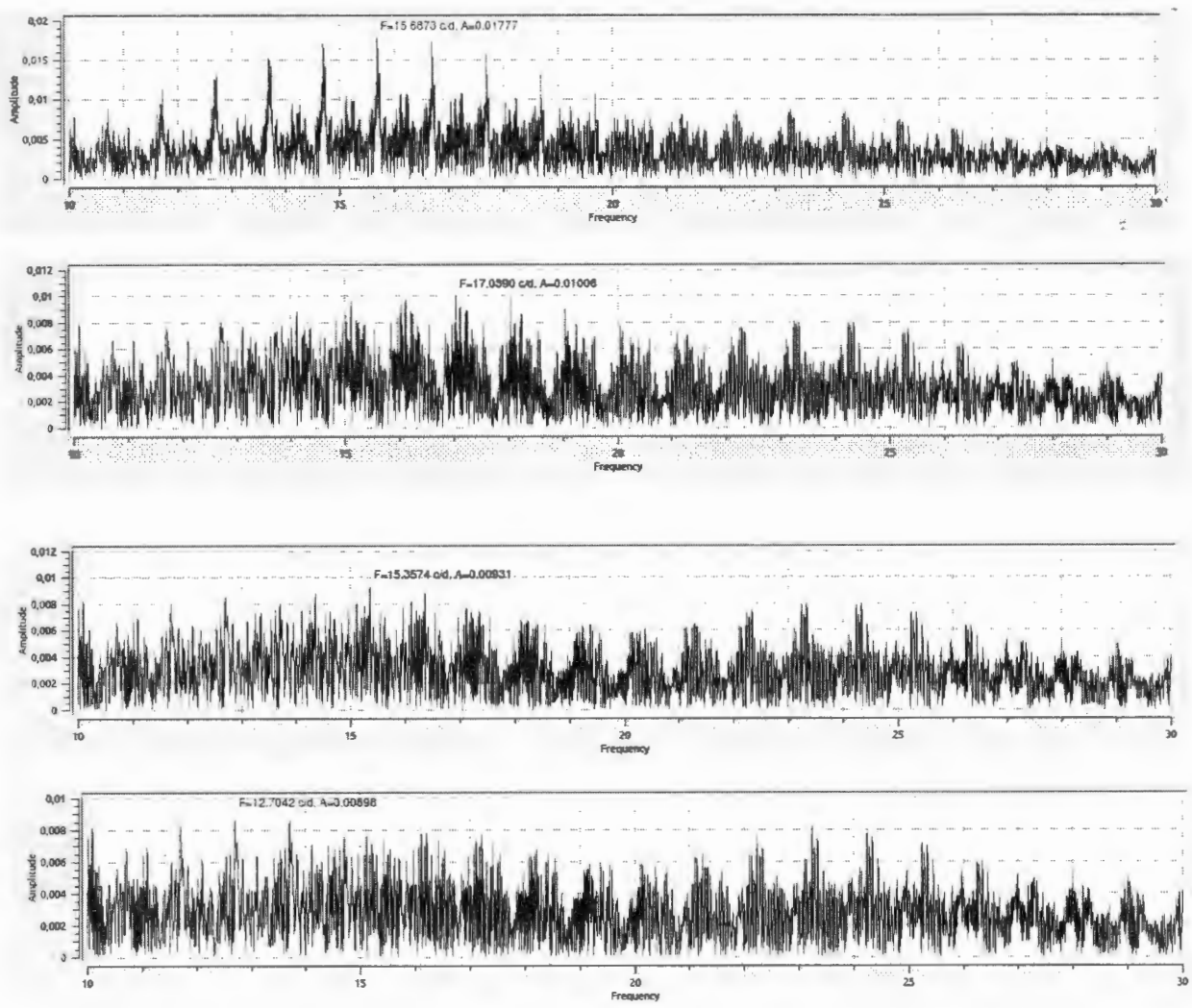

Figure 4.8 Periodograms of UBVRI photometry. The top panel is the periodogram of the unmodified data. Subsequent panels show the periodogram sequentially pre-whitened by frequencies 17.038c/d, 15.357 c/d and 12.704 c/d.

Table 4.5 Frequencies, amplitudes and phases derived from the Fourier analysis of the data in R filter.

Frequency (c/d)	Amplitude (mag)	ΔA (mag)	Phase φ (radians)	Δ φ (radians)
15.690	0.0152	0.0030	0.0767	0.0321
14.622	0.0094	0.0031	0.6383	0.0532
14.257	0.0113	0.0032	0.2538	0.0456
15.112	0.0108	0.0032	0.4735	0.0473

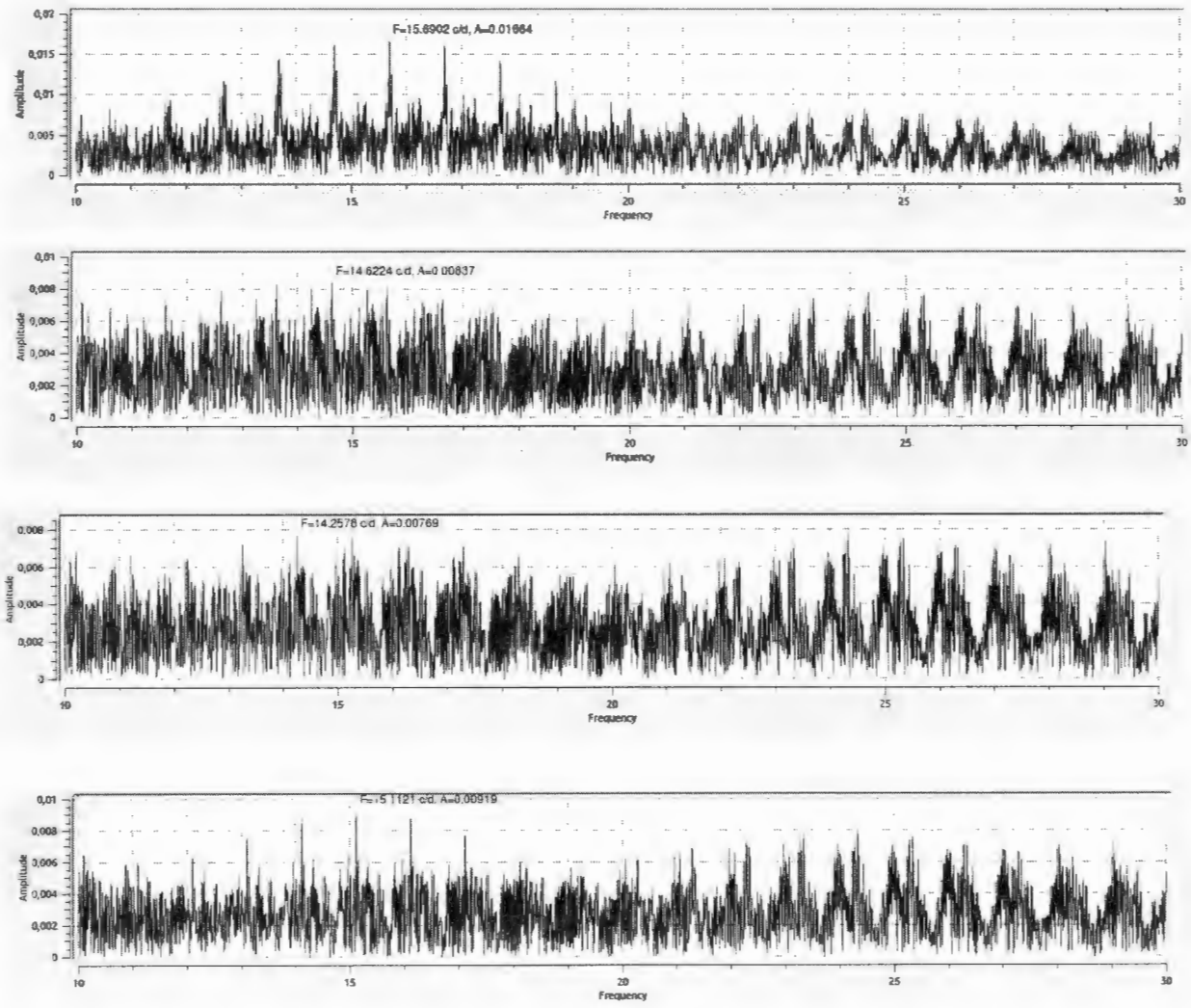

Figure 4.9 Periodograms of UBVRI photometry. The top panel is the periodogram of the unmodified data. Subsequent panels show the periodogram sequentially pre-whitened by frequencies 14.622 c/d, 14.257c/d and 15.112 c/d.

Table 4.6 Frequencies, amplitudes and phases derived from the Fourier analysis of the data in I filter.

Frequency (c/d)	Amplitude (mag)	ΔA (mag)	Phase φ (radians)	Δ φ (radians)
15.692	0.0102	0.0027	0.9518	0.0435
16.116	0.0128	0.0028	0.7355	0.0360
14.262	0.0104	0.0028	0.8978	0.0443
22.002	0.0083	0.0027	0.2615	0.0528

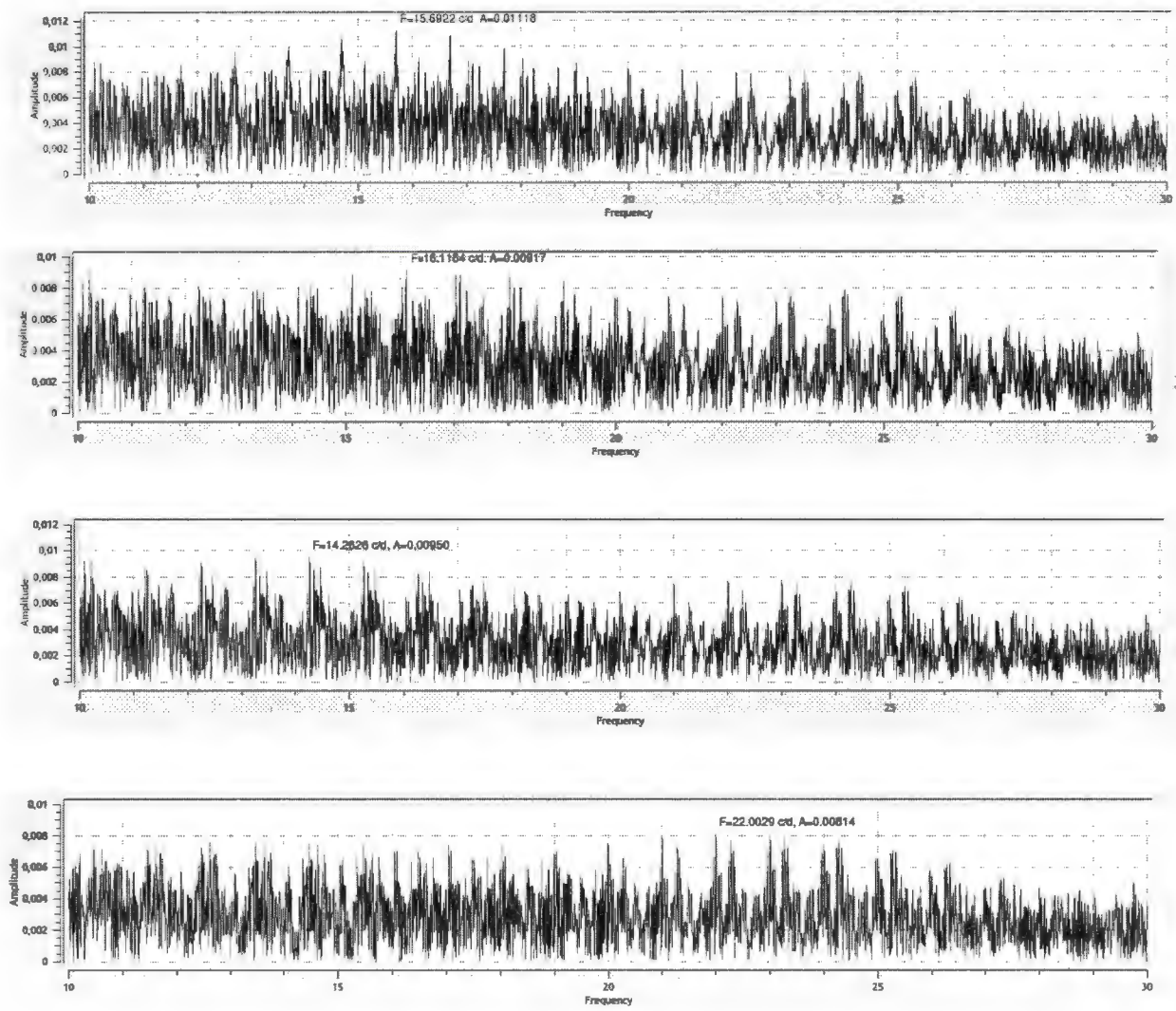

Figure 4.10 Periodograms of UBVRI photometry. The top panel is the periodogram of the unmodified data. Subsequent panels show the periodogram sequentially pre-whitened by frequencies 16.116 c/d, 14.262 c/d and 22.002 c/d.

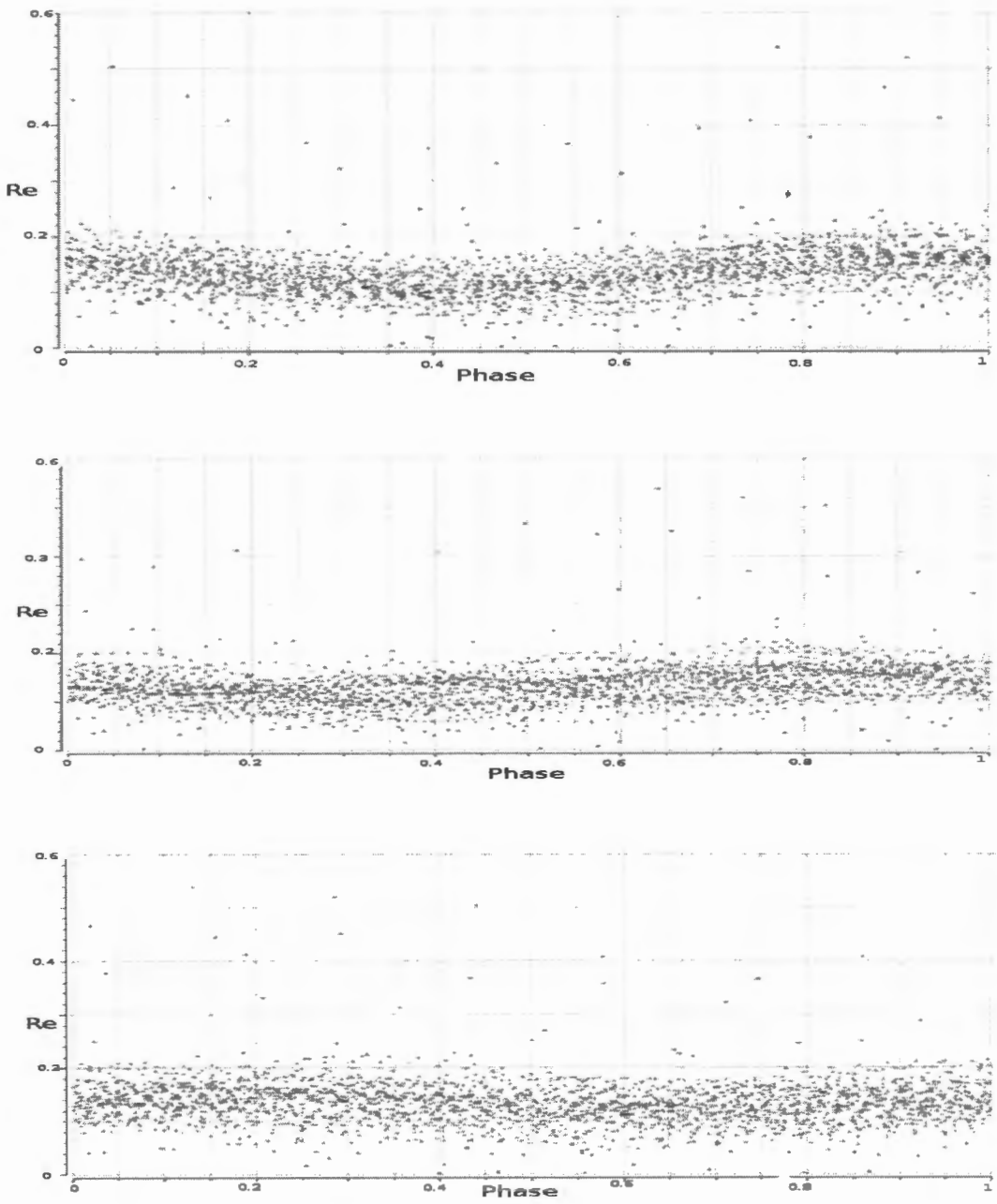

Figure 4.11 Phase plots for the three frequencies listed in Table 4.2 for filter U. From top to bottom the data has been phased using frequencies 15.686 c/d, 15.317 c/d and 17.303 c/d. Phase is given in units of period and y-axis (Re) shows residuals of Johnson U.

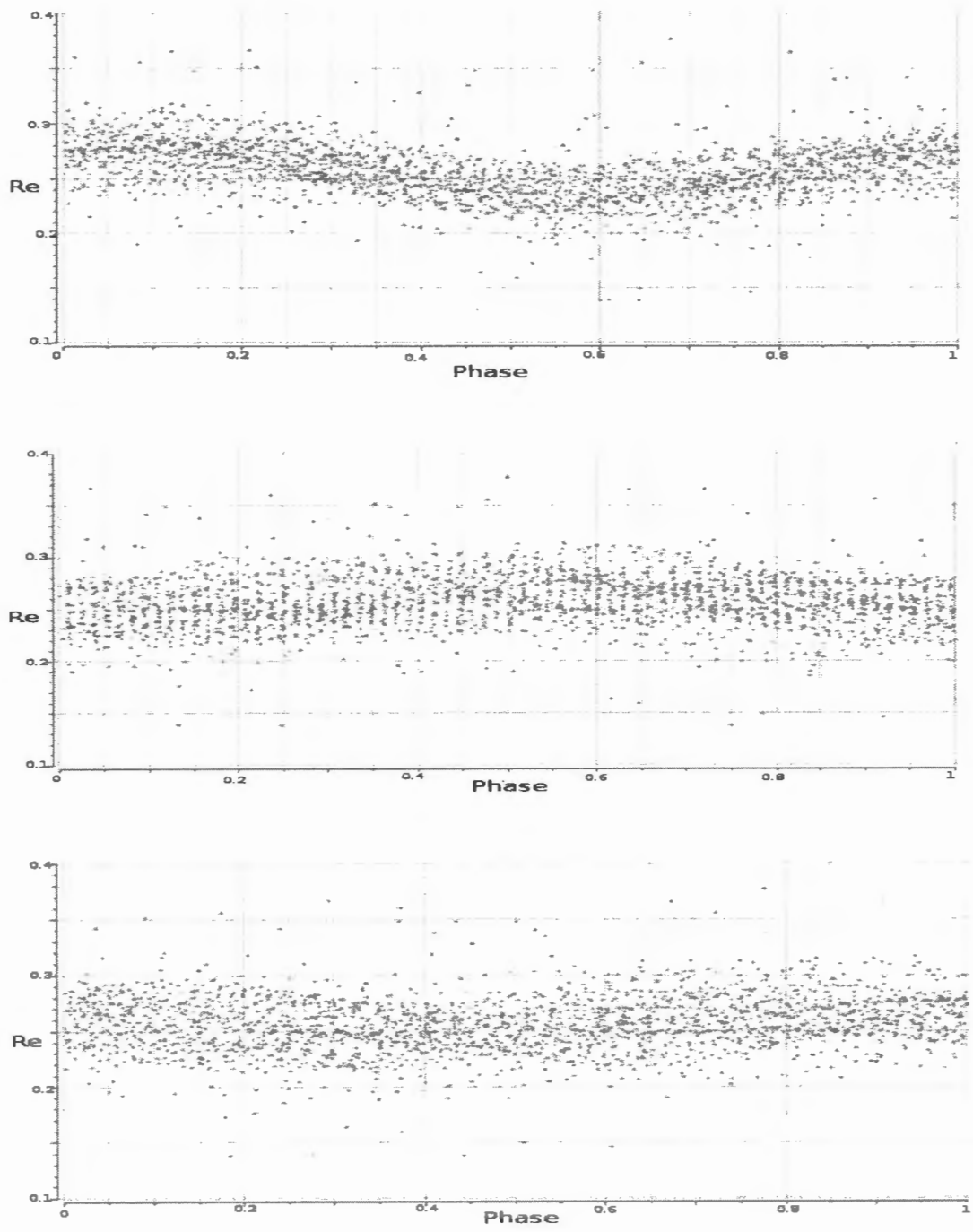

Figure 4.12 Phase plots for the three frequencies listed in Table 4.3 for filter B. From top to bottom the data has been phased using frequencies 15.688 c/d, 15.842 c/d, and 15.332 c/d. Phase is given in units of period and y-axis (Re) shows residuals of Johnson B.

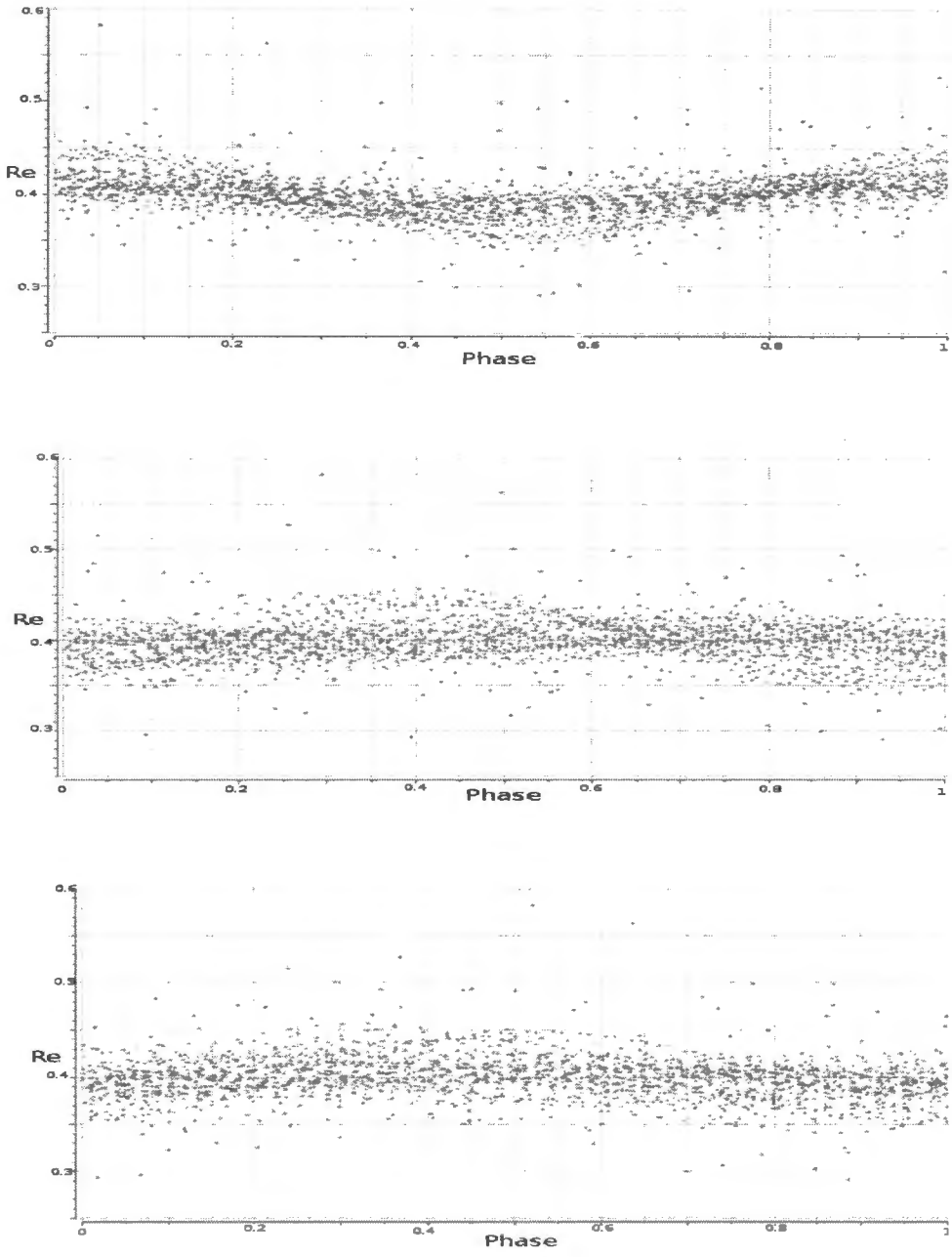

Figure 4.13 Phase plots for the first three frequencies listed in Table 4.4 in filter V. From top to bottom the data has been phased using frequencies15.687 c/d, 17.038 c/d, & 15.357 c/d. Phase is given in units of period and y-axis (Re) shows residuals of Johnson V.

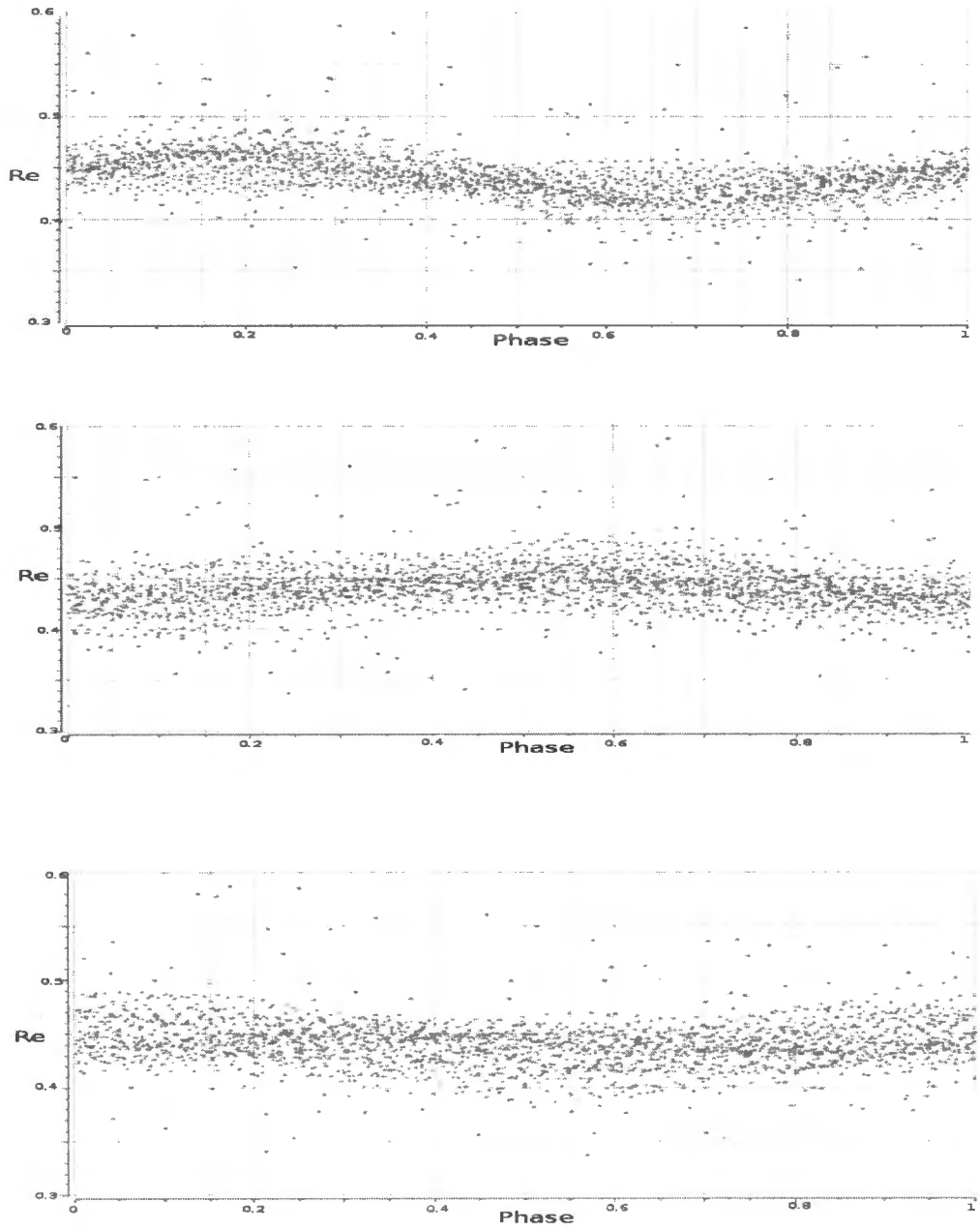

Figure 4.14 Phase plots for the first three frequencies listed in Table 4.5 in filter R. From top to bottom the data has been phased using frequencies 15.690 c/d, 14.622 c/d & 14.257 c/d. Phase is given in units of period and y-axis (Re) shows residuals of Johnson R.

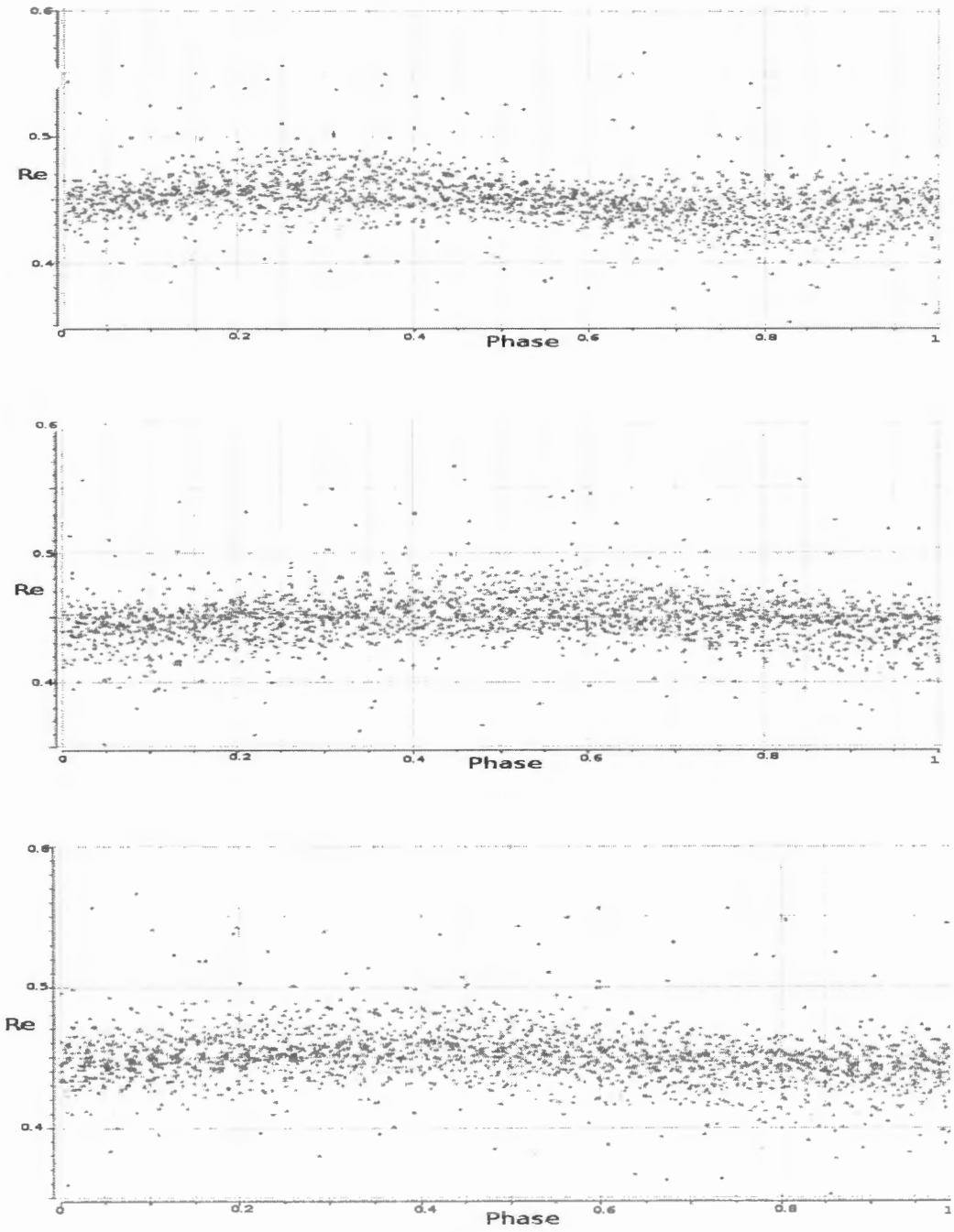

Figure 4.15 Phase plots for the first three frequencies listed in Table 4.6 in filter I. From top to bottom the data has been phased using frequencies 15.692 c/d, 16.116 c/d & 14.262 c/d. Phase is given in units of period and y-axis (Re) shows residuals of Johnson I.

4.2 Results from Mode Identification

To carry out a photometric mode identification, light curves from different filters must be imported to FAMIAS, and amplitudes and phases of the pulsation frequencies must be determined by least-squares fitting which was done in section 4.1. Therefore, the values of pulsation frequency, amplitude, uncertainty of the amplitude, phase and uncertainty of the phase were copied to the Mode Identification Tab to carry out mode identification using amplitude ratios and phase differences. FAMIAS derives the theoretical values from pre-computed model grids and displays the results of the mode identification. It is also Known that parameters like temperature T and ΔT can affect the variations of pulsation amplitude with wavelength (Medupe 1996). According to Medupe (1996), the temperature decreases with increasing wavelength in the atmosphere of stars like Ap stars. The adiabatic parameters R and Ψ_T were also estimated using pulsation code written by Medupe (2002).

FAMIAS requires T_{eff}, log g, stellar mass, metallicity, microturbulence, source of the atmospheric grid, and the source of the non-adiabatic observables. In most literatures, e.g, Kovalchuk & Pugach (1998), Balona et al. (2002) and Choudhury et al. (2011), microturbulence is given a value of 2 km/s for V351 Ori. We also used the same value for all our mode identification analysis. In most literatures the value of temperature of V351 Ori is given in the range with a minimum value of 7350 K, e.g. Marconi et al. (2001) and maximum value of 7700 K, e.g. Kovalchuk and Pugach (1998). In recent papers like Choudhury et al. (2011), a temperature value of 7500 K, which was calculated by Balona et al. (2002) is used. In most mode identification calculation we also used this temperature value. Alecian et al. (2012) used temperature value of 7750 K and uncertainty of $\pm$ 250 K in temperature which we also used for our calculations. We also used the other parameters from literature as follows.

Values of log g are also given as 3.6 Kurucz (1991), Balona et al. (2002) and recent studies show log g = 4 (see also Choudhury et al. 2011). Uncertainties of ± 0.1 or ± 0.02 are also used for log g. In all cases Kurucz atmospheres were used. The choice of mass depends on the choice of non-adiabatic observable source. For mode-identification analysis, mostly we used Delta Scuti model and Warsaw-New Jersey models. Usually mass of V351 Ori ranges between 1.85 $M_{\odot}$ and 2.7 $M_{\odot}$ or 3 $M_{\odot}$. For metallicity we tried to use 0.0 but we have also checked by slightly changing these values to see how this affects our results. For instance when we put T_{eff} =7750 K, with uncertainty in temperature ± 250 K (Alecian et al. 2002), log g = 4 from Choudhury et al. (2011) with uncertainty of ± 0.1, metalicity = 0.0, mass value 2 $M_{\odot}$ from non-adiabatic observable source of Warsaw-New Jersey, we obtained the plot shown in Figure 4.29. For the rest of the plots, the parameters that were changed to get that specific figure is mentioned in the caption of each Figure.

The evolutionary stellar model grid for the indicated mass is searched for models that lie in the given range of T_{eff} and log g. The amplitude ratios and phase differences are computed with respect to a selected filter. The results module displays the results of the photometric mode identifications. It gave us the observed and theoretical values of the amplitude ratio and phase difference (relative to U band) in different filters in a text file (Appendix E). In searching for best fit, we attempted various input parameters as shown in Table 4.7 to plot fitted amplitude ratios in (Figure 4.16 to Figure 4.35). In Figure 4.28 the fits go through all data points. In plots like Figure 4.31, the fits are very poor suggesting that initial parameters might be wrong. On the other hand, the fit is better in Figure 4.34. The Fortran program used to plot these graphs is given in Appendix C.2.

Table 4.7 List of different parameters we used to plot amplitude ratio of photometric mode identification.

Source: Balona et al. (2002), van den Ancker et al. (1996), Marconi et al. (2000), Marconi et al. (2001), Koval'chuk and Pugach (1998), Ripepi et al. (2003a), Choudhury et al. (2011), Alecian et al. (2012).

	T_{eff} (K)	Uncertainty in T_{eff} (ΔT_{eff})	log g	Uncertainty in log g	Mass of the star	metallicity	Non adiabatic source
1	7500	250	3.6	0.1	2	+0.0	Delta Sct
2	7500	200	3.6	0.1	2	+0.0	Delta Sct
3	7500	250	3.6	0.1	2	+1	Delta Sct
4	7500	250	3.6	0.1	2	+0.3	Delta Sct
5	7500	500	3.6	0.1	2	+0.0	Delta Sct
6	7400	250	3.6	0.1	2	+0.0	Delta Sct
7	7350	250	3.6	0.1	2	+0.0	Delta Sct
8	7500	250	4	0.1	2	+0.0	Warsaw
9	7500	150	3.6	0.1	2	+0.0	Delta Sct
10	7500	250	4	0.1	1.8	+0.0	Warsaw
11	7700	250	4	0.1	2	+0.0	Warsaw
12	7425	250	4	0.1	2	+0.0	Warsaw
13	7425	250	4	0.1	2	+0.3	Warsaw
14	7750	250	4	0.1	2	+0.0	Warsaw

We selected the non-adiabatic source based on whether it lead to a solution or whether it failed to produce fits.

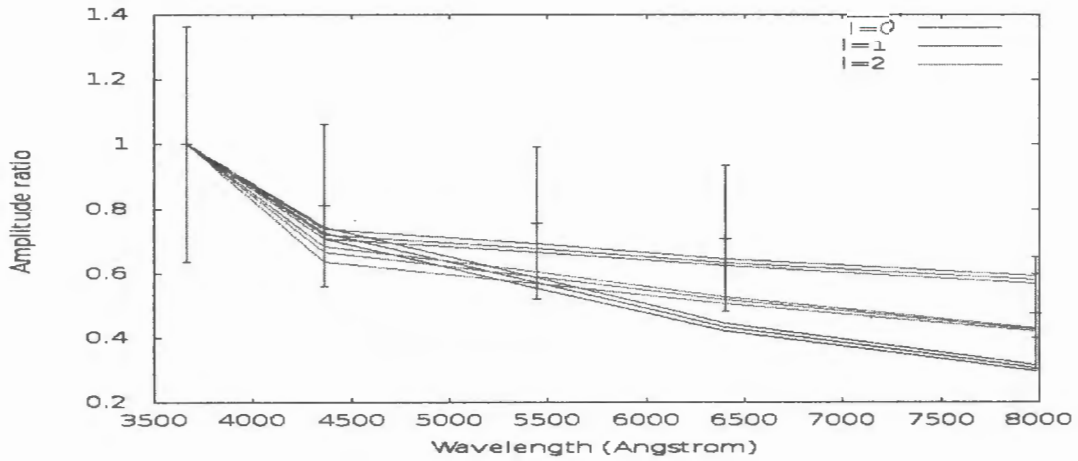

Figure 4.16: The result of the photometric mode identification for V351 Ori when T_{eff}=7500 ± 250 K, log g = 3.6 ± 0.1, mass = $2M_{\odot}$, metallicity = + 0.0 and source of non-adiabatic observable is Delta Scuti model. The red (bottom), green (middle) and blue (top) colours represent $l = 0$, $l = 1$ and $l = 2$ respectively.

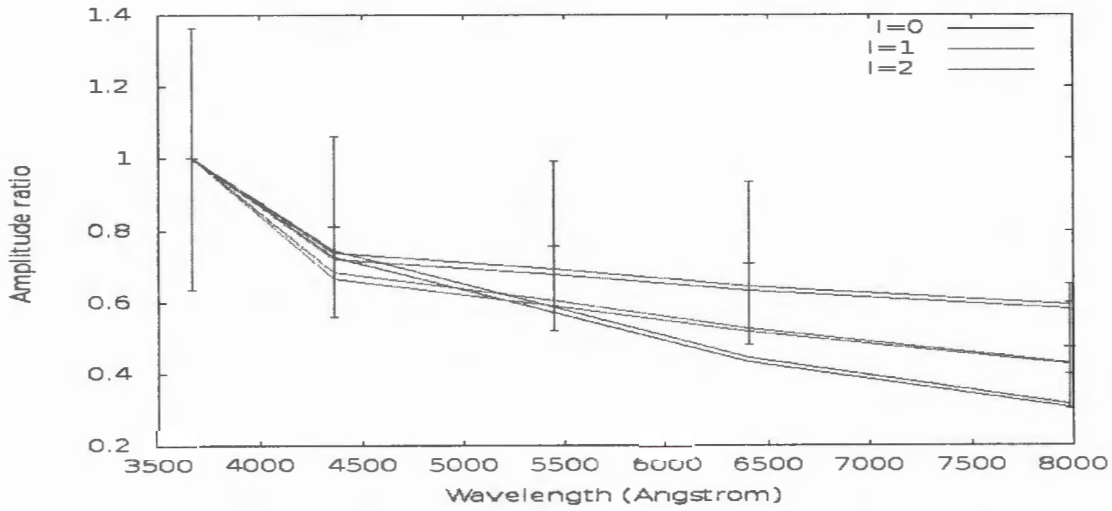

Figure 4.17: The result of the photometric mode identification for V351 Ori when T_{eff}=7500 ± 200 K, log g = 3.6 ± 0.1, mass = $2M_{\odot}$, metallicity = + 0.0 and source of non-adiabatic observable is Delta Scuti model. The red (bottom), green (middle) and blue (top) colours represent $l = 0$, $l = 1$ and $l = 2$ respectively.

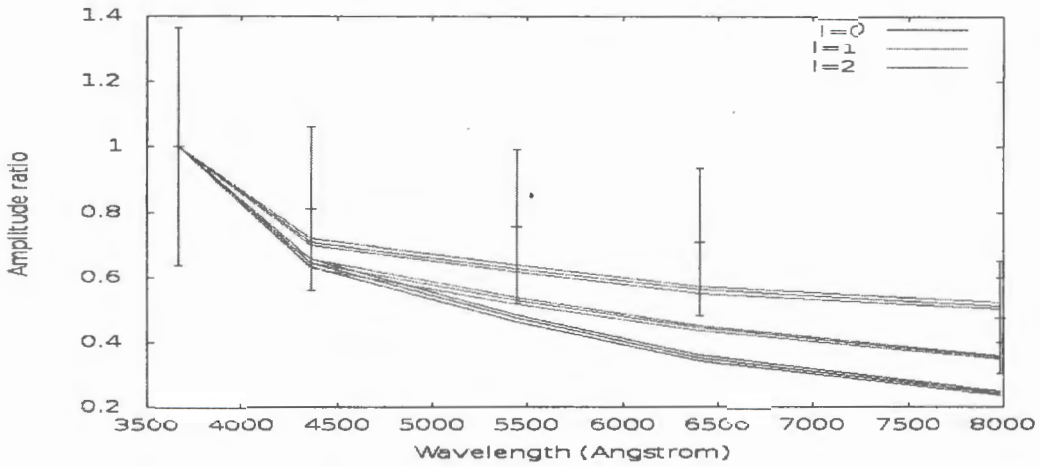

Figure 4.18: The result of the photometric mode identification for V351 Ori when T_{eff}=7500 ± 250 K, log g = 3.6 ± 0.1, mass = $2M_{\odot}$, metallicity = + 1.0 and source of non-adiabatic observable is Delta Scuti model. The red (bottom), green (middle) and blue (top) colours represent $l = 0$, $l = 1$ and $l = 2$ respectively.

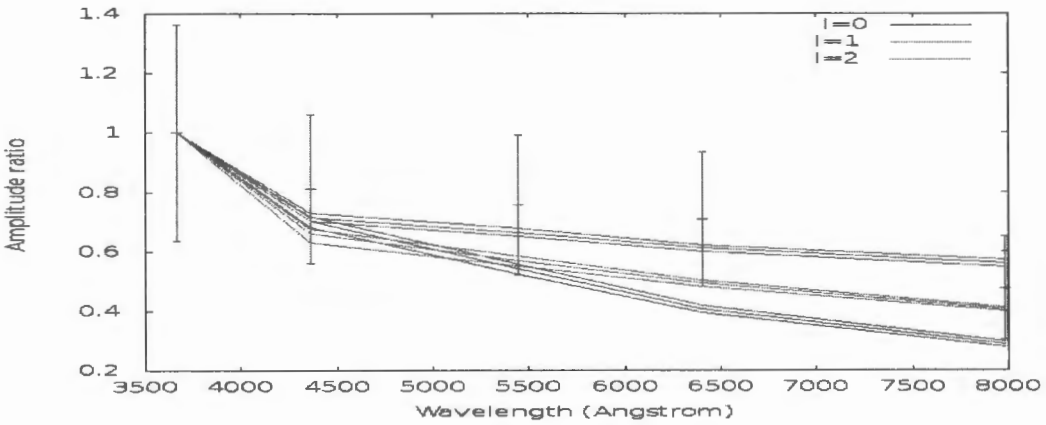

Figure 4.19: The result of the photometric mode identification for V351 Ori when T_{eff}=7500 ± 250 K, log g = 3.6 ± 0.1, mass = $2M_{\odot}$, metallicity = + 0.3 and source of non-adiabatic observable is Delta Scuti model. The red (bottom), green (middle) and blue (top) colours represent $l = 0$, $l = 1$ and $l = 2$ respectively.

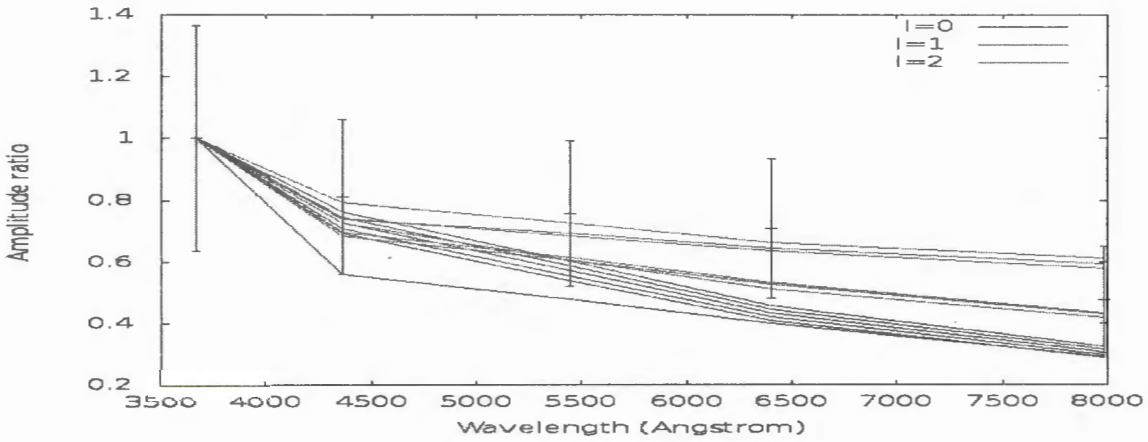

Figure 4.20: The result of the photometric mode identification for V351 Ori when T_{eff}=7500 ± 500 K, log g = 3.6 ± 0.1, mass = $2M_{\odot}$, metallicity = + 0.0 and source of non-adiabatic observable is Delta Scuti model. The red (bottom), green (middle) and blue (top) colours represent $l = 0$, $l = 1$ and $l = 2$ respectively.

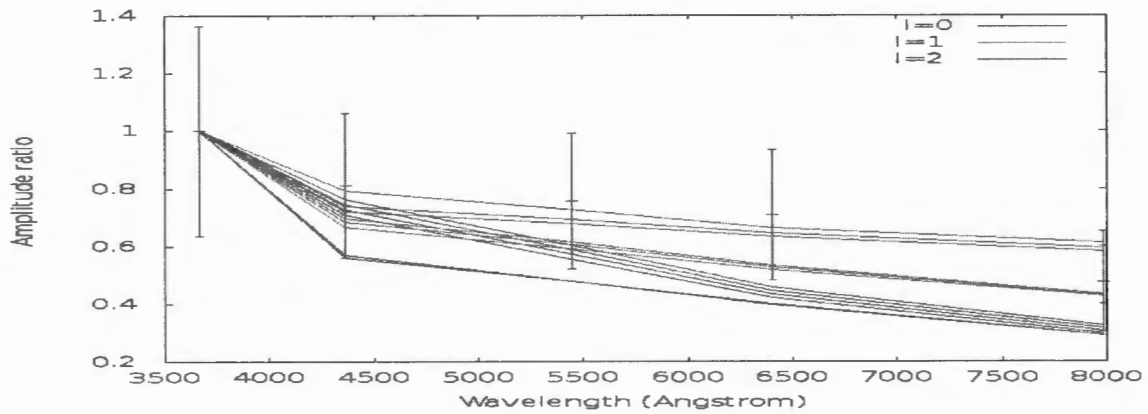

Figure 4.21: The result of the photometric mode identification for V351 Ori when T_{eff}=7400 ± 250 K, log g = 3.6 ± 0.1, mass = $2M_{\odot}$, metallicity = + 0.0 and source of non-adiabatic observable is Delta Scuti model. The red (bottom), green (middle) and blue (top) colours represent $l = 0$, $l = 1$ and $l = 2$ respectively.

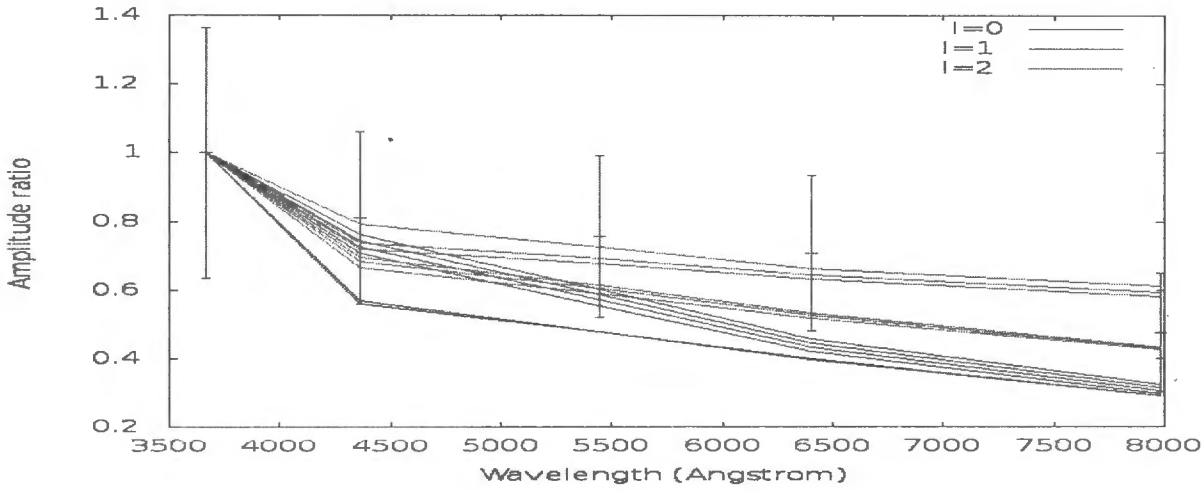

Figure 4.22: The result of the photometric mode identification for V351 Ori when T_{eff}=7350 ± 250 K, log g = 3.6 ± 0.1, mass = $2M_{\odot}$, metallicity = + 0.0 and source of non-adiabatic observable is Delta Scuti model. The red (bottom), green (middle) and blue (top) colours represent $l = 0$, $l = 1$ and $l = 2$ respectively.

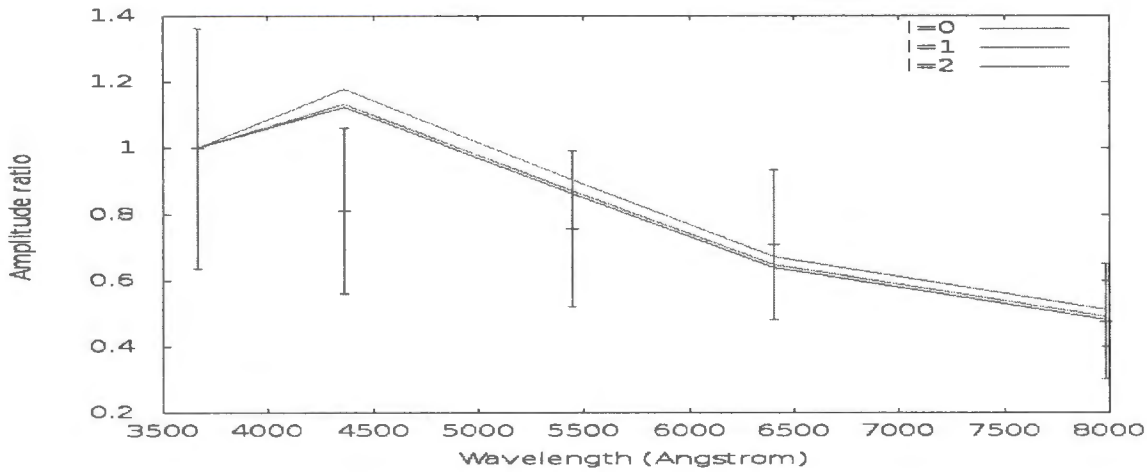

Figure 4.23: The result of the photometric mode identification for V351 Ori when T_{eff}=7500 ± 250 K, log g = 4 ± 0.1, mass = $2M_{\odot}$, metallicity = + 0.0 and source of non-adiabatic observable is Warsaw-New Jersy/Dziembowski. The red (bottom), green (middle) and blue (top) colours represent $l = 0$, $l = 1$ and $l = 2$ respectively.

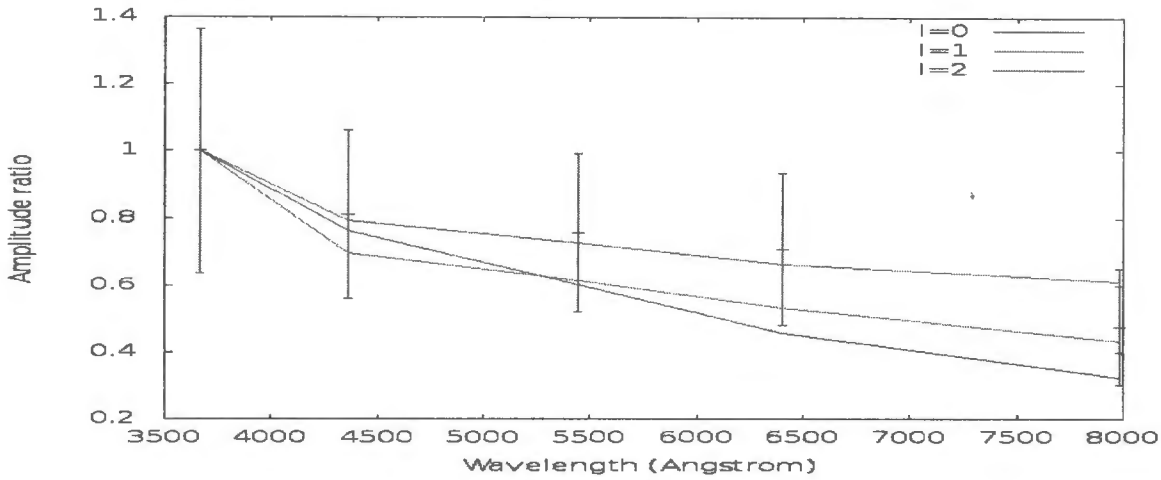

Figure 4.24: The result of the photometric mode identification for V351 Ori when T_{eff}=7500 ± 150 K, log g = 3.6 ± 0.1, mass = $2M_{\odot}$, metallicity = + 0.0 and source of non-adiabatic observable is Delta Scuti model. The red (bottom), green (middle) and blue (top) colours represent $l = 0$, $l = 1$ and $l = 2$ respectively.

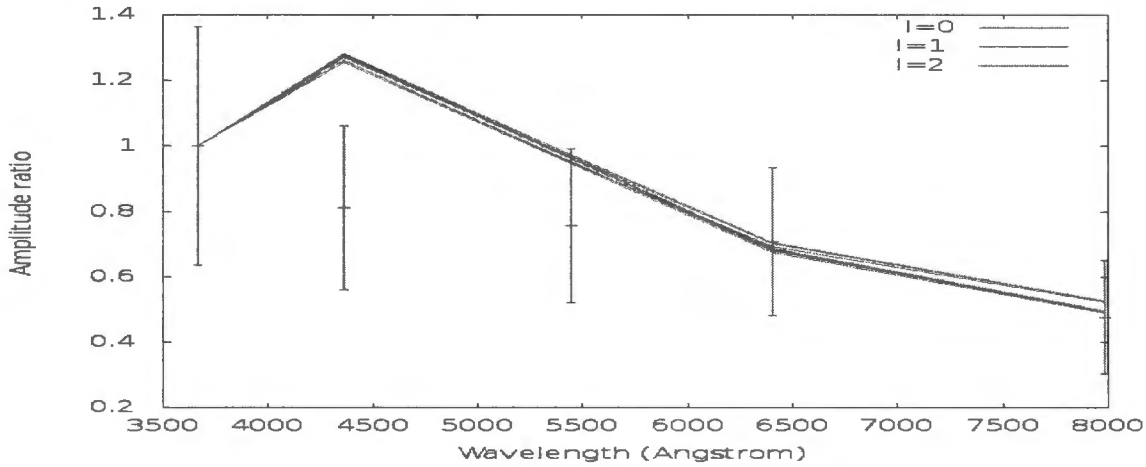

Figure 4.25: The result of the photometric mode identification for V351 Ori when T_{eff}=7500 ± 250 K, log g = 4 ± 0.1, mass = $1.8M_{\odot}$, metallicity = + 0.0 and source of non-adiabatic observable is Warsaw-New Jersy/Dziembowski. The red (bottom), green (middle) and blue (top) colours represent $l = 0$, $l = 1$ and $l = 2$ respectively.

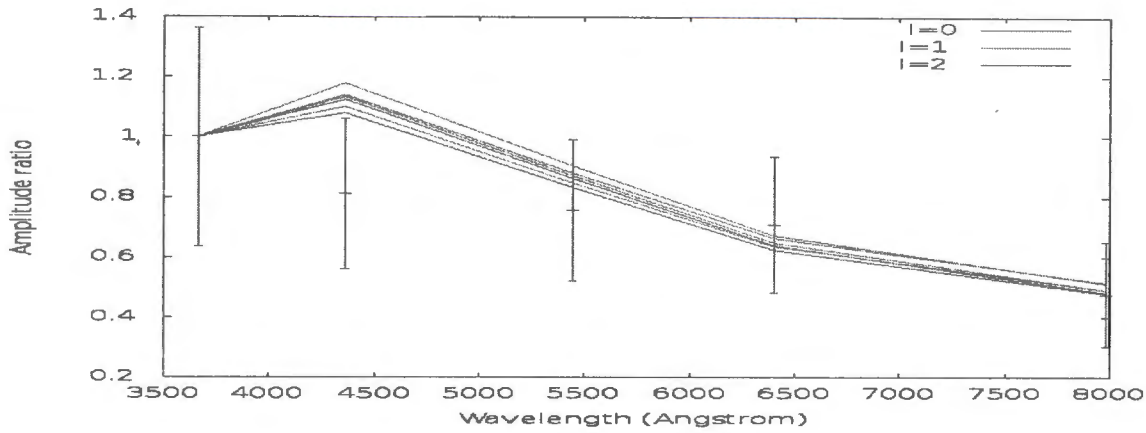

Figure 4.26: The result of the photometric mode identification for V351 Ori when T_{eff}=7700 ± 250 K, log g = 4 ± 0.1, mass = $2M_{\odot}$, metallicity = + 0.0 and source of non-adiabatic observable is Warsaw-New Jersy/Dziembowski. The red (bottom), green (middle) and blue (top) colours represent $l = 0$, $l = 1$ and $l = 2$ respectively.

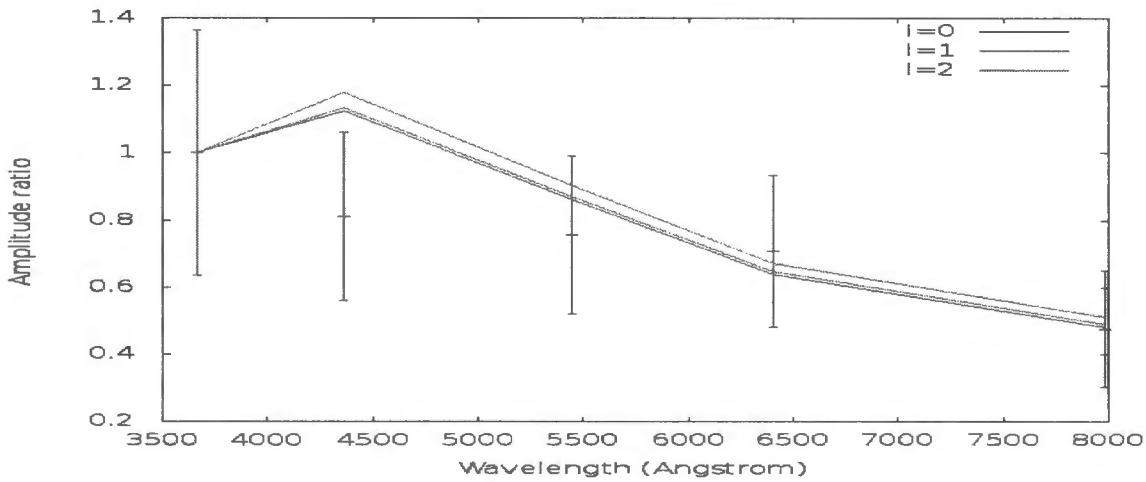

Figure 4.27: The result of the photometric mode identification for V351 Ori when T_{eff}=7425 ± 250 K, log g = 4 ± 0.1, mass = $2M_{\odot}$, metallicity = + 0.0 and source of non-adiabatic observable is Warsaw-New Jersy/Dziembowski. The red (bottom), green (middle) and blue (top) colours represent $l = 0$, $l = 1$ and $l = 2$ respectively.

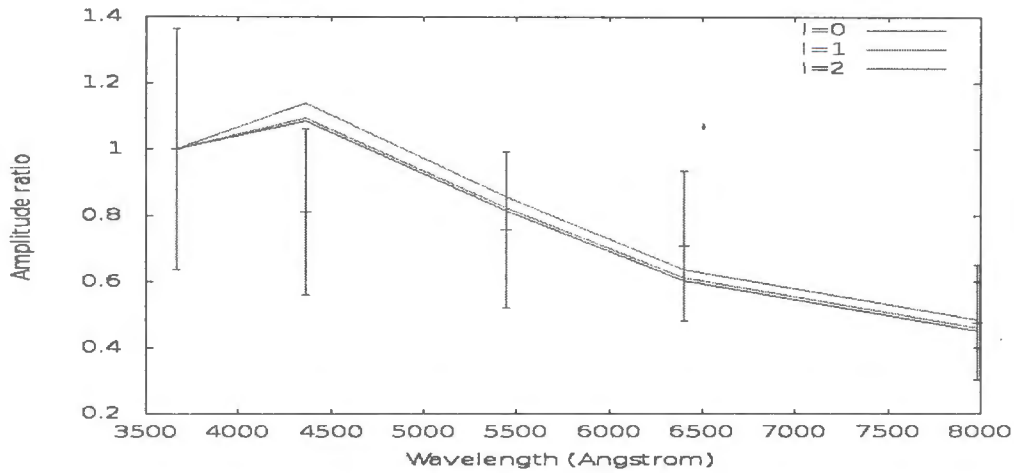

Figure 4.28: The result of the photometric mode identification for V351 Ori when T_{eff}=7425 ± 250 K, log g = 4 ± 0.1, mass = $2M_{\odot}$, metallicity = + 0.3 and source of non-adiabatic observable is Warsaw-New Jersy/Dziembowski. The red (bottom), green (middle) and blue (top) colours represent $l = 0$, $l = 1$ and $l = 2$ respectively.

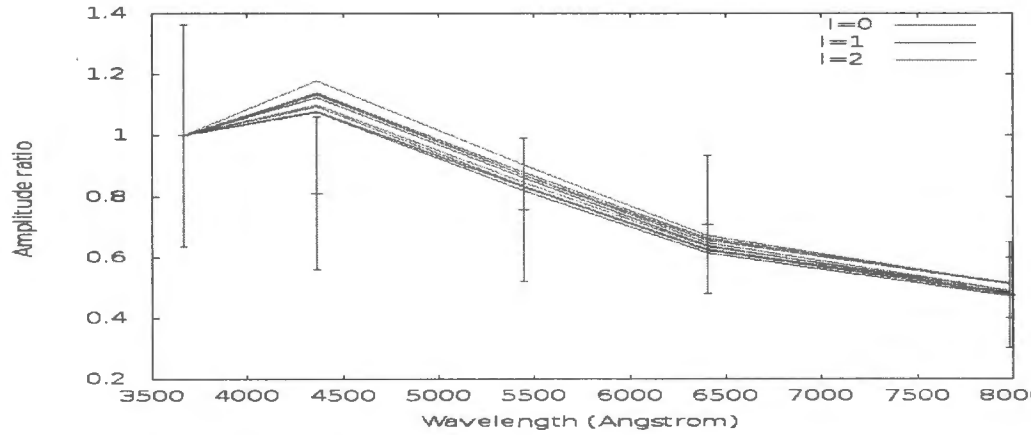

Figure 4.29: The result of the photometric mode identification for V351 Ori when T_{eff}=7750 ± 250 K, log g = 4 ± 0.1, mass = $2M_{\odot}$, metallicity = + 0.0 and source of non-adiabatic observable is Warsaw-New Jersy/Dziembowski. The red (bottom), green (middle) and blue (top) colours represent $l = 0$, $l = 1$ and $l = 2$ respectively.

Balona et al. (2002) calculated multiperiodic Fourier fit to the photometric data of V351 Ori using the frequency value of 15.675 c/d as shown in Table 4.8. To compare with our results, we have done photometric mode identification using these values and the resulted plots are shown in Figure 4.30-4.35. As it can be seen in the Figures, the plots are similar with ours except the fact that error bars in our case are larger.

Table 4.8 Amplitude and phase calculated by Balona et al. (2002) using frequency value of 15.675 c/d.

Filter	Amplitude (mmag)	Phase (radians)
U	28.6 ± 0.9	1.86 ± 0.03
B	28.6 ± 1.0	1.81 ± 0.03
V	22.9 ± 0.8	1.85 ± 0.04
R	18.5 ± 0.8	1.91 ± 0.05
I	14.5 ± 0.8	1.94 ± 0.06

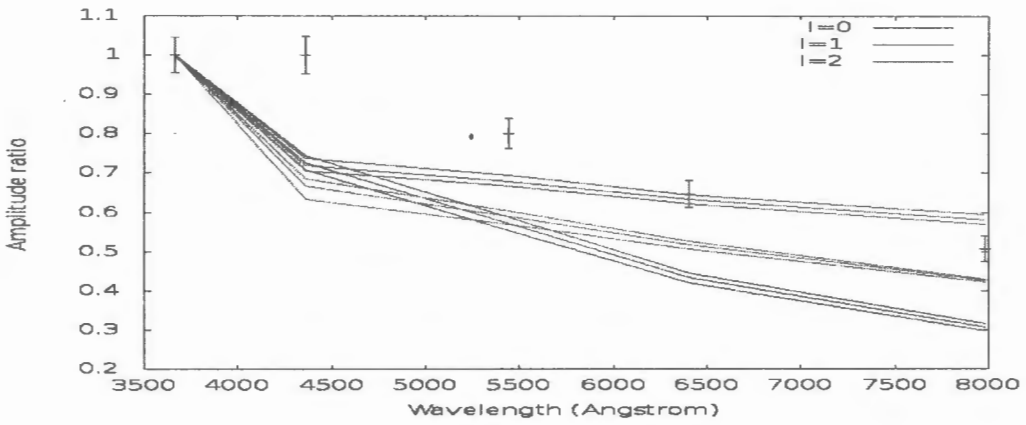

Figure 4.30: The result of the photometric mode identification using data from Balona et al. (2002) for V351 Ori when T_{eff}=7500 ± 250 K, log g = 3.6 ± 0.1, mass = $2M_{\odot}$, metallicity = + 0.0 and source of non-adiabatic observable is Delta Scuti model. The red (bottom), green (middle) and blue (top) colours represent $l = 0$, $l = 1$ and $l = 2$ respectively.

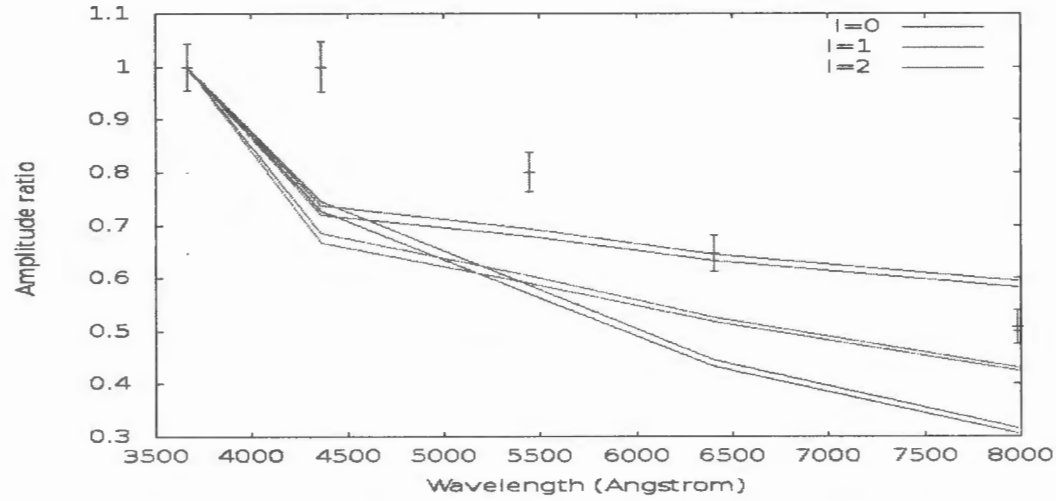

Figure 4.31: The result of the photometric mode identification using data from Balona et al. (2002) for V351 Ori when T_{eff}=7500 ± 200 K, log g = 3.6 ± 0.1, mass = $2M_{\odot}$, metallicity = + 0.0 and source of non-adiabatic observable is Delta Scuti model. The red (bottom), green (middle) and blue (top) colours represent $l = 0$, $l = 1$ and $l = 2$ respectively.

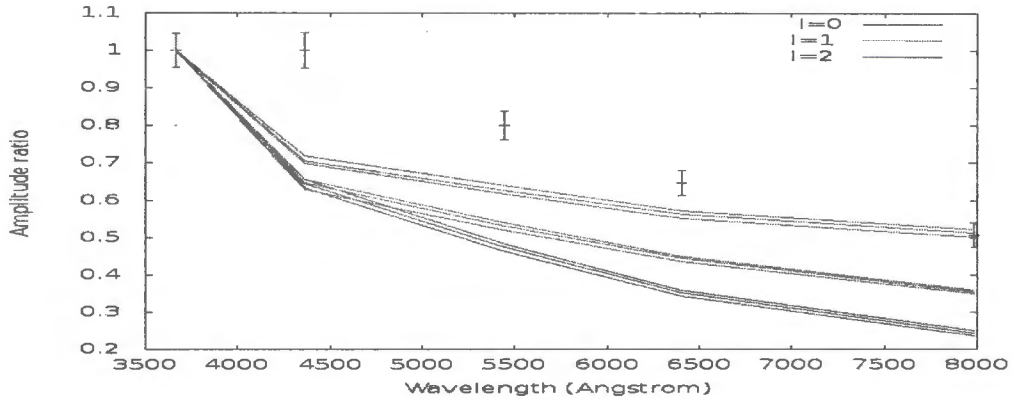

Figure 4.32: The result of the photometric mode identification using data from Balona et al. (2002) for V351 Ori when T_{eff}=7500 ± 250 K, log g = 3.6 ± 0.1, mass = 2$M_{\odot}$, metallicity = + 1.0 and source of non-adiabatic observable is Delta Scuti model. The red (bottom), green (middle) and blue (top) colours represent l = 0, l = 1 and l = 2 respectively.

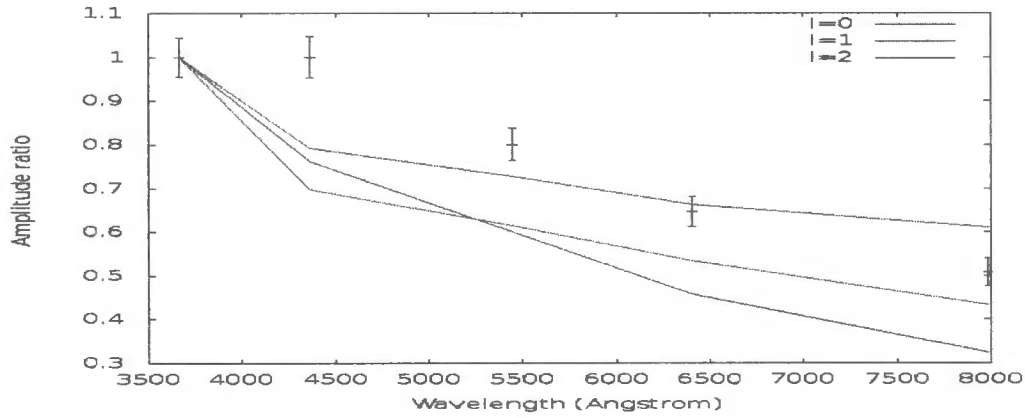

Figure 4.33: The result of the photometric mode identification using data from Balona et al. (2002) for V351 Ori when T_{eff}=7500 ± 150 K, log g = 3.6 ± 0.1, mass = 2$M_{\odot}$, metallicity = + 0.0 and source of non-adiabatic observable is Delta Scuti model. The red (bottom), green (middle) and blue (top) colours represent l = 0, l = 1 and l = 2 respectively.

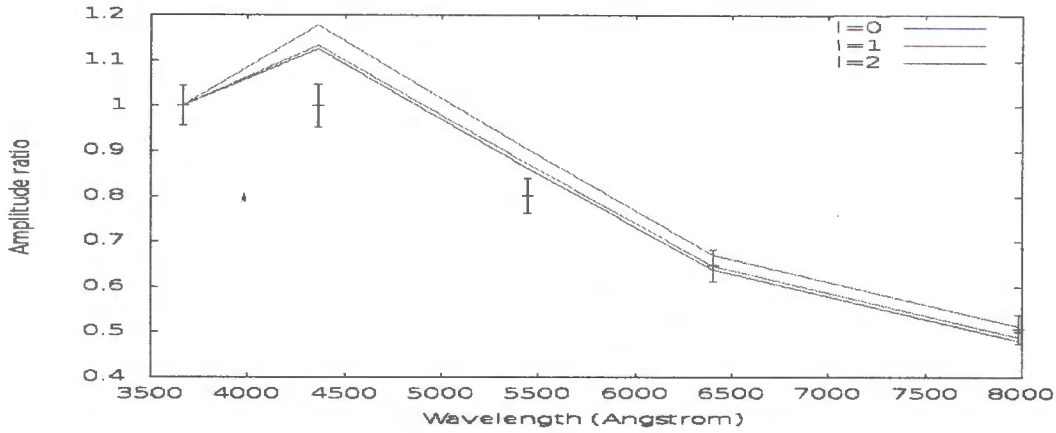

Figure 4.34: The result of the photometric mode identification using data from Balona et al. (2002) for V351 Ori when T_{eff}=7500 ± 250 K, log g = 4 ± 0.1, mass = $2M_{\odot}$, metallicity = + 0.0 and source of non-adiabatic observable is Warsaw-New Jersy/Dziembowski. The red (bottom), green (middle) and blue (top) colours represent $l = 0$, $l = 1$ and $l = 2$ respectively.

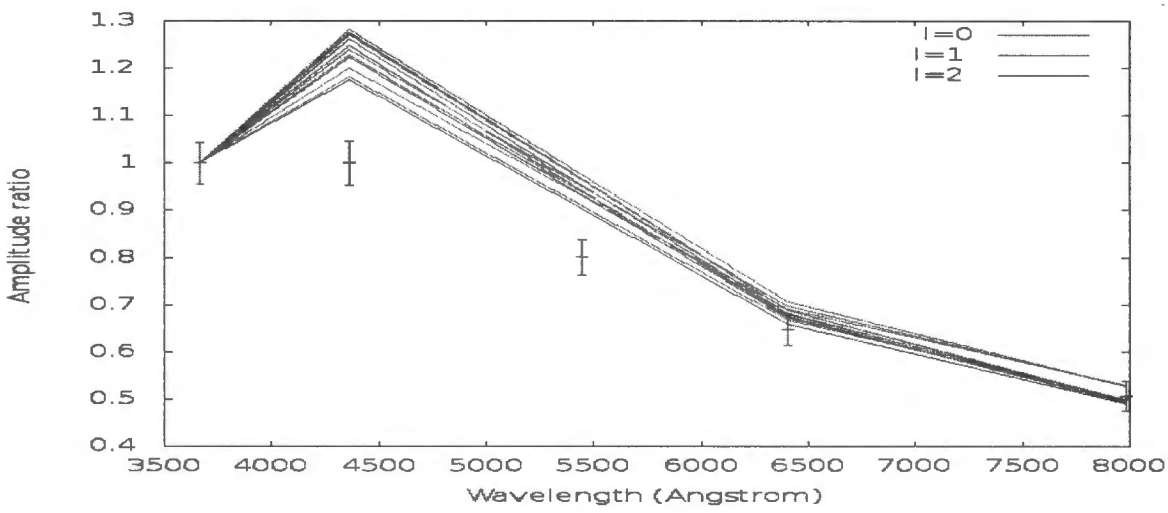

Figure 4.35: The result of the photometric mode identification using data from Balona et al. (2002) for V351 Ori when T_{eff}=7500 ± 250 K, log g = 4 ± 0.1, mass = $1.8M_{\odot}$, metallicity = + 0.0 and source of non-adiabatic observable is Warsaw-New Jersy/Dziembowski. The red (bottom), green (middle) and blue (top) colours represent $l = 0$, $l = 1$ and $l = 2$ respectively.

The points with error bars show the observed values and the fits can be used to tell l values. As can be seen in the Figures above, it does not seem simple to identify which best identification to choose for different l values since the error bars are large and sometimes outside the theoretically predicted lines. However, when we use Delta Scuti MAD model, l = 0, 1 and 2 seems to fit the theoretical values ambiguously. The error bars are too large in our 2013 data to allow distinction between l = 0, 1 and 2 modes to be made. This might be a result of our noisy data.

In most of our plots, the result shows unclear agreement between observed and calculated amplitudes for the given choice of mode. Therefore, comparing with the results shown in the text files (Appendix E), it is not to some extent clear which observed amplitudes ratios are most consistent with the theoretical models that have values l = 0, 1, 2 and 3. A unique identification of all detected pulsation modes is therefore not possible from photometry only. We therefore hope the spectroscopic mode identifications to give us further explanations. In some of the plots where the full error bar falls outside the grid, it was not possible to perform mode identification.

Actually Balona et al. (2002) performed spectroscopic observation on the same star to identify modes and was not successful as it was explained as follows. The mode identification gave calculated amplitude ratios and phase differences relative to the U band for l = 0, 1, and 2 for the same frequency value f =15.675 c/d. From the Figures plotted, Balona et al. (2002) suggested that the areas of interest were not sufficiently distinct to be useful as mode discriminants. The reason was that, at these relatively high frequencies, the light variation is caused predominantly by variations in temperature during the pulsation and very little by geometrical distortion of the star. Since the information regarding l is stored in the geometrical term, and not in the temperature term, there is practically no dependence of the amplitude and phase on l. We used Balona et al. (2002) data to confirm theses results and comments.

4.3 Frequency Evolution of V351 Ori

Photometric observations were done by Balona et al. (2002), Marconi et al. (2001), Pipepi et al. (2003a) and Ripepi et al. (2003b). We plot frequency verses year of observation in Figure 4.36 to Figure 4.38. Unfortunately, we could not find frequency errors for each of the observation campaigns. Hence we cannot reliably determine if the frequencies f_1 = 15.675 c/d , f_2 = 14.380 c/d and f_3 = 11.890 c/d of this star changed with time.

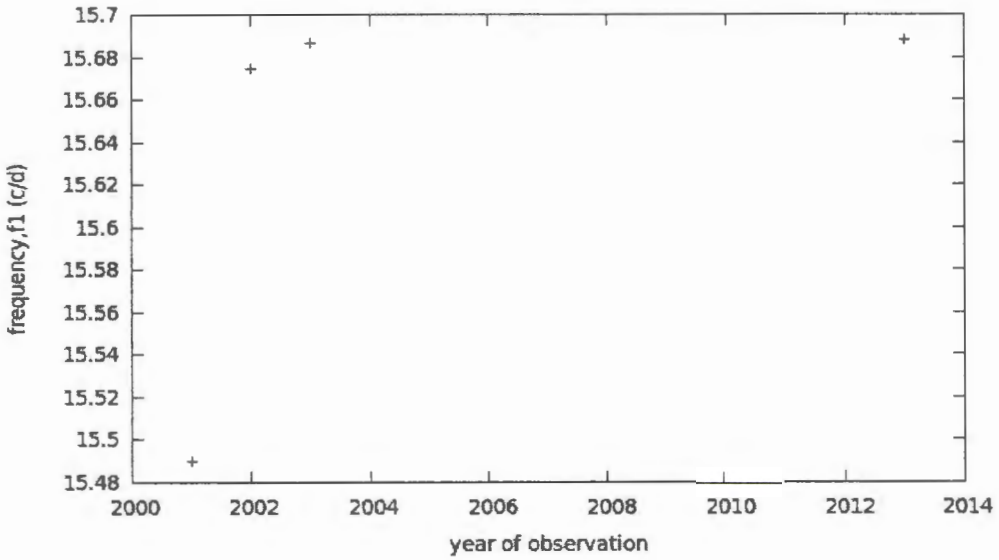

Figure 4.36 The frequency evolution of V351 Ori between 2001 and 2013 for frequency value of f_1.

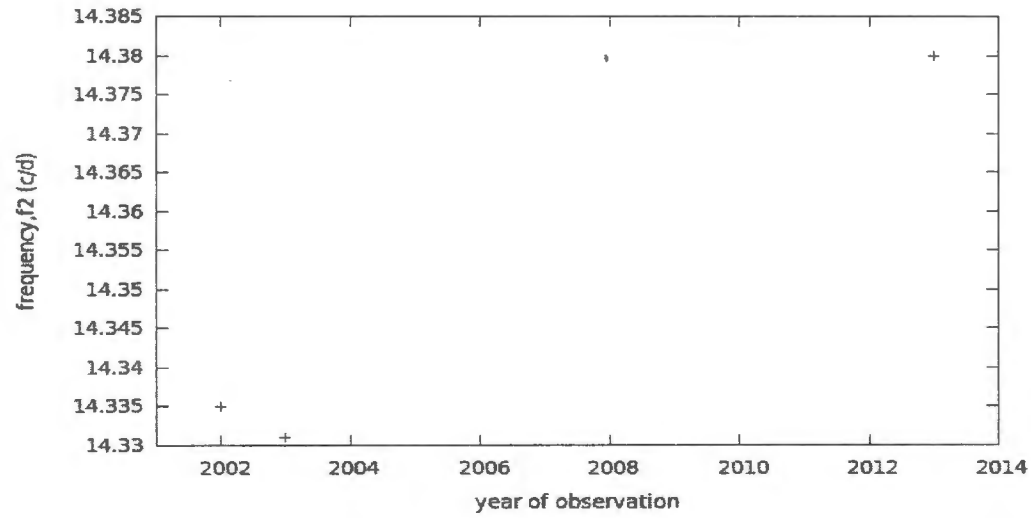

Figure 4.37 The frequency evolution of V351 Ori between 2001 and 2013 for frequency value of f_2.

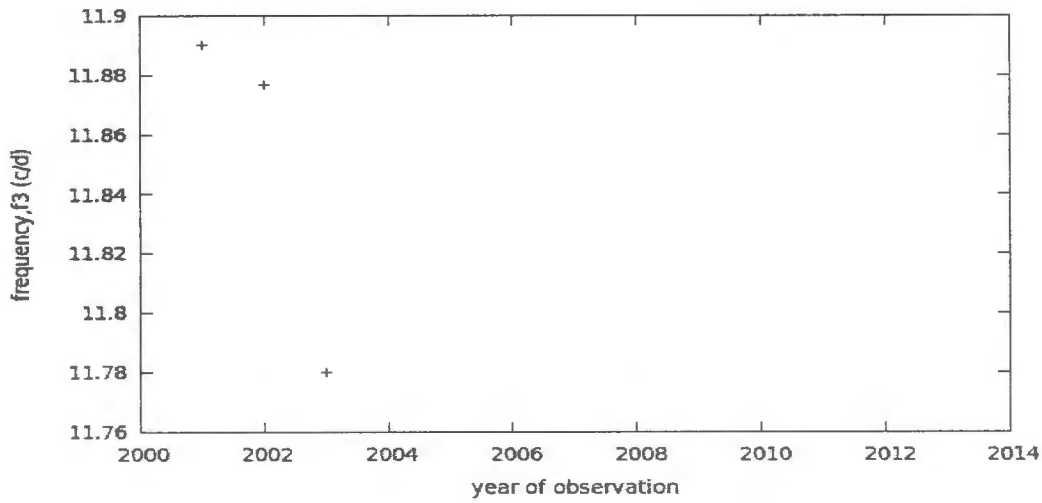

Figure 4.38 The frequency evolution of V351 Ori between 2001 and 2013 for frequency value of f_3.

Chapter 5

Conclusions and Future Work

The objective of this study was to carry out time series multicolour photometry of Herbig Ae star V351 Orionis using five Johnson filters (UBVRI) to observe pulsations in this star. The task was to measure, specifically the frequencies of oscillation of the star using Fourier analysis and then to make comparisons with values of frequencies from previous research work of theoretical predictions in order to determine the frequency evolution of this star. The other related objective was to determine amplitudes of oscillation with a high relative accuracy in different colours and as an additional idea to attempt mode identification to see if there are any systematic changes and whether we can model the change.

Frequency analysis was done using a software package called FAMIAS. The Fourier analysis and least squares fitting performed gave a periodogram plot with the frequency of pulsation of the star to be 15.688 cycles per day which was also observed in Marconi et al. (2001), Balona et al. (2002), Ripepi et al. (2003a) and Ripepi et al. (2003b). This result was obtained for all filters (UBVRI). The amplitude values also match the predicted values although our amplitude errors are much larger than those of previous authors. In addition to this frequency, the following frequency values were obtained in some of the filters which also agrees with results from literature: 14.622 c/d and 14.257 c/d in filter R, 14.262 c/d in filter I, 16.116 c/d in filter I and 12.704 in filter V. We also observed the additional frequencies listed in Table 4.9 after pre-whitening the result.

Table 4.9 List of additional frequencies we observed in different filters.

Frequency (c/d)	Filter
15.317	U
17.303	U
15.842	B
15.332	B

Frequency (c/d)	Filter
17.038	V
15.357	V
15.112	R
22.020	I

The light curve of the star shows the δ Scuti pulsation and the other aspect of the light curve is that it seems to show a variation which might be due to dust obscuration. The main pulsation frequency found (15.688 c/d) was used to perform mode identification. From the plots, it does not seem simple to identify the best identification of the different l values. The amplitude errors were large and sometimes outside the theoretically predicted lines. We believe that this is may be due to the noisy data we have. Therefore, conclusive results on mode identification cannot be ascertained only from the result we have obtained. To say which observed amplitudes ratios are most consistent with the theoretical models that have values $l = 0, 1, 2$ and 3, it seems that more observations for a greater number of nights might be needed for a better result in mode identification. Even with better data of Balona et al. (2002) mode identification for this star is not possible using photometric data alone. Balona et al. (2002) explains this as due to the way the star pulsates. According to them, in V351 Ori temperature variations dominate geometry variations and since the l-dependence is mostly in geometry terms, there is no dependence of amplitude and phase on l.

Future Work

It is possible to do the same thing (search for pulsation and mode identification) in high resolution spectroscopy to get some additional results. For instance we planned to use 1.9 M telescope or even SALT (10M), based on the results we would get from 1.9M telescope. One of the challenges in studying these stars is the fact that they are usually found within clouds of gas and dust, which will obscure or hide them at visible wavelengths. As a best alternative, for a complete understanding of the physical processes causing the photometric variability of pre-main sequence systems, simultaneous optical and near-IR observations are required to disentangle the emission from the stars and that from their associated circumstellar disks. Radio observations have also been found useful, and new sub-millimeter and mid-IR facilities respectively, will be ideally suited to get detailed additional information about this star.

Bibliography

Aerts, C., Christensen-Dalsgaard, J., & Kurtz, D.W., 2010, *Asteroseismology*, libraries, Springer

Alecian, E., Wade, G.A., Catala, C., Grunhut, J.H., Landstreet,J.D., Bagnulo,S., Bohm,T., Folsom, C.P., Marsden,S.,Waite, I., 2012, MNRAS, **429**, 1001

Balona, L.A., 1998, *ASP* Conference Series, Vol. **135 ,** 120

Balona, L. A., Koen, C., & van Wyk, F., 2002, MNRAS, **333**, 923

Balona, L.A., Medupe,T., Abedigamba,O.P., Ayane,G., Keeley,L., Matsididi, M., Mekonnen,G., Nhlapo,M.D., Sithole, N., 2013, MNRAS, **430**, 3472B

Barcza, S., 2003, A&A, **403**, 683

Breger, M.,1972, ApJ, **171**, 539

Breger, M., & Pamyatnykh, A. 1998, A&A, **332**, 958

Carroll, B.W., & Ostlie, D. A., 2007, *An Introduction to Modern Astrophysics*, 2nd ed, Pearson, New York, USA

Chaisson, M., 1998, Astronomy Today, 3rd ed, Pearson, New Jersey, USA

Choudhury, R., Bhatt, H.C., Pandey, G., 2011, A&A, **526**, 797

Doering, R.L., & Meixner, M., 2009, APS, **138**, 780

Donati, J.F., Semel, M., Carter, B. D., Rees, D. E., & Cameron, A. C. 1997, MNRAS, **291**, 658

Doucet, C., Pantin, E., Lagage, P.O., & Dullemond, C.P., 2006, n.p.

Eiroa, C., Oudmaijer, R.D., Davies, J.K., de Winter D., Garzon, F., Palacios, J. A. Alberdi, A., Ferlet, R., Grady, C.A., Cameron, A., H. J. Deeg, H. J, Harris, A.W., Horne, K., Mern, B., Miranda, L.F., Montesinos, B., Mora, A., Penny, A., Quirrenbach, A., H. Rauer, H., Schneider, J., Solano, E., Tsapras, Y., & Wesselius, P.R., 2002, A&A, **384**, 1038

Gautschy, A. and Saio, H., 1995, ARAA, Vol. 33, 75-113

Grinin VP, The PS, DeWinter D, Giampana M, Rostopchina AN, et al. 1994. A & A 292:165–7

Guenther, E.W., Joergens, V., Neuhauser, R., Torres, G., Batalha, N.S., Vijapurkar, J., Fernandez, M., & Mundt, R., 2001, *The Formation of Binary Stars*, IAU Symposium, Vol. **200**, 165

Handler, G., 2008, AAS, Vol. **157**, 106

Herbig, G. H. 1960, ApJS, 4, 337

Hartmann, L., 2009, *Accretion processes in star formation*, 2nd ed, Cambridge University Press, Cambridge, UK

Kilkenny, D., Whitter D.C.B., Davies, J.K.,Evans, A., Bode, M.F., Robson, E.I., & Banfield, R.M., 1985, SAAO Circ., 9, 55

Kilkenny, D., Balona, L.A., Carter, D.B, Ellis, D.T., & Woodhouse, G.F.W., 1988, MNSSA, **47**, 69K

Koval'chuk, G. U., & Pugach, A. F., 1998, AstL, **24**, 106

Koval'chuk., G.U., 1984, *I.A.U, Information Bulletin* , Variable stars, No 2482

Kurtz, D.W., 2002, *ASP* Conference Series, Vol. **256**, 31

Kurtz, D., & Marang, F. 1995, MNRAS, **276**, 191

Kurtz, D. W., Muller, M. 1999, MNRAS, **310**, 1071

Kurtz, D. W., Muller, M. 2001, MNRAS, **325**, 1341

Kurucz, R.L., 1991, BAAS, **23**, 1047K

Kurucz, R.L., 1993, ASPC, **44,** 87K

Kurucz, R.L., 1997, IAUS, **198**, 217K

Manoj, P., Bhatt, H. C., Maheswar, G., & Muneer, S., 2006, ApJ, **653**, 657

Marconi, M., Ripepi, V., Alcala, J. M., Covino, E.,Palla, F., & Terranegra, 2000, A&A, **355**, L35

Marconi, M., & Palla, F., 1998, *ApJ*, 507, L141

Marconi, M., & Palla, F., 2004, The A-Star Puzzle, *Proceedings IAU Symposium,* No 224, P. 69

Marconi, M., Ripepi,V., Bernabei S., Palla, F., Alcala, J.M., Covino, E., and Terranegra, L., 2001, A & A, **272**, L21

Medupe, R., Christensen-Dalsgaard, J., & Phorah, M., 2009, American Institute of Physics, *International Conference*, New Mexico, 1170, 506

Medupe, R., 2002, Ph.D. thesis, University of Cape Town

Medupe, R., 1996, MSc thesis, University of Cape Town.

Medupe, R., & Kurtz, D.W., 1998, MNRAS, **299**, 371

Miroshnichenko, A.S., Gray, R.O., Vieira, S.L.A., Kuratov, K.S., & Bergner, Yu. K., 1999, A&A, **347**, 137

Palla, F., & Stahler, S.W.,1993, APJ, **418**, 414P

Percy, J., 2007, *Understanding Variable stars*, 1st ed, Cambridge University Press, Cambridge, UK

Ripepi, V., Marconi, M., Bernabei, S., Palla, F., Pinheiro, F.J.G., Folha, D.F.M., Oswalt, T.D., Terranegra, L., Arellano Ferro, A., Jiang, X.J., Alcala, J.M., Marinoni, S., Monteiro,M.J.P.F.G., Rudkin, M., & Johnston, K., 2003a, A&A, **408**, 1047

Ripepi, V., Marconi, M., Silvotti, R., 2003b, *Baltic Astronomy*, Vol. **12**, 119

Ripepi, V., Marconi, M., Palla, F. & Bernabei, S., 2006, Mem. S.A.It. Suppl. , Vol. **9**, 200

Ruoppo, A., Marconi, M., Marques, J.P., Monteiro, M.J.P.F., Christensen-Dalsgaard, J., Palla, F., & Ripepi, V., 2007, A&A, **466**, 261

Seeds, M.A., & Backman, D.E., 2011, *Stars and Galaxies*, 7th ed, Thomson learning inc., Toronto, Canada

Semokov, E.H., 2011, *Bulgarian Astronomical Journal* (Conference Talk), 49

Spezzi, L., De Marchi, G., Panagia, N., Sicilia-Aguilar, A., & Ercolano, B., 2012, MNRAS, **421**, 78

Stahler S.W., & Palla, F., 2004, *The formation of Stars*, Wiley, Weinheim, Germany

The, P.S., de Winter, D., & Perez, M.R., 1994, A&A, **104**, 315

van den Ancker, M. E., de Winter, D., & Tjin A Djie, H. R. E., 1998, A&A, **330**, 145

van den Ancker, M. E., The, P. S., & de Winter, D., 1996, A&A, **309**, 809

van den Ancker, M.E., The P.S., Tjin A Djie H.R.E., Catala, C., de Winter D., Blondel, P.F.C., & Waters, L.B.F.M, 1997. A & A 324:L33–L36

Vieira, S.L.A., Corradi, W.J.B., Alencar,S .H.P., Mendes,L.T.S., Torres,C.A.O., Quast,G.R., Guimaraes, M.M., & da Silva, L., 2003, *APJ*, **126**, 2971

Waters L. B. F. M., Waelkens C., 1998, Annual Rev. Astron. Astrophys., **36**, 233

Watson, R.D,1988, Ap & SS, 140, 255W

Zima, W., 2008, CoAst, **157**, 387Z

Zwintz, K., 2008, *ASJ*, **673**, 1088

Appendix A Visibility Curve for V351 Ori

The following plots show visibility curves of the target star in January and February 2013. Since the length of time the star stays in the altitude above 30^0 determines the length of time we have to use the telescope, it is very important to know the object visibility before even going/planning to observe. For example, as it can be seen from curves for the last weeks of February, it was not possible to observe more than two hours since the star was at altitude below 30^0. The plot gives altitude of the object against time for a specific night. It is also possible to plot variation of altitude and observable hours of objects throught the year. In addition to this, the best observing night for each object, its rising, culminating and setting times and moon parameters can be shown. The altitudes displayed refer to the Astronomical horizon; this implies that, for high level observing sights, rising and setting of an object will occur below altitude 0.

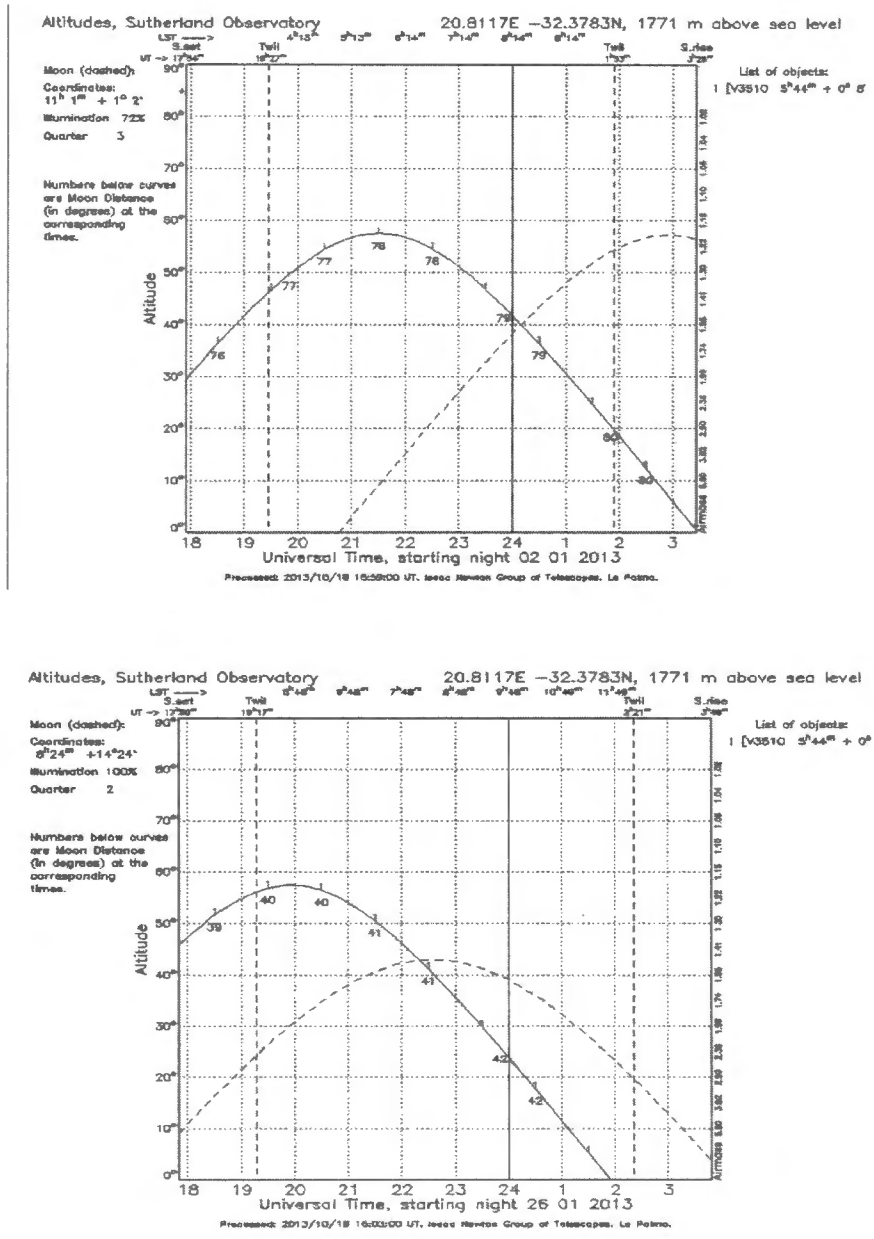

Figure A.1: Visibility curve of V351 Ori at beginning and end of January 2013. The vertical axis shows altitude of the star and horizontal axis is Universal Time. The solid line marks the altitude of the star above the horizon and the dashed curve marks the altitude of the moon (taken from http://catserver.ing.iac.es/staralt/).

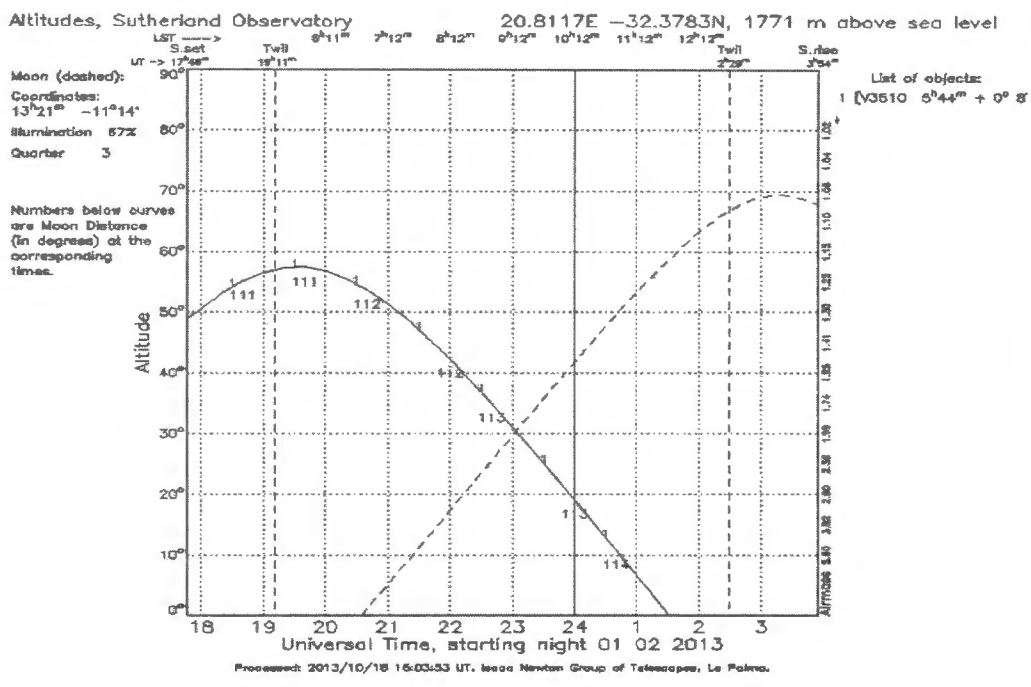

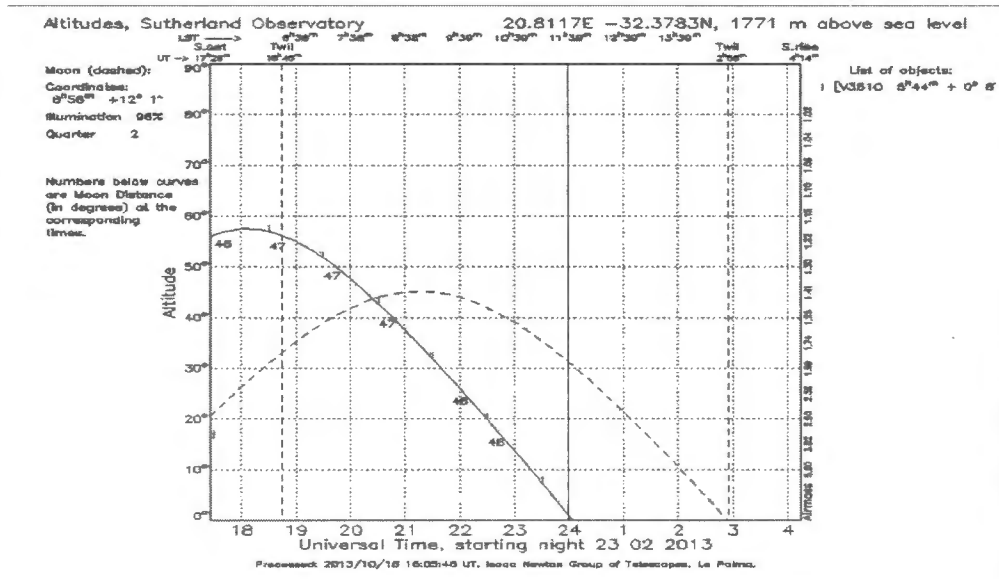

Figure A.2: Visibility curve of V351 Ori at beginning and end of February 2013. The vertical axis shows altitude of the star and horizontal axis is Universal Time. The solid line marks the altitude of the star above the horizon and the dashed curve marks the altitude of the moon (taken from http://catserver.ing.iac.es/staralt/).

Appendix B SAAO 0.5-m Telescope

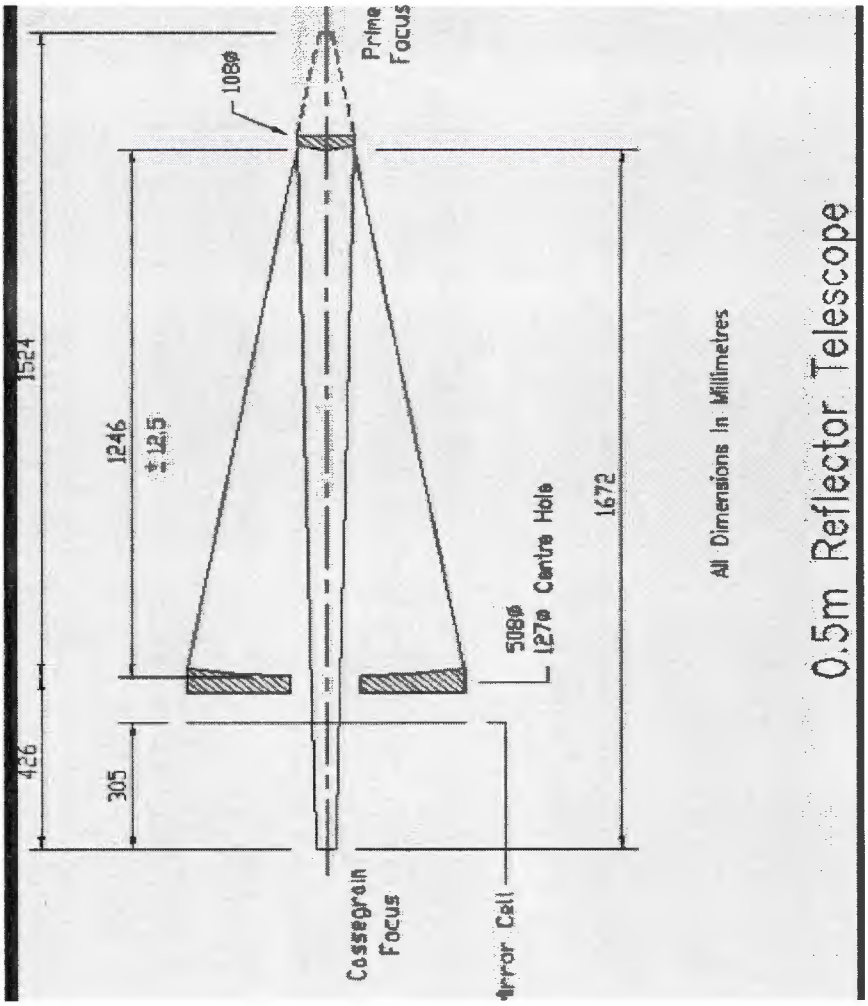

Figure B.1 Optical diagram of the SAAO 0.5-m telescope.

Figure B.2 SAAO 0.5-m telescope from outside.

Figure B.3 SAAO 0.5-m telescope from inside.

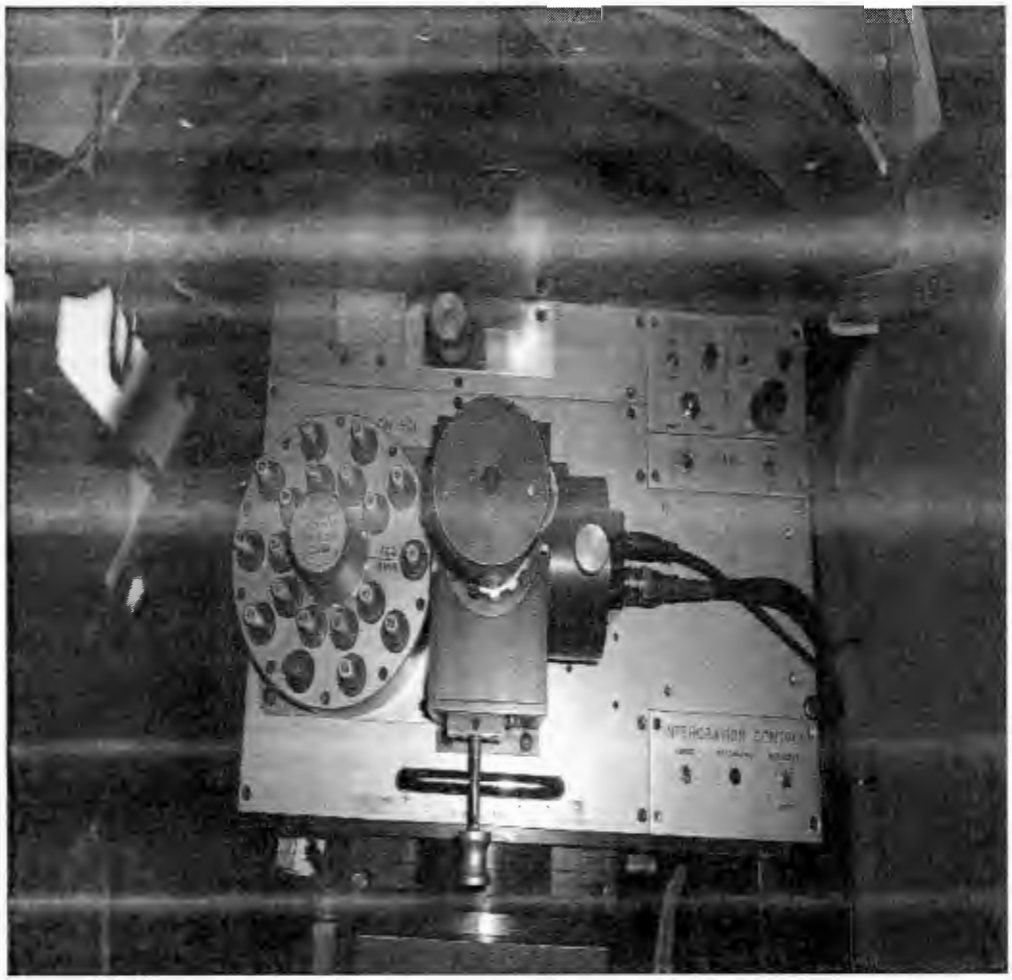

Figure B.4: The Modular Photometer (Front View). On the photometer head, the viewing eyepiece is central with the image intensifier to the right and the aperture select mechanism to the left. The thermoelectrically cooled photomultiplier housing is bolted to the bottom of the photometer head.

Appendix C Fortran Program

C.1

The following Fortran program was used to plot light curves of V351 Ori for daily reduction to check if the target star and the comparison stars we observed were appropriate. Magnitude value of each star can be seen easily from the light curve and a variable star (the target star) and constant magnitude stars (the comparison stars) were easily identified from the light curve.

```
parameter(N=5000)
real x(N),y(N)
character*5 V1,V2,V3
character*10 star1,star2,star3
character*20 tim,tim1,tim2,tim3,filnm
character*70 lin1

nflt=5
print*,'Enter Lucy data filename'
read*,filnm
print*,'Enter star names'
read*,star1,star2,star3

open(11,file=filnm,status='old')
i=1
ik1=0
ik2=0
ik3=0
```

```
 10  read(11,'(a)',end=11)lin1
c     print*,lin1
c     j=index(lin1,'HJD =')
      if(ik1.ne.1)k1=index(lin1,star1)
      if(ik2.ne.1)k2=index(lin1,star2)
      if(ik3.ne.1)k3=index(lin1,star3)
c     print*,'k1,k2,k3 =',k1,k2,k3,star1,star2,star3

      if(k1.eq.1) then
      j=index(lin1,'HJD =')
      print*,' star1 j= ',j
      if(j .eq. 1) then
       tim1=lin1(7:15)
       read(11,'(a)',end=11)lin1
       V1=lin1(9:13)
       write(12,*),tim1,' ',V1
       j=0
       ik1=0
      endif
      ik1=1
     endif

     if(k2.eq.1) then
      j1=index(lin1,'HJD =')
      print*,'star2 j= ',j
      if(j1 .eq. 1) then
       tim2=lin1(7:15)
       read(11,'(a)',end=11)lin1
       V2=lin1(9:13)
       write(13,'(a)')tim2,' ',V2
```

```
      j1=0
       ik2=0
      endif
      ik2=1
     endif

     if(k3.eq.1) then
     j2=index(lin1,'HJD =')
      print*,'star3 j= ',j
      if(j2 .eq. 1) then
       tim=lin1(7:15)
       read(11,'(a)',end=11)lin1
       V3=lin1(9:13)
       write(14,'(a)')tim3,' ',V3
       j2=0
       ik3=0
      endif
      ik3=1
     endif

    i=i+1
    goto 10
11  M=i-1

    close(11)
    close(12)
    close(13)
    close(14)
    stop
    end
```

C.2

A little program for calculating amplitude ratios and error in amplitude ratios. It reads in file 'data' and prints amplitude ratios and errors in file "dat"

```
      real*8 wav(5),amp(5),err(5),er,am
      integer i,N,filt
      open(11,file='data2',status='unknown')
      i=1
10    read(11,*,end=12)wav(i),amp(i),err(i)
      print*,wav(i),amp(i),err(i)

      i=i+1
      goto 10
12    N=i-1
      print*,'Enter reference filter '
      read*,filt
   open(12,file='dat',status='unknown')
      do i=1,N
       am=amp(i)/amp(filt)
       er=sqrt((err(i)/amp(filt))**2+
     &    (amp(i)*err(filt)/amp(filt)**2)**2)
       print*,wav(i),am,er
       write(12,*)wav(i),am,er
      enddo
      close(11)
      close(12)
      end
```

Appendix D V351 Ori (HD 38238)

This section gives basic data of the target star from different resources and its location relative to Milky Way galaxy and finally location of the comparison stars with respect to the target star.

Summary of basic data of the star

Source: SIMBAD Astronomical Database, van dan Ancker et al. (1996), Choudhury et al. (2011), Koval'chuk and Pugach (1998), Palla & Stahler (1993), Ripepi et al. (2003a), Marconi et al. (2000), Balona et al. (2002), Kurtz & Muller (1999).

Star name: V351 Ori/HD 38238/HIP 27059
Galaxy: Milky Way
Constellation: Orion
Coor.: RA=05 44 18.8
Dec.= +00 08 40.4
Gal.coor.: 204.971
+00 07 26.3
Distance: 210 pc (lower limit according to Hipparcos)
450 pc (upper limit if located if located in Orion nebula; star forming region)
Mass: 2.5 - 3M⊙
Radius: 3.9R⊙
Age : 1- 2 Mill.yr
T_{eff}=7500K
Period: 0.058d± 0.002
Spectral type: A7IIIe
Amplitude: 0.02 mag
Luminosity: 13L⊙

Magnitude: U= 9.58 B=9.3 V=8.98 R=8.57 I=8.47 J=7.95 H=7.5 K=6.8

Rotational velocity, v sin I: 102 km /s

Radial velocity :13.3 km/s

log g: 4.00

Microturbulent velocity: 2 km /s

Additional Properties:

- Algol-like dimming
- δ Scuti type variability
- Inverse P Cygni profile (in Hα profile)

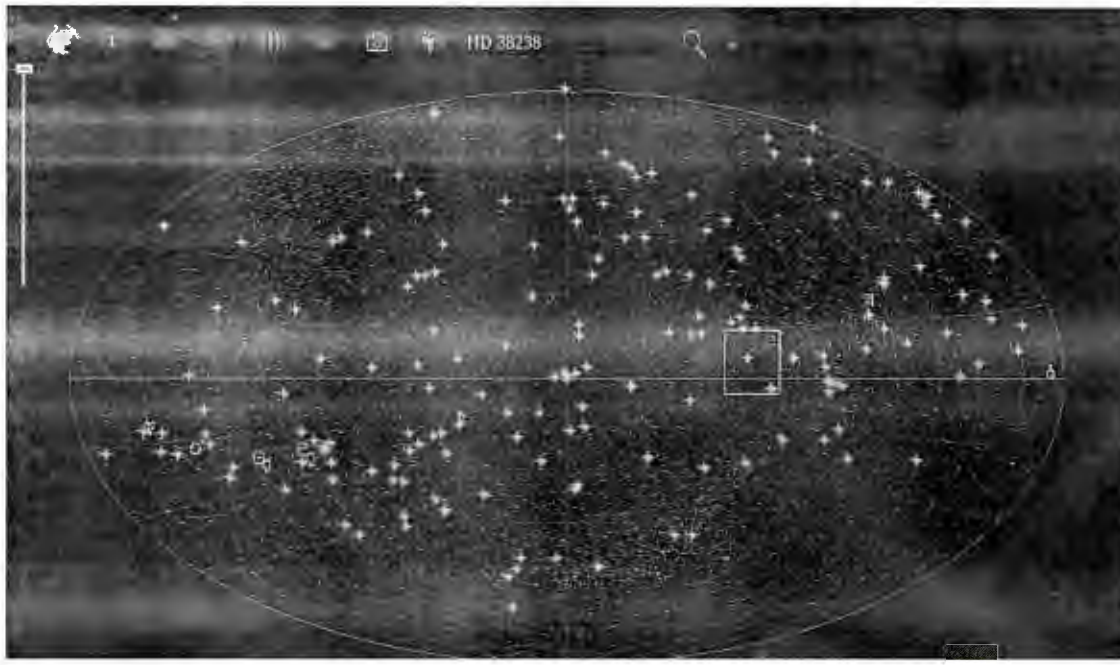

Figure D.1 Location of V351 Ori (at the centre of the rectangle) with respect to Celestial Sphere and Milky Way Galaxy (the white S-shaped band) as seen outside the the sphere (www.sky-map.org).

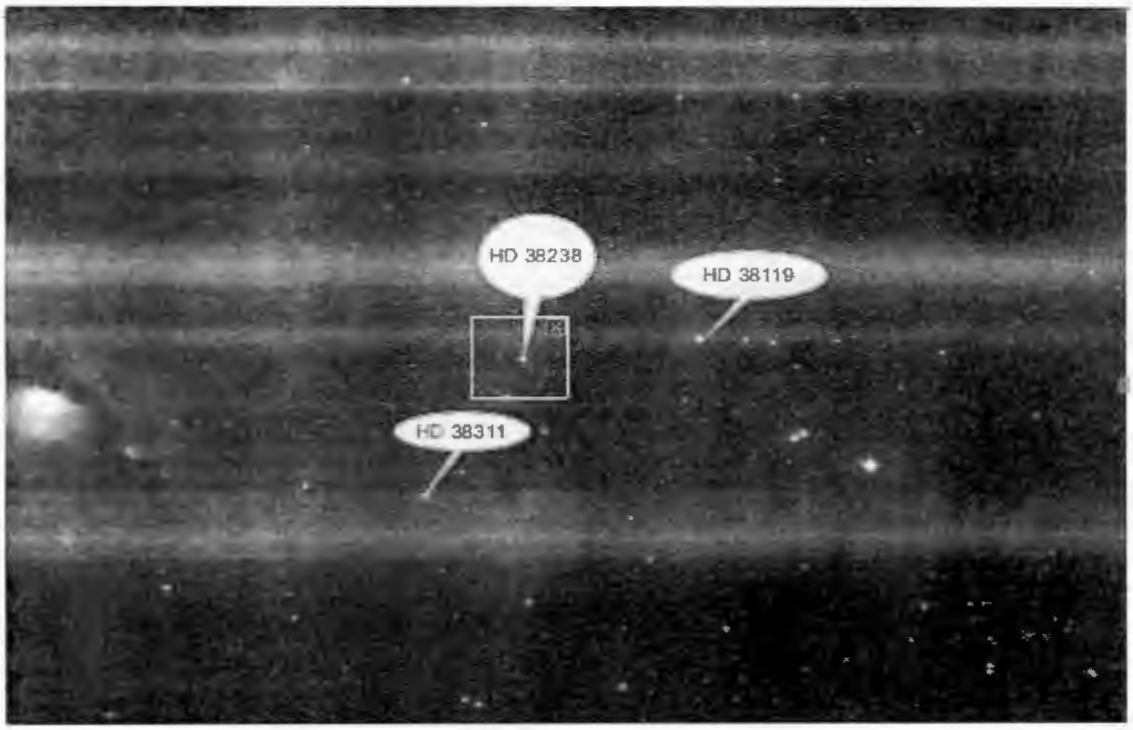

Figure D.2 Relative location of the target star (HD 38238) and the two comparison stars (HD 38119 and HD 38311), (www.sky-map.org).

Appendix E Mode Identification Report

This field displays the main information about the observed and theoretical parameters for the obtained mode identification. It lists the input values and settings for the models, the observed amplitude ratios and phase differences, and for each pulsation model that matches the search criteria, its degree and corresponding amplitude ratio and phase differences. This report shows only for the first four mode identification plots taken as a sample.

1

Input values:

Frequency = 15.6889

Teff = 7500+/-250

log g = 3.6+/-0.1

Model Parameters:

M = 2.00 Mo

Atmosphere Model: Kurucz

without overshooting

Metallicity = +0.0

Microturbulence velocity = 2 km/s

Model source: Delta Sct Models MAD

Grids of atmospheric parameters have been computed by Leszek Kowalczuk and Jagoda Daszynska-Daszkiewicz

(http://helas.astro.uni.wroc.pl/deliverables.php) using Kurucz and NEMO atmospheres.

Pulsational grid for Delta Scuti Stars computed with ATON (Ventura et al. 2007) and MAD by Montalban and Dupret (2007).

Observed values:

A(U)/A(U) = 1 +/- 0.363603

A(B)/A(U) = 0.809561 +/- 0.248895

A(V)/A(U) = 0.752964 +/- 0.234953

A(R)/A(U) = 0.704469 +/- 0.225537

A(I)/A(U) = 0.475639 +/- 0.175064

P(U - U) = 0 +/- 29.6682 °

P(B - U) = -56.2074 +/- 24.5903 °

P(V - U) = -28.412 +/- 25.08 °

P(R - U) = -93.857 +/- 25.8965 °

P(I - U) = -132.48 +/- 30.0544 °

Results from mode identification:

Found 4 different models in the given range of Teff, logg and mass.

----------Model 1----------

Teff = 7386.35 K

logg = 3.6882

l = 0

Frequency = 15.9707 c/d

A(U)/A(U) = 1

A(B)/A(U) = 0.761418

A(V)/A(U) = 0.601104

A(R)/A(U) = 0.457099

A(I)/A(U) = 0.323853

P(U - U) = 0 °

P(B - U) = -33.9955 °

P(V - U) = -27.4477 °

P(R - U) = -22.5688 °

P(I - U) = -28.2162 °

l = 1

Frequency = 16.3015 c/d

A(U)/A(U) = 1

A(B)/A(U) = 0.69627

A(V)/A(U) = 0.614614

A(R)/A(U) = 0.532997

A(I)/A(U) = 0.433628

P(U - U) = 0 °

P(B - U) = -22.6451 °

P(V - U) = -13.7068 °

P(R - U) = -6.25191 °

P(I - U) = -3.05741 °

l = 2

Frequency = 14.937 c/d

A(U)/A(U) = 1

A(B)/A(U) = 0.791583

A(V)/A(U) = 0.726583

A(R)/A(U) = 0.663727

A(I)/A(U) = 0.611217

P(U - U) = 0 °

P(B - U) = -15.9332 °

P(V - U) = -7.00854 °

P(R - U) = 0.489097 °

P(I - U) = 5.73866 °

----------Model 2----------

Teff = 7349.88 K

logg = 3.6753

l = 0

Frequency = 15.6167 c/d

A(U)/A(U) = 1

A(B)/A(U) = 0.745088

A(V)/A(U) = 0.586762

A(R)/A(U) = 0.445945

A(I)/A(U) = 0.315396

P(U - U) = 0 °

P(B - U) = -34.8777 °

P(V - U) = -28.5036 °

P(R - U) = -23.2721 °

P(I - U) = -28.4775 °

l = 1

Frequency = 15.9393 c/d

A(U)/A(U) = 1

A(B)/A(U) = 0.685069

A(V)/A(U) = 0.604187

A(R)/A(U) = 0.525878

A(I)/A(U) = 0.430051

P(U - U) = 0 °

P(B - U) = -22.7216 °

P(V - U) = -13.973 °

P(R - U) = -6.41319 °

P(I - U) = -3.06275 °

l = 2

Frequency = 15.756 c/d

A(U)/A(U) = 1

A(B)/A(U) = 0.736861

A(V)/A(U) = 0.693818

A(R)/A(U) = 0.643659

A(I)/A(U) = 0.59382

P(U - U) = 0 °

P(B - U) = -13.4594 °

P(V - U) = -6.1134 °

P(R - U) = -0.143011 °

P(I - U) = 3.84573 °

----------Model 3----------

Teff = 7311.39 K

logg = 3.6626

l = 0

Frequency = 15.2731 c/d

A(U)/A(U) = 1

A(B)/A(U) = 0.726661

A(V)/A(U) = 0.570792

A(R)/A(U) = 0.433718

A(I)/A(U) = 0.306239

P(U - U) = 0 °

P(B - U) = -35.7021 °

P(V - U) = -29.5507 °

P(R - U) = -23.9166 °

P(I - U) = -28.5563 °

l = 1

Frequency = 15.724 c/d

A(U)/A(U) = 1

A(B)/A(U) = 0.665962

A(V)/A(U) = 0.589569

A(R)/A(U) = 0.517091

A(I)/A(U) = 0.425886

P(U - U) = 0 °

P(B - U) = -22.1191 °

P(V - U) = -13.7801 °

P(R - U) = -6.34048 °

P(I - U) = -2.94428 °

l = 2

Frequency = 15.8348 c/d

A(U)/A(U) = 1

A(B)/A(U) = 0.718508

A(V)/A(U) = 0.679075

A(R)/A(U) = 0.632541

A(I)/A(U) = 0.581827

P(U - U) = 0 °

P(B - U) = -12.1306 °

P(V - U) = -5.67432 °

P(R - U) = -0.364266 °

P(I - U) = 3.0838 °

----------Model 4----------

Teff = 7270.6 K

logg = 3.6499

l = 0

Frequency = 14.9381 c/d

A(U)/A(U) = 1

A(B)/A(U) = 0.70675

A(V)/A(U) = 0.553553

A(R)/A(U) = 0.420693

A(I)/A(U) = 0.296726

P(U - U) = 0 °

P(B - U) = -36.4496 °

P(V - U) = -30.577 °

P(R - U) = -24.4881 °

P(I - U) = -28.426 °

l = 1

Frequency = 15.8959 c/d

A(U)/A(U) = 1

A(B)/A(U) = 0.633941

A(V)/A(U) = 0.569104

A(R)/A(U) = 0.506494

A(I)/A(U) = 0.421218

P(U - U) = 0 °

P(B - U) = -18.938 °

P(V - U) = -11.8753 °

P(R - U) = -5.44603 °

P(I - U) = -2.44767 °

l = 2

Frequency = 15.8234 c/d

A(U)/A(U) = 1

A(B)/A(U) = 0.706624

A(V)/A(U) = 0.666865

A(R)/A(U) = 0.622138

A(I)/A(U) = 0.569641

P(U - U) = 0 °

P(B - U) = -10.9904 °

P(V - U) = -5.30892 °

P(R - U) = -0.521314 °

P(I - U) = 2.50868 °

2

Input values:

Frequency = 15.6889

Teff = 7500+/-200

log g = 3.6+/-0.1

Model Parameters:

M = 2.00 Mo

Atmosphere Model: Kurucz

without overshooting

Metallicity = +0.0

Microturbulence velocity = 2 km/s

Model source: Delta Sct Models MAD

Grids of atmospheric parameters have been computed by Leszek Kowalczuk and Jagoda Daszynska-Daszkiewicz

(http://helas.astro.uni.wroc.pl/deliverables.php) using Kurucz and NEMO atmospheres.

Pulsational grid for Delta Scuti Stars computed with ATON (Ventura et al. 2007) and MAD

by Montalban and Dupret (2007).

Observed values:

A(U)/A(U) = 1 +/- 0.363603

A(B)/A(U) = 0.809561 +/- 0.248895

A(V)/A(U) = 0.752964 +/- 0.234953

A(R)/A(U) = 0.704469 +/- 0.225537

A(I)/A(U) = 0.475639 +/- 0.175064

P(U - U) = 0 +/- 29.6682 °

P(B - U) = -56.2074 +/- 24.5903 °

P(V - U) = -28.412 +/- 25.08 °

P(R - U) = -93.857 +/- 25.8965 °

P(I - U) = -132.48 +/- 30.0544 °

Results from mode identification:

Found 3 different models in the given range of Teff, logg and mass.

----------Model 1----------

Teff = 7386.35 K

logg = 3.6882

l = 0

Frequency = 15.9707 c/d

A(U)/A(U) = 1

A(B)/A(U) = 0.761418

A(V)/A(U) = 0.601104

A(R)/A(U) = 0.457099

A(I)/A(U) = 0.323853

P(U - U) = 0 °

P(B - U) = -33.9955 °

P(V - U) = -27.4477 °

P(R - U) = -22.5688 °

P(I - U) = -28.2162 °

l = 1

Frequency = 16.3015 c/d

A(U)/A(U) = 1

A(B)/A(U) = 0.69627

A(V)/A(U) = 0.614614

A(R)/A(U) = 0.532997

A(I)/A(U) = 0.433628

P(U - U) = 0 °

P(B - U) = -22.6451 °

P(V - U) = -13.7068 °

P(R - U) = -6.25191 °

P(I - U) = -3.05741 °

l = 2

Frequency = 14.937 c/d

A(U)/A(U) = 1

A(B)/A(U) = 0.791583

A(V)/A(U) = 0.726583

A(R)/A(U) = 0.663727

A(I)/A(U) = 0.611217

P(U - U) = 0 °

P(B - U) = -15.9332 °

P(V - U) = -7.00854 °

P(R - U) = 0.489097 °

P(I - U) = 5.73866 °

----------Model 2----------

Teff = 7349.88 K

logg = 3.6753

l = 0

Frequency = 15.6167 c/d

A(U)/A(U) = 1

A(B)/A(U) = 0.745088

A(V)/A(U) = 0.586762

A(R)/A(U) = 0.445945

A(I)/A(U) = 0.315396

P(U - U) = 0 °

P(B - U) = -34.8777 °

P(V - U) = -28.5036 °

P(R - U) = -23.2721 °

P(I - U) = -28.4775 °

l = 1

Frequency = 15.9393 c/d

A(U)/A(U) = 1

A(B)/A(U) = 0.685069

A(V)/A(U) = 0.604187

A(R)/A(U) = 0.525878

A(I)/A(U) = 0.430051

P(U - U) = 0 °

P(B - U) = -22.7216 °

P(V - U) = -13.973 °

P(R - U) = -6.41319 °

P(I - U) = -3.06275 °

l = 2

Frequency = 15.756 c/d

A(U)/A(U) = 1

A(B)/A(U) = 0.736861

A(V)/A(U) = 0.693818

A(R)/A(U) = 0.643659

A(I)/A(U) = 0.59382

P(U - U) = 0 °

P(B - U) = -13.4594 °

P(V - U) = -6.1134 °

P(R - U) = -0.143011 °

P(I - U) = 3.84573 °

----------Model 3----------

Teff = 7311.39 K

logg = 3.6626

l = 0

Frequency = 15.2731 c/d

A(U)/A(U) = 1

A(B)/A(U) = 0.726661

A(V)/A(U) = 0.570792

A(R)/A(U) = 0.433718

A(I)/A(U) = 0.306239

P(U - U) = 0 °

P(B - U) = -35.7021 °

P(V - U) = -29.5507 °

P(R - U) = -23.9166 °

P(I - U) = -28.5563 °

l = 1

Frequency = 15.724 c/d

A(U)/A(U) = 1

A(B)/A(U) = 0.665962

A(V)/A(U) = 0.589569

A(R)/A(U) = 0.517091

A(I)/A(U) = 0.425886

P(U - U) = 0 °

P(B - U) = -22.1191 °

P(V - U) = -13.7801 °

P(R - U) = -6.34048 °

P(I - U) = -2.94428 °

l = 2

Frequency = 15.8348 c/d

A(U)/A(U) = 1

A(B)/A(U) = 0.718508

A(V)/A(U) = 0.679075

A(R)/A(U) = 0.632541

A(I)/A(U) = 0.581827

P(U - U) = 0 °

P(B - U) = -12.1306 °

P(V - U) = -5.67432 °

P(R - U) = -0.364266 °

P(I - U) = 3.0838 °

3

Input values:

Frequency = 15.6889

Teff = 7500+/-200

log g = 3.6+/-0.1

Model Parameters:

M = 2.00 Mo

Atmosphere Model: Kurucz

without overshooting

Metallicity = +1.0

Microturbulence velocity = 2 km/s

Model source: Delta Sct Models MAD

Grids of atmospheric parameters have been computed by Leszek Kowalczuk and Jagoda Daszynska-Daszkiewicz

(http://helas.astro.uni.wroc.pl/deliverables.php) using Kurucz and NEMO atmospheres.

Pulsational grid for Delta Scuti Stars computed with ATON (Ventura et al. 2007) and MAD by Montalban and Dupret (2007).

Observed values:

A(U)/A(U) = 1 +/- 0.363603

A(B)/A(U) = 0.809561 +/- 0.248895

A(V)/A(U) = 0.752964 +/- 0.234953

A(R)/A(U) = 0.704469 +/- 0.225537

A(I)/A(U) = 0.475639 +/- 0.175064

P(U - U) = 0 +/- 29.6682 °

P(B - U) = -56.2074 +/- 24.5903 °

P(V - U) = -28.412 +/- 25.08 °

P(R - U) = -93.857 +/- 25.8965 °

P(I - U) = -132.48 +/- 30.0544 °

Results from mode identification:

Found 3 different models in the given range of Teff, logg and mass.

----------Model 1----------

Teff = 7386.35 K

logg = 3.6882

l = 0

Frequency = 15.9707 c/d

A(U)/A(U) = 1

A(B)/A(U) = 0.66756

A(V)/A(U) = 0.493327

A(R)/A(U) = 0.366259

A(I)/A(U) = 0.255485

P(U - U) = 0 °

P(B - U) = -23.1016 °

P(V - U) = -19.1151 °

P(R - U) = -17.4904 °

P(I - U) = -26.0274 °

l = 1

Frequency = 16.3015 c/d

A(U)/A(U) = 1

A(B)/A(U) = 0.66306

A(V)/A(U) = 0.545962

A(R)/A(U) = 0.45607

A(I)/A(U) = 0.361732

P(U - U) = 0 °

P(B - U) = -14.6672 °

P(V - U) = -7.47149 °

P(R - U) = -2.25417 °

P(I - U) = -0.676519 °

l = 2

Frequency = 14.937 c/d

A(U)/A(U) = 1

A(B)/A(U) = 0.759007

A(V)/A(U) = 0.661877

A(R)/A(U) = 0.589179

A(I)/A(U) = 0.537021

P(U - U) = 0 °

P(B - U) = -10.2194 °

P(V - U) = -1.34668 °

P(R - U) = 4.88567 °

P(I - U) = 9.29205 °

----------Model 2----------

Teff = 7349.88 K

logg = 3.6753

l = 0

Frequency = 15.6167 c/d

A(U)/A(U) = 1

A(B)/A(U) = 0.656291

A(V)/A(U) = 0.483898

A(R)/A(U) = 0.358887

A(I)/A(U) = 0.249616

P(U - U) = 0 °

P(B - U) = -23.1613 °

P(V - U) = -19.7044 °

P(R - U) = -18.2121 °

P(I - U) = -26.6573 °

l = 1

Frequency = 15.9393 c/d

A(U)/A(U) = 1

A(B)/A(U) = 0.656342

A(V)/A(U) = 0.538955

A(R)/A(U) = 0.450407

A(I)/A(U) = 0.357986

P(U - U) = 0 °

P(B - U) = -14.4049 °

P(V - U) = -7.6674 °

P(R - U) = -2.57937 °

P(I - U) = -0.91957 °

l = 2

Frequency = 15.756 c/d

A(U)/A(U) = 1

A(B)/A(U) = 0.719385

A(V)/A(U) = 0.638863

A(R)/A(U) = 0.57283

A(I)/A(U) = 0.522677

P(U - U) = 0 °

P(B - U) = -8.58027 °

P(V - U) = -1.69916 °

P(R - U) = 3.07112 °

P(I - U) = 6.4304 °

----------Model 3----------

Teff = 7311.39 K

logg = 3.6626

l = 0

Frequency = 15.2731 c/d

A(U)/A(U) = 1

A(B)/A(U) = 0.644227

A(V)/A(U) = 0.473674

A(R)/A(U) = 0.35093

A(I)/A(U) = 0.243316

P(U - U) = 0 °

P(B - U) = -23.0452 °

P(V - U) = -20.184 °

P(R - U) = -18.8616 °

P(I - U) = -27.1855 °

l = 1

Frequency = 15.724 c/d

A(U)/A(U) = 1

A(B)/A(U) = 0.645585

A(V)/A(U) = 0.530035

A(R)/A(U) = 0.443966

A(I)/A(U) = 0.353874

P(U - U) = 0 °

P(B - U) = -13.6196 °

P(V - U) = -7.55548 °

P(R - U) = -2.78882 °

P(I - U) = -1.11897 °

l = 2

Frequency = 15.8348 c/d

A(U)/A(U) = 1

A(B)/A(U) = 0.706445

A(V)/A(U) = 0.626929

A(R)/A(U) = 0.562004

A(I)/A(U) = 0.512031

P(U - U) = 0 °

P(B - U) = -7.56703 °

P(V - U) = -1.76961 °

P(R - U) = 2.34296 °

P(I - U) = 5.26988 °

4

Input values:

Frequency = 15.6889

Teff = 7500+/-200

log g = 3.6+/-0.1

Model Parameters:

M = 2.00 Mo

Atmosphere Model: Kurucz

without overshooting

Metallicity = +0.3

Microturbulence velocity = 2 km/s

Model source: Delta Sct Models MAD

Grids of atmospheric parameters have been computed by Leszek Kowalczuk and Jagoda Daszynska-Daszkiewicz

(http://helas.astro.uni.wroc.pl/deliverables.php) using Kurucz and NEMO atmospheres.

Pulsational grid for Delta Scuti Stars computed with ATON (Ventura et al. 2007) and MAD by Montalban and Dupret (2007).

Observed values:

A(U)/A(U) = 1 +/- 0.363603

A(B)/A(U) = 0.809561 +/- 0.248895

A(V)/A(U) = 0.752964 +/- 0.234953

A(R)/A(U) = 0.704469 +/- 0.225537

A(I)/A(U) = 0.475639 +/- 0.175064

P(U - U) = 0 +/- 29.6682 °

P(B - U) = -56.2074 +/- 24.5903 °

P(V - U) = -28.412 +/- 25.08 °

P(R - U) = -93.857 +/- 25.8965 °

P(I - U) = -132.48 +/- 30.0544 °

Results from mode identification:

Found 3 different models in the given range of Teff, logg and mass.

----------Model 1----------

Teff = 7386.35 K

logg = 3.6882

l = 0

Frequency = 15.9707 c/d

A(U)/A(U) = 1

A(B)/A(U) = 0.73382

A(V)/A(U) = 0.568701

A(R)/A(U) = 0.42832

A(I)/A(U) = 0.304072

P(U - U) = 0 °

P(B - U) = -31.7674 °

P(V - U) = -26.2561 °

P(R - U) = -22.4893 °

P(I - U) = -27.8158 °

l = 1

Frequency = 16.3015 c/d

A(U)/A(U) = 1

A(B)/A(U) = 0.686319

A(V)/A(U) = 0.593394

A(R)/A(U) = 0.508077

A(I)/A(U) = 0.414678

P(U - U) = 0 °

P(B - U) = -20.977 °

P(V - U) = -12.722 °

P(R - U) = -5.93564 °

P(I - U) = -2.74543 °

l = 2

Frequency = 14.937 c/d

A(U)/A(U) = 1

A(B)/A(U) = 0.781662

A(V)/A(U) = 0.707559

A(R)/A(U) = 0.641473

A(I)/A(U) = 0.590807

P(U - U) = 0 °

P(B - U) = -14.8879 °

P(V - U) = -6.10733 °

P(R - U) = 1.0288 °

P(I - U) = 6.16364 °

----------Model 2----------

Teff = 7349.88 K

logg = 3.6753

l = 0

Frequency = 15.6167 c/d

A(U)/A(U) = 1

A(B)/A(U) = 0.718068

A(V)/A(U) = 0.555257

A(R)/A(U) = 0.417894

A(I)/A(U) = 0.296063

P(U - U) = 0 °

P(B - U) = -32.5084 °

P(V - U) = -27.2956 °

P(R - U) = -23.2472 °

P(I - U) = -28.223 °

l = 1

Frequency = 15.9393 c/d

A(U)/A(U) = 1

A(B)/A(U) = 0.675831

A(V)/A(U) = 0.583452

A(R)/A(U) = 0.501111

A(I)/A(U) = 0.410705

P(U - U) = 0 °

P(B - U) = -21.0097 °

P(V - U) = -13.0268 °

P(R - U) = -6.15282 °

P(I - U) = -2.82871 °

l = 2

Frequency = 15.756 c/d

A(U)/A(U) = 1

A(B)/A(U) = 0.730314

A(V)/A(U) = 0.676494

A(R)/A(U) = 0.62162

A(I)/A(U) = 0.573163

P(U - U) = 0 °

P(B - U) = -12.557 °

P(V - U) = -5.44979 °

P(R - U) = 0.206378 °

P(I - U) = 4.11344 °

----------Model 3----------

Teff = 7311.39 K

logg = 3.6626

l = 0

Frequency = 15.2731 c/d

A(U)/A(U) = 1

A(B)/A(U) = 0.700428

A(V)/A(U) = 0.540342

A(R)/A(U) = 0.4065

A(I)/A(U) = 0.287399

P(U - U) = 0 °

P(B - U) = -33.1917 °

P(V - U) = -28.3311 °

P(R - U) = -23.9577 °

P(I - U) = -28.4719 °

l = 1

Frequency = 15.724 c/d

A(U)/A(U) = 1

A(B)/A(U) = 0.658262

A(V)/A(U) = 0.569713

A(R)/A(U) = 0.492563

A(I)/A(U) = 0.406122

P(U - U) = 0 °

P(B - U) = -20.4001 °

P(V - U) = -12.9029 °

P(R - U) = -6.14941 °

P(I - U) = -2.79884 °

l = 2

Frequency = 15.8348 c/d

A(U)/A(U) = 1

A(B)/A(U) = 0.713344

A(V)/A(U) = 0.662273

A(R)/A(U) = 0.610472

A(I)/A(U) = 0.560919

P(U - U) = 0 °

P(B - U) = -11.3036 °

P(V - U) = -5.12974 °

P(R - U) = -0.106037 °

P(I - U) = 3.28183 °